UNIVERSIDAD PERUANA
CAYETANO HEREDIA

“EVALUACIÓN DE LA CALIDAD ECOLÓGICA DE LA BAHÍA DE PARACAS (PERÚ, 14°S) USANDO BIOINDICADORES DE LOS SEDIMENTOS: LOS FORAMINÍFEROS BENTÓNICOS”

TESIS PARA OPTAR EL GRADO DE DOCTOR EN CIENCIAS DE LA VIDA

LANDER MERMA MORA

LIMA-PERÚ

2024

“ECOLOGICAL QUALITY ASSESSMENT OF THE PARACAS BAY (PERU, 14°S) THROUGH BIOINDICATORS OF THE SEDIMENTS: THE BENTHIC FORAMINIFERA”

THESIS FOR COMPLETING DOCTORAL DEGREE IN LIFE SCIENCES

LANDER MERMA MORA

LIMA-PERU

2024

ASESOR

Dr. Jorge Aquiles Cardich Salazar

CO ASESOR

Dr. Dimitri Alexey Gutiérrez Aguilar

CO ASESOR

Dr. Abdelfettah Sifeddine

JURADO EVALUADOR

Dr. Matthieu Carré

PRESIDENTE

Dr. Raúl Loayza Muro

VOCAL

Dra. Laura Tavera Martínez

SECRETARIA

Dedicated to my nuclear family and special friends
who despite all these years still keep in touch.

ACKNOWLEDGMENTS

To my advisor (Director of Thesis) Jorge Cardich for the guidance, support and friendship.

To my co-advisors Dimitri Gutiérrez and Abdelfettah Sifeddine for facilitating the development of this study and for their comments to the manuscript.

To the project CONCYTEC-World Bank “Improvement and Expansion of Services of the National System of Science, Technology and Technological Innovation” 8682-PE, through its executing unit FONDECYT (Grant n◦ 08-2018-E033-FONDECYT-BM-Programas de Doctorado en Áreas Estratégicas y Generales), for the financial support.

RESEARCH FUNDING

CONCYTEC - PROCIENCIA - Grant n° 08-2018-E033-FONDECYT-Banco Mundial - Programas de Doctorado en Áreas Estratégicas y Generales.

EVALUACIÓN DE LA CALIDAD ECOLÓGICA DE LA BAHÍA DE PARACAS (PERÚ, 14°S) USANDO BIOINDICADORES DE LOS SEDIMENTOS: LOS FORAMINÍFEROS BENTÓNICOS

INFORME DE ORIGINALIDAD

10%	8%	8%	3%
INDICE DE SIMILITUD	FUENTES DE INTERNET	PUBLICACIONES	TRABAJOS DEL ESTUDIANTE

FUENTES PRIMARIAS

1	Submitted to Universidad Peruana Cayetano Heredia Trabajo del estudiante	<1%
2	research-repository.st-andrews.ac.uk Fuente de Internet	<1%
3	revistasinvestigacion.unmsm.edu.pe Fuente de Internet	<1%
4	hdl.handle.net Fuente de Internet	<1%
5	repositorio.upch.edu.pe Fuente de Internet	<1%
6	Alexis Castillo, Tatiana Hromic, Roberto A. Uribe, Jorge Valdés et al. " Living (stained) calcareous benthic foraminiferal assemblages ( ) in a coastal upwelling zone of the Humboldt Current System, Northern Chile (S) ", Regional Studies in Marine Science, 2021 Publicación	<1%

TABLE OF CONTENTS

TABLE OF FIGURES

TABLE OF TABLES

THESIS ABSTRACT

Eutrophication of coastal marine environments is described as an increasing rate of supply of organic matter to the bottom ecosystem. In the coastal area of Pisco-Paracas, Peru, a process of eutrophication induced by organic pollution from the fishmeal industry developed between 1964 and 2004, the effects of which on communities of benthic organisms have not been studied.

Currently, Paracas Bay is a shallow marine environment (<15 m deep) in which there are natural conditions of bottom hypoxia, of a poorly described regime, which is habitat for a benthic fauna that is low diverse but tolerant to such conditions.

Among benthic organisms, foraminifera (testate protists) represent one of the main dominant groups in oxygen-deficient environments such as the Peruvian coast. Due to their diversity and adaptations to specific environmental conditions, benthic foraminifera are suitable to be used as indicators of the ecological quality of coastal ecosystems. Furthermore, the tests of foraminifera are potentially preserved in the sedimentary record, allowing us to reconstruct the ecological quality of an environment in the past.

The main objective of this study was to evaluate the ecological quality of Paracas Bay associated with the eutrophication process induced by the fishmeal industry, by integrating environmental, ecological, and paleo-ecological approach based on benthic foraminifera. For this, specific objectives were addressed in the chapters of this document, such as: the determination of the main factors that control the bottom oxygen regime on time scales using environmental monitoring data (Chapter 2), the characterization of the assemblages of benthic foraminifera, their spatiotemporal

variability and associated abiotic factors (Chapters 3 and 4); and finally, historical changes in the organic enrichment of the sediments and the preserved assemblages of benthic foraminifera were evaluated, along with their relationships with the geochemical variability of the sediments in the last 100 years, through the analysis of a sedimentary record from the Paracas Bay (Chapter 5).

Between 1964 and 2004, industrial organic pollution in the Pisco-Paracas coastal area induced eutrophic conditions in the environments at the bottom of Paracas Bay, which did not affect, however, the structure of the benthic foraminiferal assemblage of the bay, given that the same dominant species (adapted to tolerate anoxic and sulfurous conditions) characterized the assemblages before, during and after the period of greatest industrial influence. This led to the conclusion that the ecological quality of Paracas Bay was not degraded in that period.

However, the sediments of Paracas Bay accumulated more and more organic matter derived from phytoplankton that along with changes associated with other natural or anthropogenic processes, would have caused a recent change in the dominant foraminiferal species (from *Bolivina costata* to *Buliminella elegantissima*) reflecting the current severe eutrophic conditions.

Keywords: organic pollution, coastal eutrophication, foraminifera indicators, ecological quality.

RESUMEN DE TESIS

La eutrofización de ambientes marinos costeros es descrita como una tasa creciente de suministro de materia orgánica al ecosistema de fondo. En la zona costera de Pisco-Paracas, Perú, se desarrolló un proceso de eutrofización inducida por la contaminación orgánica de la industria de harina de pescado, entre 1964 y 2004, cuyos efectos sobre las comunidades de organismos bentónicos no han sido estudiados.

Actualmente, la Bahía de Paracas es un ambiente marino somero (<15 m de profundidad) en el que existen condiciones naturales de hipoxia de fondo, de régimen poco descrito, que alberga una fauna bentónica poco diversa y tolerante a tales condiciones.

Entre los organismos bentónicos, los foraminíferos (protistas testados) representan uno de los principales grupos dominantes en ambientes deficientes de oxígeno como la costa peruana. Debido a su diversidad y adaptaciones a condiciones ambientales específicas, los foraminíferos bentónicos son aptos para ser utilizados como indicadores de la calidad ecológica de los ecosistemas costeros. Además, las testas de los foraminíferos potencialmente se preservan en el registro sedimentario, permitiendo reconstruir la calidad ecológica de un ambiente en el pasado.

El objetivo principal de este estudio fue evaluar la calidad ecológica de la Bahía de Paracas asociado al proceso de eutrofización inducida por la industria harinera, mediante la integración del estudio ambiental y un enfoque ecológico-paleoecológico basado en foraminíferos bentónicos. Para esto, se abordaron objetivos específicos en los capítulos del presente documento, como: la

determinación de los principales factores que controlan el régimen de oxígeno de fondo en escalas de tiempo usando datos de monitoreo ambiental (Capítulo 2), la caracterización de los ensambles de foraminíferos bentónicos, su variabilidad espaciotemporal y los factores abióticos asociados (Capítulos 3 y 4); y finalmente se evaluaron los cambios históricos del enriquecimiento orgánico de los sedimentos y de los ensambles preservados de foraminíferos bentónicos, y su relación con la variabilidad geoquímica de los sedimentos en los últimos 100 años, a través del análisis de un registro sedimentario de la Bahía de Paracas. (Capítulo 5).

Entre los años 1964 y 2004, la contaminación orgánica industrial en la zona costera de Pisco-Paracas indujo condiciones más eutróficas en los ambientes del fondo de la Bahía de Paracas, que no afectó, sin embargo, a la estructura del ensamble de foraminíferos bentónicos de la bahía, dado que las mismas especies dominantes (adaptadas para tolerar condiciones anóxicas y sulfurosas) caracterizaron los ensambles antes, durante y después del período de mayor influencia industrial. Esto llevó a concluir que la calidad ecológica de la Bahía de Paracas no fue degradada en ese periodo.

Sin embargo, los sedimentos de la Bahía de Paracas acumularon cada vez más materia orgánica derivada del fitoplancton que, junto con los cambios asociados a otros procesos naturales o antropogénicos, habrían ocasionado un cambio reciente de especie de foraminífero dominante (de *Bolivina costata* a *Buliminella elegantissima*) que refleja las condiciones eutróficas severas de la actualidad.

Palabras clave: contaminación orgánica, eutrofización costera, foraminíferos indicadores, calidad ecológica.

I. CHAPTER 1: General introduction

1.1. Marine eutrophication

Marine eutrophication is the process of the nutritional enrichment of a marine coastal environment by increasing the organic and inorganic nutrient resources, specially forms of nitrogen (N) and phosphorus (P). The immediate effect of eutrophication is the increased primary production which can lead to changes in the ecosystem's energy flow. In order to differentiate the phenomenon from its causes (*e.g.*, nutrient enrichment and increasing water resident time) and consequences (*e.g.*, hypoxia and defaunation), eutrophication has also been described as the increasing rate of organic matter supply to the marine ecosystem (Nixon, 2009).

Most scientific studies have focused in the inorganic forms of N as nutrients, and nitrates as the most limiting factor for marine autotrophic production of organic matter (Jessen *et al*., 2015). The sources of N can be natural or anthropogenic. The natural ones comprise atmospheric deposition, upwelling, river runoff, whereas the main anthropogenic sources are sewage, fertilizers and industrial runoffs.

The eastern boundary ocean margins, such as the American Pacific coast, are subjected to natural nutrient enrichment due to wind-driven coastal upwelling that transports deeper nutrient-rich waters into the surface (Wilkerson and Dugdale, 2008). On the other hand, human activities like the large-scale use of synthetic N fertilizers in agriculture, the rapid expansion of industrial fossil fuel combustion and the coastal urbanization, produced an increasing terrigenous discharge and atmospheric N emissions affecting marine areas until the present (Paerl and Piehler, 2008).

1.2. The Pisco-Paracas coastal area

The Pisco-Paracas coastal area (Figure 1a) is located in the Ica region (13.5-16°S), which is subjected to the most intense (*e.g.*, Goubanova *et al.*, 2010) alongshore winds off the Peruvian coast as a consequence of the influence of the South Pacific Anticyclone. These winds are permanently favorable to coastal upwelling, giving rise to the main upwelling center of the Peruvian coast that is active year-round but stronger during austral winter and early spring, while less intense during austral summer (Gutiérrez *et al.*, 2011, 2016).

In this coastal area, the bottom topography is bordered by a steep depth gradient between 50 and 25 m, becoming gradually shallower into the intermediate zone and the Paracas Bay, whereas exhibiting an even more gentle slope in the northern zone, off the Pisco River (Figure 1b). The bottom substrate is predominantly composed of terrigenous muddy sediments with sandier and gravelly sediments restricted to the shores (Velazco and Solis, 2000).

The Paracas Bay is a small (<100 km^2) and shallow (<15 m depth) environment in the southern part of the Pisco-Paracas coastal area, where occurrences of bottom hypoxia and anoxia are predominantly observed during the austral summer months (Cabello *et al.*, 2002; Aguirre-Velarde *et al.*, 2019). The mechanisms and controls of hypoxia have been insufficiently investigated in this coastal area, however, the potential contributing factors include the advection of oxygen-depleted upwelled waters into the bay, in-situ oxygen depletion following thermohaline stratification, and the decay of harmful algal blooms (Pitcher *et al.*, 2021). Moreover, the spatiotemporal patterns of hypoxic conditions in the bay and adjacent coastal areas,

as well as the extent of the relationship between hypoxia and physicochemical factors at different time scales, remain unexplored.

1.3. Eutrophication in the Pisco-Paracas coastal area

The Pisco-Paracas coastal area has been exposed to a process of anthropogenic eutrophication since the 1960s, due to the industrial effluents of fishmeal processing plants, located in the industrial zone of Pisco adjacent to the Paracas Bay (Figure 1b), until 2004, when a new system of wastewater treatment and a pipeline that transports waste out of this area, were stablished.

This anthropogenic eutrophication was associated with frequent mortality events of the marine fauna (fish and benthic invertebrates) due to anoxic events mainly observed during the 1990s and the early 2000s (Cabello *et al*., 2002; Jacinto, 2014) in Pisco and the Paracas Bay. In addition, aquaculture of the Peruvian scallop *Argopecten purpuratus* in the bay was affected due to high mortality and production drops in those years, but also recently since 2012 (Cueto-Vega *et al*., 2021).

The influence of eutrophication on the bottom hypoxic conditions of this coastal area was evidenced by time-series data that showed the lowest bottom oxygen concentrations prior the deployment of wastewater pipeline, and an increase of concentrations after that (Pitcher *et al.,* 2021). However, signs of eutrophic conditions are still observed in the water column such as a deficit of nitrates with respect to phosphates, particularly in summer (N:P ratio << 16; Pitcher *et al*., 2021),

and in the bottom such as anoxic sediments with high content of particulate organic matter (Solís *et al*., 2022).

1.4. Benthic Foraminifera and the Ecological Quality

Among benthic organisms, the foraminifera (shell-bearing protists) are trophic links between phytodetritus and metazoans (Nomaki *et al*., 2008), and represent one of the major dominant groups of the benthic biota from oxygen-deficient environments such as the Peruvian upper continental margin (Levin *et al*., 2002).

The concept of Ecological Quality (EcoQ) encompasses both the environmental and biological conditions of aquatic ecosystems that have been impacted by human activities. The assessment of the EcoQ relies on bioindicators such as benthic foraminifera, whose abundance and diversity make them a promising tool for this purpose (Bouchet *et al*., 2012). Moreover, benthic foraminifera are particularly advantageous because they have inorganic external structures (tests) that manage to be preserved in the sedimentary record, allowing paleoecological reconstructions (Alve *et al*., 2009; Dolven *et al*., 2013).

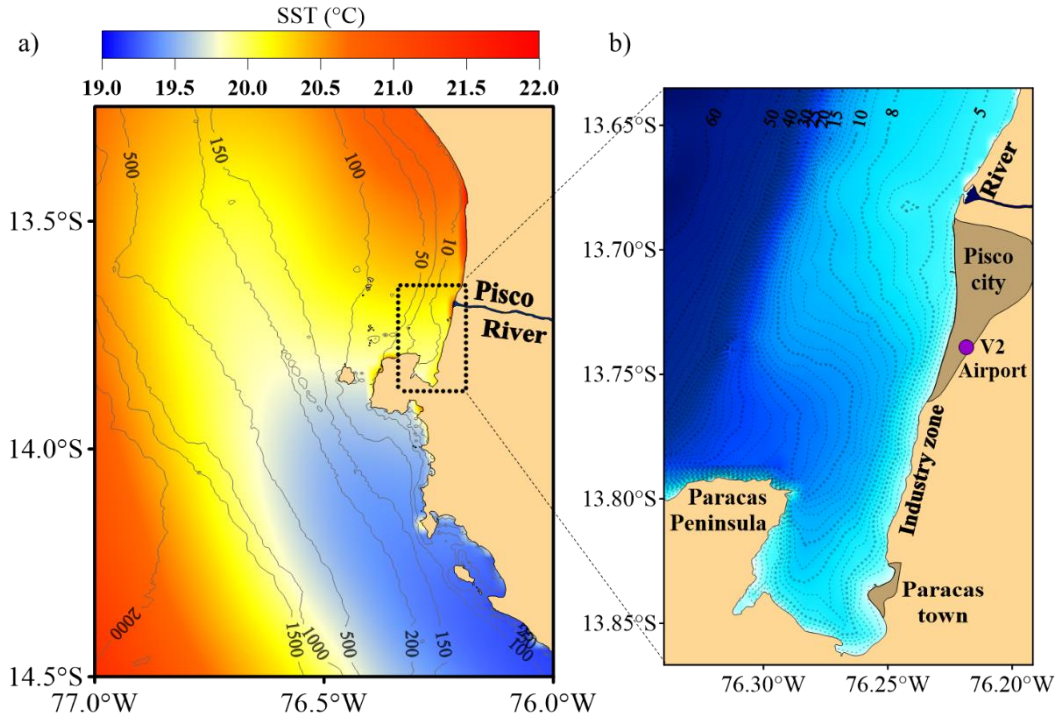

Figure 1. The study area in the environmental context of the Pisco region. a) Isobathic contours in meters (black lines) are superimposed on the summer distribution of Sea Surface Temperature (SST) in °C (color shading), adapted from Pitcher *et al*. (2021). Colder SST in blue represents the extension of the upwelling center off Pisco. b) The Pisco-Paracas coastal area, with Paracas Bay in its southernmost part, including the bathymetry (in color shading and dashed lines).

1.5. Research question and hypothesis

Considering that benthic foraminifera are bioindicators of the ecological quality of marine environments, the question that motivated this study was: How did the industrial organic pollution of the Pisco coast affect the assemblage of benthic foraminifera in the hypoxia-stressed Paracas Bay?

In order to answer this question, the present study formulates the following hypothesis:

The industrial organic pollution in the Pisco-Paracas coastal area affected the structure of the benthic foraminiferal assemblage in the Paracas Bay, decreasing its species diversity and generating a strong dominance of very few tolerant species, which characterize the current living foraminiferal assemblage.

1.6. Objectives

General

Evaluate the ecological quality of the hypoxia-stressed Paracas Bay, associated to a eutrophication process, through the integration of environmental, ecological and paleo-ecological approaches, based on benthic foraminifera.

Specific

- Determine the main natural factors that control oxygen regime at different time scales of the bottom water of the Pisco-Paracas coastal area using historical environmental monitoring data (Chapter 2).
- Characterize the benthic foraminiferal assemblages, their spatial and temporal variability, and the abiotic factors that control them in the Pisco-Paracas coastal area, through field surveys and monitoring (Chapters 3 and 4).
- Analyze the historical changes of the preserved assemblages of benthic foraminifera, and their relationship with the variability of sediment geochemistry in the last hundred years, based on the analysis of a sedimentary record from the Paracas Bay. (Chapter 5).

II. CHAPTER 2: Bottom-water hypoxia in the Paracas Bay (Peru, 13.8°S) in seasonal and synoptic time scale variability.

2.1. Introduction

In general, the formation and persistence of coastal hypoxia are related to physical and biogeochemical processes that act as sources or sinks of oxygen. The complexity of these processes and their interactions in the coastal zone make it difficult to identify specific causes of hypoxia. However, in many coastal systems, hypoxia develops seasonally during periods of strong stratification of the water column, resulting from increased insolation and/or freshwater inputs (Fennel and Testa, 2019), and it is becoming more frequent and persistent mainly due to the increasing anthropogenic discharges of nutrients and organic matter in the ocean (Diaz and Rosenberg, 2008; Breitburg *et al*., 2018).

Coastal hypoxia can also occur naturally in the Eastern Boundary Upwelling Systems (EBUS; Helly and Levin, 2004). In these regions, the upwelling dynamics may influence the development of hypoxia and anoxia even in small bays (upwelling bays; Largier, 2020), through its control on the water column stratification and mixing, the productivity and development of algal blooms, and the nearshore advection of the low-oxygen upwelled waters (Pitcher *et al*., 2014).

The Paracas Bay is a small and shallow environment in the Peruvian coast in which the events of bottom hypoxia and anoxia occur mainly during austral summer months (Cabello *et al.,* 2002; Aguirre-Velarde *et al.,* 2019). The processes and control mechanisms of hypoxia in this bay have been little explored, and it has been suggested that potential factors could be the advection of oxygen-depleted upwelled

waters into the bay, the in-situ oxygen depletion following thermohaline stratification, and/or the decay of harmful algal blooms (Pitcher *et al.*, 2021). However, neither the spatiotemporal patterns of hypoxic conditions in the bay and adjacent coastal areas, nor the degree of relationship between hypoxia and physicochemical factors at different time scales, have yet been assessed. In particular, the relative role of the wind forcing variability of the outside upwelling area, and the local area, were not yet compared despite the potential relevance of the wind-driven advection of oxygen-depleted waters, since the upwelling water source is associated with a shallow and intense oxygen minimum zone (OMZ) that impinges the shelf (*e.g.*, Fuenzalida *et al.*, 2009).

Therefore, we aim to explore the development of hypoxic conditions in Paracas Bay, through the following objectives: (1) to describe the temporal and spatial variability of bottom-water hypoxia in the Pisco-Paracas coastal area; and (2) to analyze the association between physical factors (water temperature, river flow, and intensity of winds) and hypoxic conditions in the Paracas Bay across daily to seasonal time-scales.

2.2. Methods

2.2.1. Study area

Since the Pisco-Paracas coastal area is located downstream an upwelling center (Figure 2.1a), its oceanographic regime is influenced by the coastal upwelling variability. During winter, when the alongshore winds and coastal upwelling are prominent, the vertical mixing and intrusion of cold waters characterize the water column of this coastal area; while during summer, when the alongshore winds and

coastal upwelling weaken, the surface temperature increases and water stratification intensifies (Pitcher *et al.*, 2021). In the latter conditions, the Sea Surface Temperature (SST) typically exhibits a spatial distribution with colder waters off the Paracas Peninsula, warmer waters in the northern coast of Pisco, and intermediate values of SST in the Paracas Bay (Figure 2.1a). Furthermore, the highly seasonal freshwater input from the Pisco River, which is discharged 15 km north of the bay mouth, ranges 100 – 150 m^3s^{-1} on average in summer months, peaking occasionally more than 250 m^3s^{-1}, while during the rest of the year it is less than 25 m^3s^{-1} (Cuellar-Martinez *et al*., 2021).

2.2.2. Monitoring design and data sources

The analyzed data come from three different datasets. The first one was obtained by the IMARPE-Pisco Coastal Laboratory ('IMARPE dataset'), containing records of water temperature and dissolved oxygen concentration from the Pisco-Paracas coastal area. These were determined during oceanographic surveys, with a frequency of at least once per month, between 2005 and 2015, according to a sampling stations grid (Figure 2.1). At each station surface and bottom (1 m above seafloor) water samples were collected with Niskin bottles and temperature and oxygen were determined with a mercury thermometer and by the modified Winkler titration method (Strickland and Parsons, 1972), respectively. Moreover, the salinity was measured in water samples since 2010 with a Portasal Salinometer 8410A. The inshore subtidal area was divided in three zones for spatial comparisons, corresponding to groups of nearby monitoring stations with a similar depth range (Table 2.1): the zone off the river mouth or "river mouth" zone (r1 and r2), the bay zone (b1, b2 and b3) and the intermediate zone (i1, i2 and i3), all of

them with a depth range between 8 and 12 m. Additionally, a deep zone was defined (d1, d2 and d3) with a depth range between 25 and 30 m.

The second dataset ('daily dataset') consists of daily records of water temperature and dissolved oxygen in Paracas Bay (p1), surface wind speed at two specific sites (V1 and V2) and Pisco River flows (Figure 2.1), during the 2006 to 2015 period. The p1 site is a nearshore environmental monitoring station of the PLUSPETROL Company, in which surface and bottom (1m above seafloor) water temperature and dissolved oxygen were measured with a portable multiparameter HACH Sension 156. Wind speed data from V1 come from the ASCAT satellite-borne scatterometer at about 10 km off the coastline, and correspond to the intensity of an upwelling-favorable wind (upwelling wind henceforth), since it is almost ever southeasterly (parallel to the coast). Wind speed data from V2 come from the Meteorological Aerodrome Reports (METAR) of the Pisco airport station. Since this station is located less than 1 km from the seashore in a zone with no major orographic feature, wind speed from V2 was considered as a proxy of the local wind intensity in the bay. The river flows were measured at a hydrological station located 60km upstream from the coast (source: National Water Authority, ANA), and were considered as a proxy of the river discharge into the ocean, 15 km north of the bay.

The third set of high-frequency data ('HF dataset') contains hourly records of water temperature and dissolved oxygen at a bay station (p2, Figure 2.1). The surface water temperature was recorded by an autonomous data-logger (HOBO U22-001; Onset Corp., Bourne, MA), while bottom water temperature and oxygen were recorded by a MiniDOT data logger (PME Inc., Vista, CA) deployed near the muddy bottom (20 cm above the sediments), between April 2015 and January 2016.

Hourly records of the zonal and meridional components of the METAR local wind speed (V2), were also available for this period.

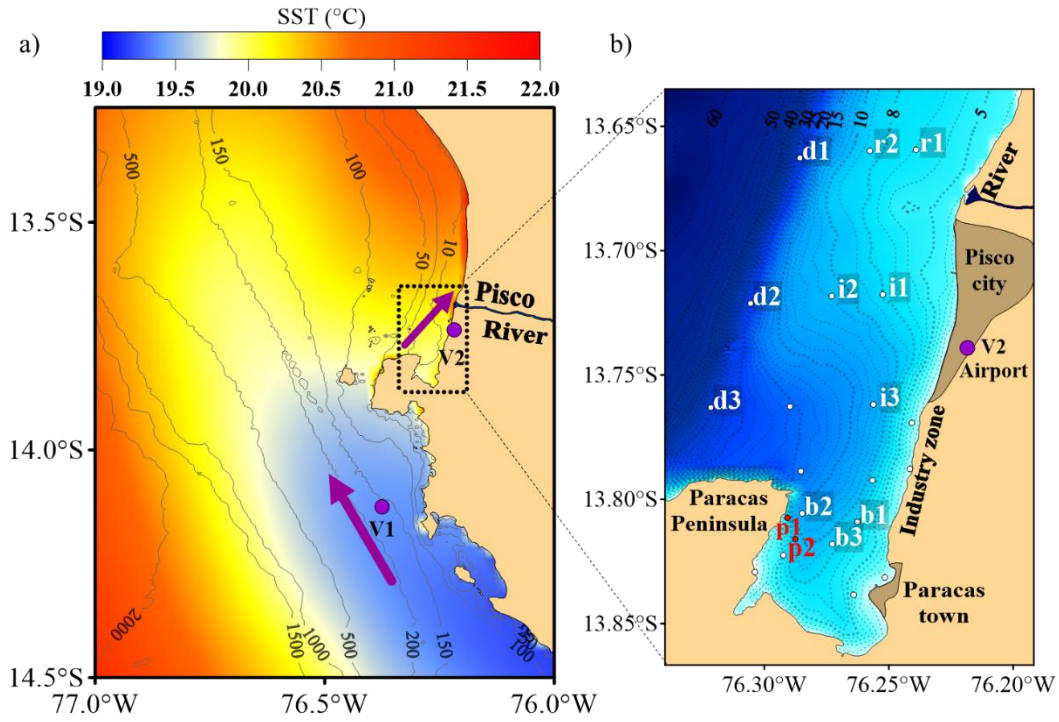

Figure 2.1. Features of the study area. a) Isobathic contours (black lines) are superimposed on the summer distribution (color shading) of SST, adapted from Pitcher *et al.* (2021). The sites of recording satellite wind data (V1) over the upwelling cell, and local wind data (V2) at the Pisco airport, are shown with their predominant directions in purple arrows. b) The Pisco-Paracas coastal area including a bathymetry (color shading and dashed lines). IMARPE monitoring stations are plotted as white dots and some were grouped in 4 sub-areas: the deep zone (d1, d2 and d3), river mouth zone (r1 and r2), intermediate zone (i1, i2 and i3), and bay zone (b1, b2, b3). The other monitoring stations (p1 and p2) are shown in red.

Table 2.1. Characteristics of the monitoring sites in the Pisco-Paracas coastal area. The “river mouth” zone corresponds to the marine area off the river mouth.

Site	Zone	Frequency	Longitude	Latitude	Depth (m)
r1	River mouth	Once to four times per month	-13.65939	-76.23906	8
r2			-13.65986	-76.25758	10
i1	Intermediate		-13.71761	-76.25242	9
i2			-13.71825	-76.27292	12
i3			-13.76189	-76.25617	12
b1	Bay		-13.80911	-76.26258	9
b2			-13.80569	-76.28483	12
b3			-13.81803	-76.27272	8
d1	Deep		-13.66269	-76.28572	25
d2			-13.72122	-76.30556	26
d3			-13.76308	-76.32156	30
p1	Bay	Daily	-13.80811	-76.29289	6
V1	-	Daily	-14.12500	-76.37500	-
p2	Bay	Hourly	-13.81447	-76.28731	9
V2	-	Hourly	-13.73651	-76.21787	-

2.2.3. Data processing

2.2.2.1. Hypoxia and its spatiotemporal variability

The value of 1.4 mL L^{-1} of the bottom-water dissolved oxygen (BWDO) was considered as the upper threshold for hypoxic conditions and the lower one for normoxic conditions (Rabalais *et al.,* 2010). The BWDO levels under 0.5 mL L^{-1} were further considered as severe hypoxic conditions since they are more

characteristic of the offshore OMZ (Chan *et al.*, 2008). The spatiotemporal differences in the BWDO were first explored through maps of their average distribution in the study area in summer and winter, elaborated from all the available bottom water measurements of the IMARPE dataset, after applying a kriging method for spatial interpolation using the Golden Surfer 15 software. Then, the BWDO annual cycles were computed for the grouped monitoring stations in each defined zone.

The normoxic, hypoxic and severe bottom hypoxic conditions in the sediment-overlying waters of the bay (p2, HF dataset), in the April 2015 - January 2016 period, were characterized in duration and compared by seasons.

2.2.2.2. Physical factors and relationships

A depth-normalized index of stratification was calculated for comparing among stations of different depth, only with the IMARPE dataset. According to Li (2002), the stratification index is equal to $\Delta\sigma$ /Δdepth; where $\Delta\sigma$ is the difference in seawater density between surface and bottom calculated from temperature and salinity records, and Δdepth is the depth difference. On the other datasets of water-column single station monitoring (p1 or p2), the temperature difference between surface and bottom waters (ΔT) was calculated and used as a stratification proxy for temporal comparisons, since ΔT was linearly well associated with $\Delta\sigma$ (Figure A.A1).

The average annual cycle (for the 2006-2015 period) of the Pisco River runoff and of the speed of winds were compared with the average annual cycle of ΔT and BWDO in the bay (p1), based on the daily dataset. Missing values of the time series

were filled with linear interpolation in order to calculate daily anomalies of all these variables, as the result of subtracting the loess-smoothed average annual cycles from their actual daily values. Wavelets analyses (averaged power) and cross-correlations were applied to these anomalies, using the R software (R Core Team, 2020), in order to explore their non-seasonal variability and their relationships, respectively.

The hourly time series of the HF dataset were shown together in order to compare their intra-seasonal variability and to analyze their relationships. Thus, the associations of the zonal and meridional components of the local wind speed with ΔT and BWDO of the bay (p2) were assessed by means of cross-correlations, after applying a centered moving average (n = 25) in the time series, in order to avoid correlations related to the diurnal cycle.

2.3. Results

2.4.1. Spatiotemporal variability of BWDO and stratification

The spatial distribution of the average BWDO, for the 2005-2015 period, indicated that bottom hypoxic levels (<1.4 mL L^{-1}) were present in the study area in both summer and winter seasons. Hypoxia was typically found deeper than 15 m in winter, but it had a wider distribution in summer reaching shallower depths (Figure 2.2a). The BWDO distribution resembles the bathymetry, so that the hypoxic levels are projected towards the central area of the bay, whereas normoxic levels (>1.4 mL L^{-1}) appear to be usually restricted to depths shallower than 8 m (b3 station depth).

The spatial distribution of the average SST exhibited warmer surface waters (about 20 to 24 °C) in summer, especially on the north and east sides, whereas colder waters (about 16 to 18 °C) in winter (Figure 2.2b). Although SST was more spatially homogenous in the latter, the west side of the study area were notoriously characterized by colder surface waters in both seasons. Similar distribution was observed for the average stratification index, with greater spatial differences (0.04 to 0.33 σ unit.m^{-1}) in summer than in winter (0.01 to 0.05 σ unit.m^{-1}).

The BWDO data grouped in the four defined zones revealed that hypoxic conditions are less frequent in the river mouth zone, whereas more frequent in the bay, and almost permanent in the deep zone (Figure 2.3a). On the other hand, the stratification index in the four zones revealed that strong stratified conditions are more frequent in the river mouth zone than in the intermediate zone and the bay, whereas the deep zone is better mixed (Figure 2.3b).

Annual cycles also showed that seasonality in the bay is actually characterized by two long and contrasting seasons: December to April (late spring – summer – early autumn) and June to September (late autumn – winter – early spring). Based on bay zone records only, hypoxia (<1.4 mL L^{-1}), and even severe hypoxia (<0.5 mL L^{-1}), occurred in both of them (Figure 2.4). Although hypoxia was much more frequent (>90%) in the December-April season, it also occurred in more than half of the records of the June-September season (Figure 2.4a). At first glance in the scatter plot of BWDO vs stratification, a seasonal inverse association is not clear at all (Figure 2.4b). The grouping of data towards the origin of axes rather showed that hypoxia occurred mostly under non stratified conditions.

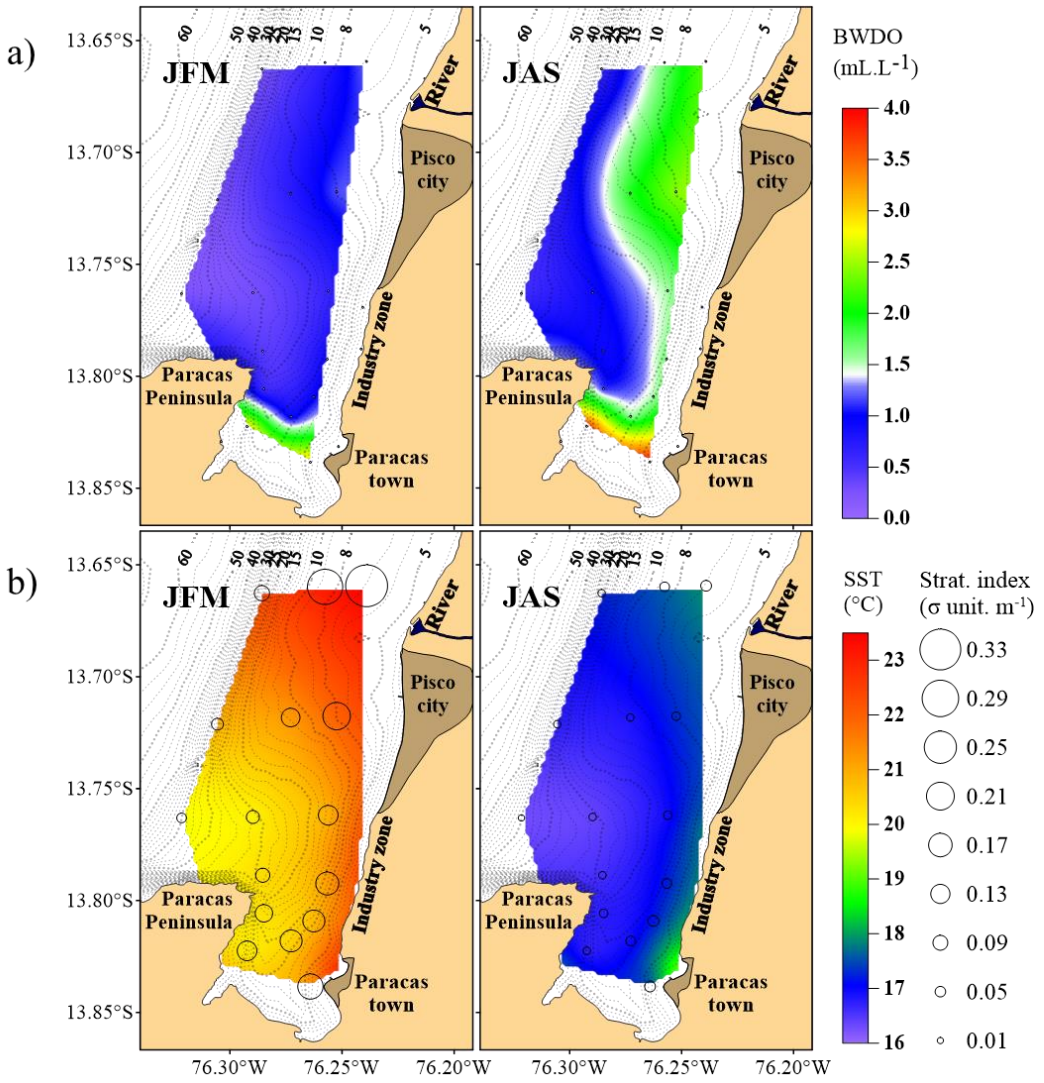

Figure 2.2. Average spatial distribution of water variables superimposed on isobaths (black contours) in austral summer (JFM) and winter (JAS), derived from the monitoring stations of IMARPE database. a) Bottom-water dissolved oxygen (BWDO) in color, with hypoxic threshold (1.4 mL L^{-1}) in white. b) Sea surface temperature (SST, °C) in color, and stratification index in bubbles at monitoring stations (additional stations for SST).

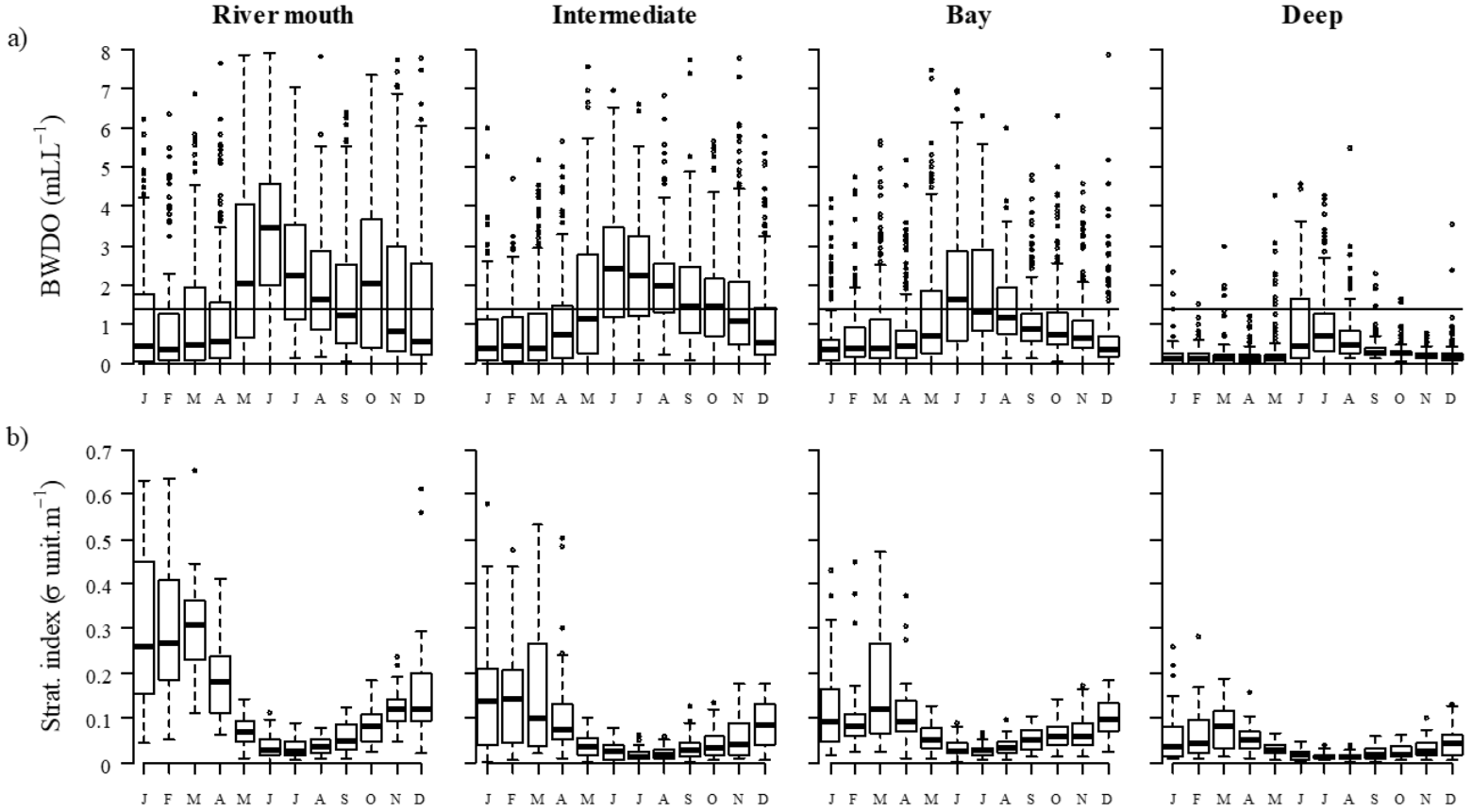

Figure 2.3. Annual cycles of the BWDO (a) and the stratification index (b), for each defined zone derived from the IMARPE-Pisco monitoring stations: the river mouth zone and the intermediate, bay and deep zones. Horizontal lines in (a) indicate the boundary for hypoxic (<1.4 mL L^{-1}) conditions.

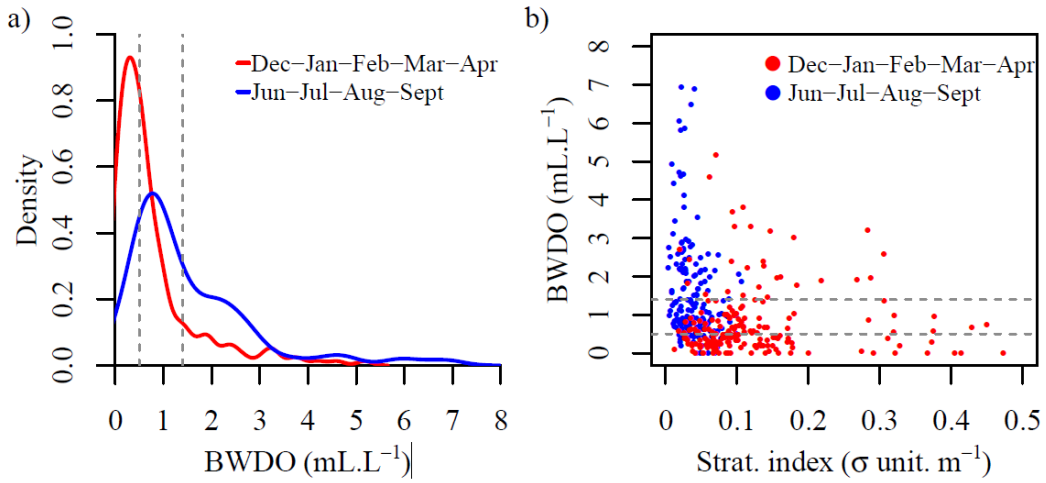

Figure 2.4. Distribution of BWDO data from Paracas Bay for the December-April (n = 271) and June-September (n = 229) seasons. (a) Probability density functions of BWDO of each season. (b) Scatter plot of BWDO vs stratification index, exhibiting data mainly grouped near the origin of axes. Dashed lines indicate the boundaries for hypoxic (<1.4 mL L^{-1}) and severe hypoxic (<0.5 mL L^{-1}) levels.

2.4.2. The BWDO and physical factors at different time scales

Average annual cycles of the daily dataset's variables showed that stratification and hypoxia intensify in the bay in the season of weaker upwelling wind and stronger local wind, as well as with higher Pisco River flows; whereas water mixing and oxygenation increase in the season of stronger upwelling wind, weaker local wind and lower river flows (Figure 2.5). Moreover, local wind and upwelling wind exhibited almost opposite seasonal cycles, with the latter exhibiting a much greater amplitude of variation.

The daily anomalies of these variables showed modes of significant and intense non-seasonal variability mainly at a synoptic time scale (from few to several days), and secondarily at an interannual scale (>400 days, Figure 2.6 f-j). Thus, the BWDO fluctuated intensely in 3-8 days, ΔT in 2-4 days, local wind in 3-5 days, and the upwelling wind in 4-10 days. Instead, the river flows fluctuated mostly on the scale of 1-8 weeks.

In addition, the BWDO anomalies in the bay revealed interannual periods of predominant oxygenation (positive values during 2008-2010) and predominant deoxygenation (negative values during 2011-2014), which coincided with less stratification (negative values of ΔT) and more stratification (positive values) during the same periods, respectively (Figure 2.6 a-b). Moreover, the trend of increasing stratification along the 2006-2015 period was opposed to a trend of decreasing upwelling winds in the same period (Figure 2.6 b, d).

The significant cross-correlations of the daily anomalies (Figure A.A2) revealed that despite the opposite seasonal patterns in the intensity of the two winds, their daily anomalies correlate directly ($r = 0.38$), with the upwelling wind 1-day lagged behind local wind. The anomalies of ΔT, as well as those of each the surface and bottom water temperatures, were negatively correlated with the anomalies of the upwelling wind ($r = -0.19$) and of the local wind ($r = -0.17$), with about 1 or 2-day lag. The anomalies of BWDO were negatively correlated, 1-day lagged, with those of the upwelling wind ($r = -0.10$) and local wind ($r = -0.20$), but also with ΔT ($r = -0.17$) with no time-lag. And finally, the river flow was very weakly correlated with BWDO and ΔT ($|r| < 0.10$) (Figure A.A2).

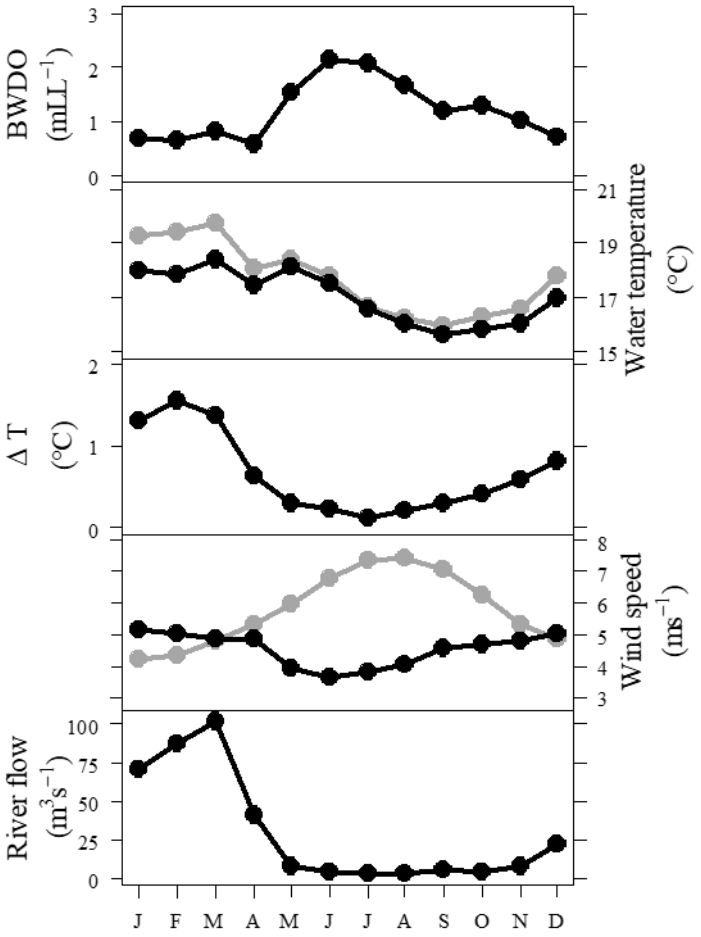

Figure 2.5. Average annual cycles based on data of the 2006-2015 period, of the (a) BWDO, the (b) water column temperatures (surface in gray and bottom in black), and (c) ΔT, of the Paracas Bay compared to the (d) upwelling wind (gray) and local wind (black) speeds, and the (e) Pisco River runoff.

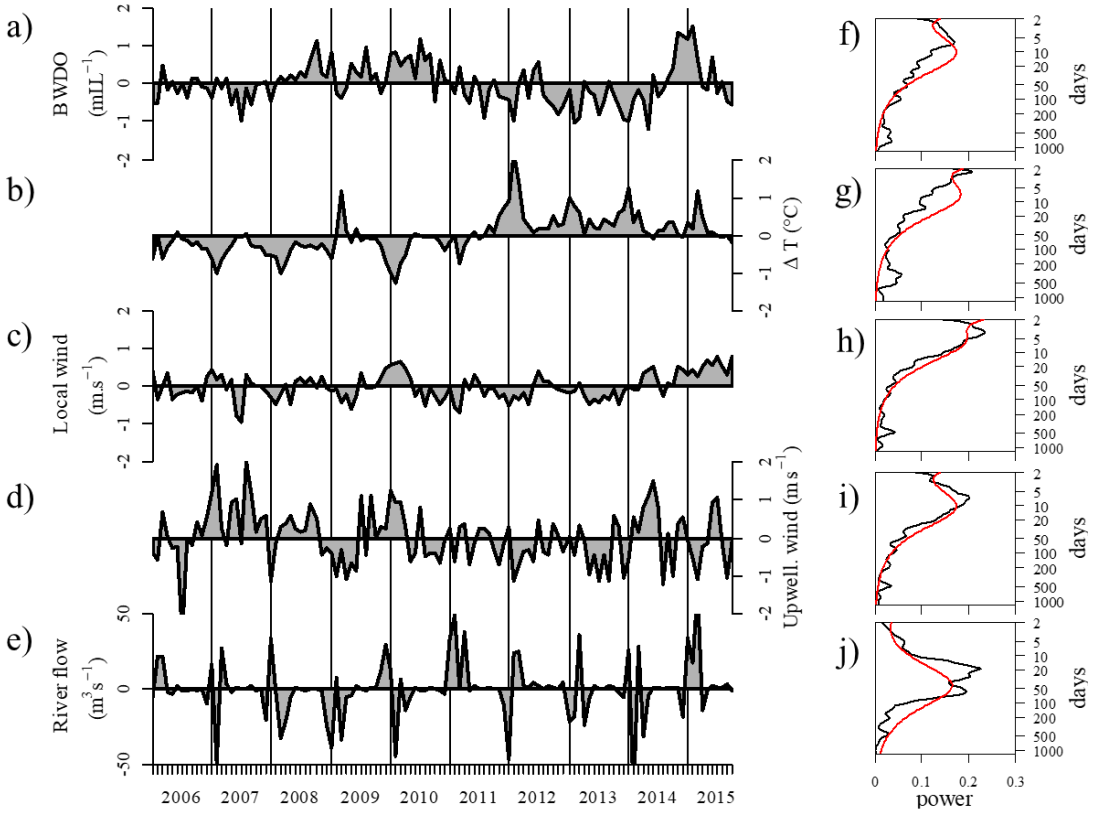

Figure 2.6. Non-seasonal variability of the BWDO, ΔT, local and upwelling winds, and river flow from the 2006-2015 period. Anomalies of the variables shown at a monthly-averaged scale in order to facilitate the observation of interannual changes (a-e), with vertical lines pointing out January of each year. The wavelets average power of daily anomalies of each variable (f-j), exhibiting peaks of significant variability at synoptic and interannual time scales, above the noise spectrum in red.

2.4.3. Analysis of hourly time series

The local wind speed (in the March 2015 – January 2016 period) exhibited a meridional component (V) with larger variability than the zonal component (U). The patterns of changing of these components were compared with those of temperatures and BWDO of sediment-overlying waters at p2 in the bay (Figure 2.7). Since the December-April season was not totally covered by this period, the available intervals March-April (i) and December-January (ii) were considered for comparing with the June-September season.

Bottom hypoxia was the predominant condition in the entire period. In the June-September season, the normoxic conditions were just intermittent, lasting up to 7 days maximum (Table 2.2), and the surface and bottom water temperatures steadily decreased (Figure 2.7c), with low values of ΔT. On the other hand, the meridional wind and water temperatures exhibited greater fluctuations during the December-April season (i and ii), whereas BWDO exhibited low variability. Yet, there were persistent and severe hypoxic conditions in this season, which were only interrupted by episodes of oxygenation of up to 2 days maximum (Table 2.2) that started simultaneously with longer lasting warming events (Figure 2.7 c-d).

The cross-correlations of the meridional wind speed with the water temperature, ΔT and BWDO were stronger, and negative, in the December-April season with about 24 hours of time-lag (Figure A.A3). Thus, the oxygenation episodes and warming events occurred one day after the relaxation of this local wind component. During most of the warming events in that season, ΔT increased due to a more intense warming of the surface relative to the bottom (Figure 2.7c). Then, BWDO and ΔT

were lag-0 positive correlated (Figure A.A3) due to their simultaneous increasing, but they tended to be negative correlated after 48-72 hours (time-lag) due to the drop of BWDO levels into hypoxia again (Figure 2.7d).

Table 2.2. Duration in hours of the normoxic, hypoxic and severe hypoxic conditions (and their percentage) in each defined period at p2 in Paracas Bay, March 2015 – January 2016. *Maximum number of consecutive days under normoxia.

Condition	Mar-Apr (i)	Jun-Sep	Dec-Jan (ii)
Normoxia	49 h (6.4%)	631 h (21.5%)	12 h (1.4%)
(>1.4mL L^{-1})	2*	7*	0.5*
Hypoxia	719 h (93.6%)	2297 h (78.5%)	948 h (98.6%)
(<1.4 mL L^{-1})			
Severe hypoxia	652 h (84.9%)	1335 h (45.6%)	929 h (96.8%)
(<0.5 mL L^{-1})			

Figure 2.7. Hourly time series of the local wind speed compared to the records of

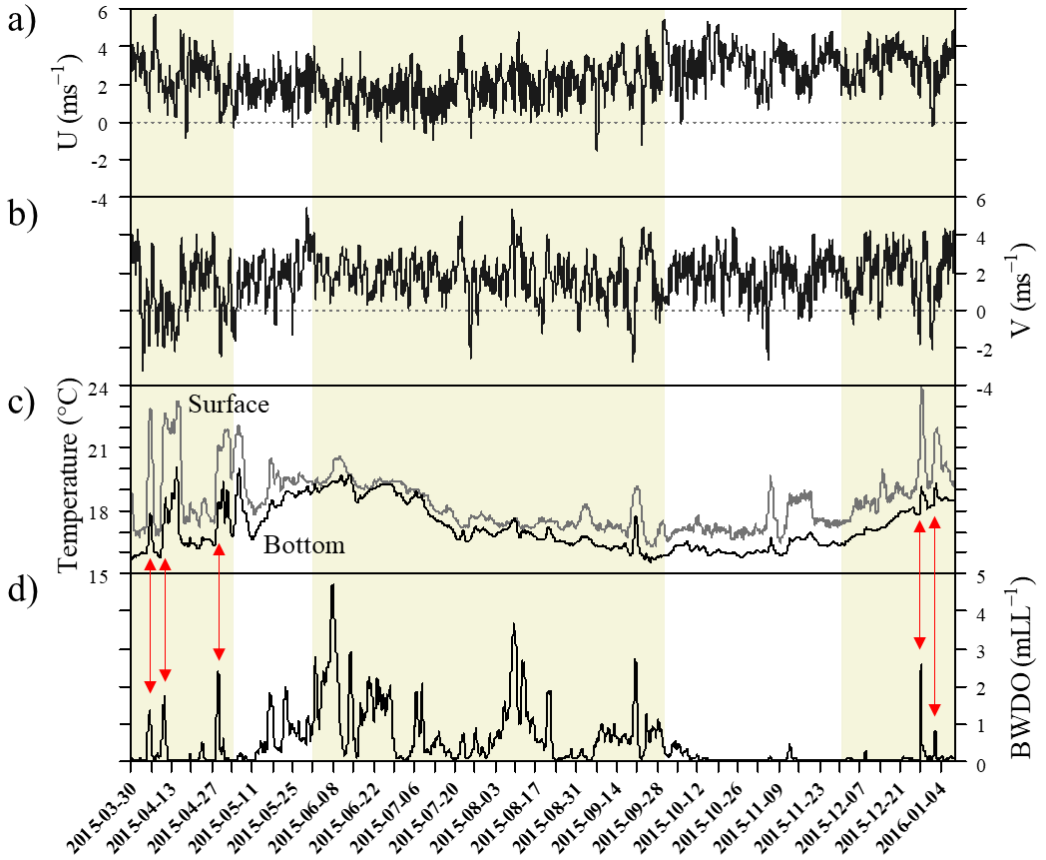

the p2 monitoring station in Paracas Bay. The zonal (a) and meridional (b) components of the wind speed. The surface and bottom water temperature, in gray and black respectively (c), and BWDO (d), in the bay. Shaded areas correspond to March-April 2015, June-September 2015 and December 2015-January 2016 periods. Red arrows point out the simultaneity of, more notorious, warming/stratification onsets and oxygenation episodes of the December-April season.

2.4. Discussion

2.4.1. General features of hypoxia on inshore bottom areas

By linking together data from different environmental monitoring programs, this study allowed us to identify the spatiotemporal patterns of the bottom water hypoxia of the Pisco-Paracas coastal area. For instance, the deeper bottom waters (25-30 m) undergo severe hypoxic conditions (<0.5 mL L^{-1}) almost permanently, only interrupted in winter months (Figure 2.3a). It is likely that this "deep zone" is mostly beneath the oxycline as a result of the shoaling of the OMZ upper boundary, which occurs off the central Peruvian coast (Paulmier and Ruiz-Pino 2009; Bertrand *et al.*, 2010), reaching up to depths of about 10 m during the spring-summer-autumn, and down to about 50 m in winter (Gutiérrez *et al.*, 2008; Graco *et al.*, 2017).

The higher frequency of bottom hypoxia (<1.4 mL L^{-1}) in the Paracas Bay than in the other shallow zones (Figure 2.3a), along with its detection in more than half of the records, even under mixed water column conditions during the June-September period (Figure 2.4, Table 2.2), points out that bottom hypoxia is a persistent feature of the bay and not just a seasonal phenomenon that develops under stratified conditions. Furthermore, the Paracas Bay (between 8 and 12 m depth) appears to be the shallowest environment in which a persistent hypoxic regime was recorded, as other embayments of the Peruvian central coast exhibited similar conditions in more than 15 m depth (Tarazona *et al.*, 1988; Tarazona and Arntz, 2001). In fact, the well-oxygenated benthic conditions in the Peruvian Upwelling System are known to characterize narrow inshore areas (Arntz *et al.*, 2006), which were observed only in sites shallower than 5 m depth in our data (not shown).

2.4.2. Water stratification variability in Paracas Bay

The analysis of the time series showed the high variability in water temperature and dissolved oxygen in the bay. Aguirre-Velarde *et al.* (2019) have already described these variations during summer months, after recording temperature fluctuations (up to ~10°C) in a matter of hours, which were inversely correlated to salinity fluctuations (up to ~2.0), and suggested that changes in water masses entering the bay are responsible of that variability. These authors also reported stratified conditions as frequent events (usually of 3-4 days long) of strong vertical differences in seawater density, associated with the coupled temperature and salinity fluctuations. Such events correspond to the significant variability that we identified using ΔT daily anomalies (Figure 2.6 g). Other similar short-duration events have been reported in shallow estuaries, where stratification is tightly coupled with variations in the freshwater discharge and wind stress (Stanley and Nixon, 1992; Ni *et al.*, 2016). Nevertheless, the short-term variability of the Pisco River flow and stratification in Paracas Bay were weakly associated (Figure 2.6 g-j, Figure A.A2), which indicates that rather than being modulated by the freshwater discharge variability, the intrusions of the river plume into the bay are linked to the patterns of wind-driven water circulation (Arellano *et al.*, 2023).

2.4.3. The winds and their control on the bay dynamics

The difference in the predominant direction of the local and upwelling winds, and the inverse annual cycles of their intensities, are features previously described in other coastal areas of the south-eastern Pacific, and associated to the effects of temperature contrast between the desert and sea, and the topography of coastal

headlands, on the local wind (Pizarro *et al.*, 1994). It has been shown that the weaker local wind relaxes 1 or 2 days prior to the upwelling-favorable wind in Bodega Bay, a small upwelling bay of the California EBUS (Roughan *et al*., 2005). This feature might also apply in Paracas Bay, accounting for the 1-day lag between them observed in this study. Furthermore, the significant cross-correlations of the winds speed with water temperature, ΔT and BWDO of Paracas Bay, indicate that the bay hydrodynamics is mainly associated with the winds' variability. This was already suggested to occur in the 'upwelling bays' of the EBUS, therefore exhibiting fluctuations at a synoptic time scale in their circulation, stratification and water properties (Largier, 2020).

Because of their permanent upwelling-favorable direction, the winds south of the Paracas Peninsula support a year-round active upwelling cell (Gutiérrez *et al*., 2011, 2016). For the June-September season of stronger upwelling winds, a persistent shoreward advection of atmospheric momentum was described as occurring just north of the peninsula (Chamorro *et al*., 2021), and a persistent wind-driven water inflow rounding the peninsula was described by modelling studies (Carbonel, 2013; Arellano *et al*., 2023). These suggest that upwelling waters are also frequently advected shoreward, explaining the negative correlations of daily anomalies of the upwelling wind speed with temperature, as well as with ΔT and BWDO, of Paracas Bay (Figure A.A2), and also explaining the usual presence of cooler waters around the peninsula (Figure 2.2a). Therefore, the circulation and physicochemical properties of the bay would be driven by upwelling winds variability, especially during the season of lower local wind speed and Pisco River flows (June-September, Figure 2.5).

The stronger association of the (meridional component) local wind speed with water temperature and oxygen during December-April indicates the relevance of local wind in modulating the bay circulation and water stratification during that season. In fact, Aguirre-Velarde *et al.* (2019) already proposed that the local wind drives the circulation in Paracas Bay in summer months, allowing the entrance of cold waters when the meridional wind is positively active, and warmer and less saline waters when it relaxes. The negative correlations of local wind speed with bottom temperature, as well as with ΔT and BWDO, suggest that rather than just producing vertical mixing, a positive meridional wind would lead to a bottom-water inflow of cold, and hypoxic, upwelling deeper waters. On the other hand, the relaxation or reversal of this wind component would lead to the southward inflow of the warmer, less saline and more oxygenated, waters from the river mouth zone. Similar cases of local wind influence on the circulation and subsurface water flux were described for other bays in EBUS (Largier, 2020). Our interpretation is also consistent with a high-resolution numerical model of the water circulation in the bay (Arellano *et al.*, 2023).

2.4.4. Drivers and sources of the hypoxic regime

The analysis of the BWDO temporal variability in the bay and its association with that of the physical factors at synoptic, seasonal and interannual time scales, allowed us to propose that both the local and offshore upwelling winds are significant drivers of hypoxia. As discussed above, the persistent hypoxic conditions in bottom waters (8 - 12 m) of Paracas Bay are likely a consequence of the persistent upwelling waters inflow from the deeper and more hypoxic zone,

which is driven by the upwelling wind mainly during June-September and by the local wind mostly during December-April.

The presence of the oxycline overlying the bottom in the 'deep zone' determines a hypoxic water source just adjacent to the bay. However, the alternation of hypoxic and normoxic conditions during June-September would be related to the variations of the oxygen content of the incoming upwelling waters due to the deepening of the oxycline in that season, *i.e.*, a deeper mixed layer (Thomsen *et al.,* 2016; Graco *et al.,* 2017). Additionally, since the interannual variability of El Niño Southern Oscillation (ENSO) affects the depth of the OMZ upper boundary (oxycline) in the Peruvian coastal zone (Espinoza-Morriberón *et al.,* 2019), this might also lead to interannual changes of the BWDO levels in the bay. Thus, predominant local El Niño conditions in the period 2008-2010, and La Niña conditions in the period 2011-2014, as inferred from thermal indexes of ENSO in the Peruvian coast (Quispe-Ccalluari *et al.,* 2018), resulted in more oxygenated and hypoxic periods in the bay, respectively (Figure 2.6a).

The simultaneous onset of the strong stratification/warming events and oxygenation episodes in the bay, in the December-April season, would originate from the inflow of the northern (warmer and less hypoxic) waters when the meridional component of local wind relaxes or reverses. Although this seems to contradict the role of strong stratification on hypoxic or anoxic events at a synoptic time-scale, the stratification persistence for a few more days could be a cause for the oxygen depletion due to the stimulated microbial respiration at the bottom. The 3-day lag of the inverse correlation between hourly time series of ΔT and BWDO (Figure

A.A3) suggests the time scale in which strong stratification generates hypoxic conditions.

As it was observed between October and early December of 2015 (Figure 2.7d), severe oxygen depletion can also occur without strong stratified conditions in the sediment-overlying waters. Since the bay is characterized by containing muddy sediments subjected to large organic matter fluxes (Velazco and Solís, 2000), in a region that is highly productive almost all year round except for winter months (Gutiérrez *et al.*, 2016), it is likely that the sediment oxygen demand is strong enough to maintain severe hypoxic conditions just over the sediment-water interface. Furthermore, although organic pollution decreased in the study area since 2004 (Pitcher *et al.*, 2021), its effects on the current organic content of sediments and the associated oxygen demand need further study.

The formation and subsequent decaying harmful algal blooms, which are more frequent in the bay from November to May (Cabello *et al.*, 2002; Sánchez *et al.*, 2019; Pitcher *et al.*, 2021), are favored by stratified conditions and thus might contribute to the oxygen depletion as an input of labile organic matter. In fact, widespread anoxic conditions were reported in the bay during an intense stratification event in mid-March 2015, with surface temperatures of up to 26°C, and associated to a succession of dinoflagellate blooms of *Prorocentrum cordatum* and *Akashiwo sanguinea* (IMARPE, 2015).

2.5. Conclusions

The bottom waters deeper than 8 m in the Paracas Bay are hypoxic most of the time, even under conditions of predominant vertical mixing of the water column. Their seasonal differences are characterized by the severity of the hypoxic regime, with predominant severe hypoxia during December-April but frequent and intermittent hypoxia during June-September. This seasonal pattern is associated with seasonal changes in the depth position of the adjacent OMZ, and the subsequent oxygen content of incoming upwelling waters, as well as with the seasonal intensification of the upwelling-favorable and local winds that drive the hydrodynamics of the bay.

The synoptic time-scale fluctuations of winds modulate the intra-seasonal variability of hypoxia in the bay. While fluctuations of upwelling-favorable winds during June-September drive the inshore expansion of mixed and less hypoxic upwelling waters, the fluctuations of local winds during December-April drive the entrance and circulation of more hypoxic upwelling waters in the bay. Thus, the positive intensification of local meridional component leads to the entrance of deep, cold and hypoxic upwelling waters, whereas its relaxation or reversal events lead to the entrance of warmer and more oxygenated waters from the northern zones.

Strong stratified conditions develop after the reversal events of meridional wind component in the December-April season only, and their extension for several days contribute to amplify the oxygen depletion and the persistence of bottom hypoxia or occurrence of anoxia.

III. CHAPTER 3: Characterization of the living assemblage of benthic foraminifera in the Pisco-Paracas coastal area.

3.1. Introduction

The Peruvian Coastal Upwelling System is the marine region of highest primary productivity of the Pacific Ocean (Pennington *et al*., 2006), which is sustained by persistent upwelling-favorable winds throughout the year (Bakun and Weeks, 2008; Gutiérrez *et al*., 2016). As a result, the Oxygen Minimum Zone (OMZ) of the southeastern Pacific is particularly intense and shallow in the subsurface coastal waters off Peru, and impinges the seafloor from depths about 50 m down to 600 m, with an oxycline (the upper boundary of OMZ) that seasonally reaches depths up to 20 m in the nearshore coastal areas (Gutiérrez *et al*., 2008; Graco *et al*., 2017).

The nearshore environments in upwelling systems exhibit characteristic physicochemical patterns and processes primarily driven by their interaction with the open ocean (*e.g.*, 'upwelling bays'; Largier, 2020). Thus, even the small bays of the southcentral Peruvian coast are influenced by coastal upwelling, which delivers waters that are not only relatively cold and nutrient-rich, but also frequently hypoxic (Tarazona *et al*., 2003) and with low pH (<7.75, Hernandez-Ayon *et al*., 2019). The oxygen concentration near the bottom of these bays varies according to the degree of coastal exposure and the local water circulation, being higher when currents are stronger such as in Independencia Bay, and reduced when there is stagnation such as in Ancon Bay (Tarazona *et al*., 1991). However, the patterns of other water properties, such as pH, in the nearshore environments are poorly known.

The benthic fauna from nearshore environments were described as controlled by the type of the bottom substrate, the interaction with the open ocean, and the anthropogenic activities affecting the ecosystem integrity (Tarazona *et al*., 2003). The benthic foraminifera, shell-bearing protists that are trophic links between phytodetritus and metazoans (Nomaki *et al*., 2008), are one of the major dominant groups of the benthic biota from the oxygen-deficient Peruvian upper continental margin (Levin *et al*., 2002). The species composition of benthic foraminifera living in sediments of upper continental shelf and nearshore bottoms of the upwelling-influenced Peruvian central coast are characterized by the dominance of a small number of calcareous species (Cardich *et al.*, 2012; Merma-Mora, 2020; Romero, 2021).

However, the effects of small-scale environmental gradients on the distribution of the foraminiferal species in an upwelling-influenced nearshore environment such as the Pisco-Paracas coastal area, are yet unexplored. Therefore, this study aimed to (1) compare the spatiotemporal variability of the subtidal benthic environment in the Paracas Bay and the adjacent Pisco coastal zones, and (2) evaluate the living benthic foraminiferal assemblage and the main environmental factors that produce variations in its structure.

3.2. Methods

3.2.1. Historical data of bottom water conditions

We used historical monitoring data (of the period 2010-2015) of bottom water temperature (BWT), salinity (BWS), dissolved oxygen (BWDO), and pH (BWpH); recorded in the Pisco-Paracas coastal area, twice a month, by the monitoring

program of the Peruvian Marine Research Institute (IMARPE). In order to determine the average spatial and temporal variability, the monitoring stations distributed in this coastal area (Figure 1b) were grouped into four zones: the bay (1, 2, and 3), deep (4 and 5), east (6 and 7), and north (8 and 9) (Table 3.1).

Table 3.1. Characteristics of the stations of the study area.

Station	Latitude	Longitude	Depth (m)	Zone	Zone color	Substrate
1	13.848667	76.271806	6.0	Paracas Bay	Red	Mud
2	13.833111	76.279500	8.0	Paracas Bay	Red	Mud
3	13.814472	76.287306	9.5	Paracas Bay	Red	Mud
4	13.788177	76.284591	19.0	Central Deep	Orange	Mud
5	13.761680	76.289665	20.5	Central Deep	Orange	Mud
6	13.791560	76.256685	10.0	Central East	Blue	Mud
7	13.761116	76.256403	12.5	Central East	Blue	Mud
8	13.716860	76.272188	10.5	North	Brown	Mud
9	13.659637	76.258094	9.5	North	Brown	Mud

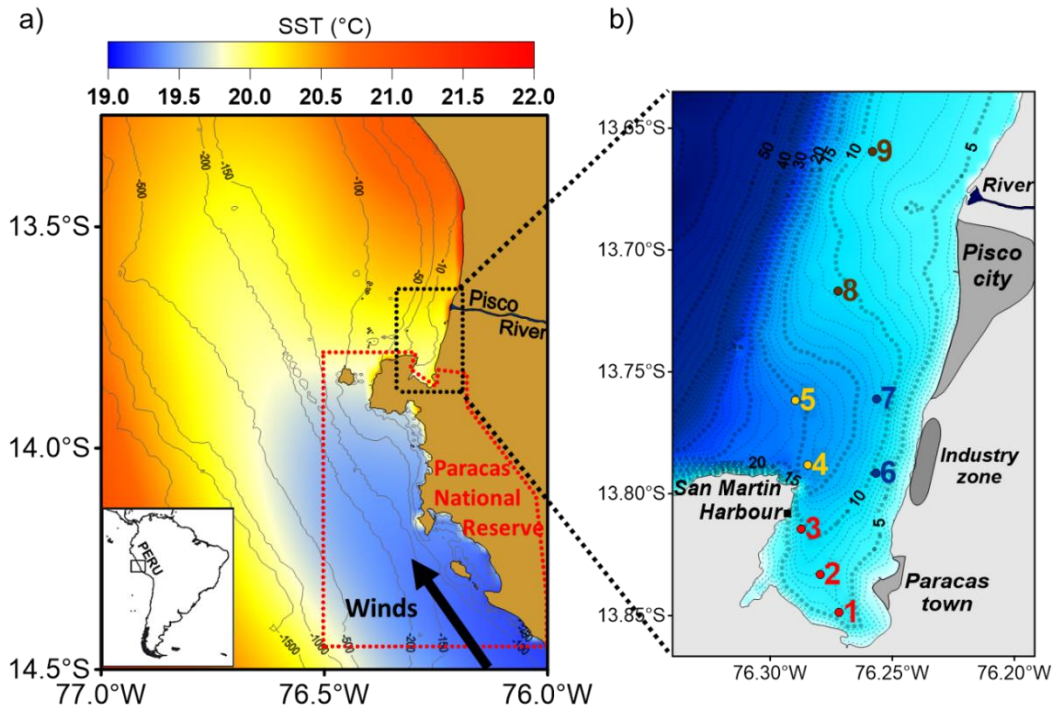

Figure 3.1. Environmental context of the study sites. a) Average distribution in summer of Sea Surface Temperature (SST) in the Pisco province, with the extension of the upwelling center in the southern area. b) The Pisco-Paracas coastal area and the bathymetry, with sampling stations in colors corresponding to the bay (red), deep (orange), east (blue), and north (brown) zones.

3.2.2. Field sampling and *in situ* measurements

Three field surveys were conducted for sampling bottom waters and sediments in the stations of the monitoring program: in November 2014, March 2015 and July 2015. Additionally, station 3 was chosen for conducting single-site monthly monitoring, throughout the period November 2014 – July 2015, of the geochemical and benthic foraminiferal dynamics in Paracas Bay.

3.2.2.1. Bottom water sampling and *in situ* determinations

On board a small artisanal fishing boat (approx. 6 m length), water samples were collected at each station from c.a. 1 m above the bottom using Niskin bottles for determination of temperature using a mercury thermometer, dissolved oxygen by a modified Winkler titration method (Strickland and Parsons, 1972), and pH by using a METTLER TOLEDO combined pH sensor, SEVEN MULTI model. Water subsamples of 200 mL were set aside and cold stored for determining the salinity and concentrations of nitrates and phosphates in the laboratory.

3.2.2.2. Sediment sampling and preservation

Two replicates of sediment samples were collected at each station using a HAPS bottom corer since it is appropriate for collecting undisturbed sediments (Kanneworff and Nicolaisen, 1972). The surface sediments were sliced (1 cm thick top) and preserved in plastic jars with a Rose Bengal solution (2g/L Methyl alcohol 70%) for staining the foraminiferal cytoplasm of living specimens, recommended as a standardized protocol (Schönfeld *et al*., 2012). Additional sediment samples were collected with a 0.05 m^2 Van Veen grab for analyses of texture and organic matter content.

In the monthly monitoring at station 3, sediment samples were collected manually by SCUBA diving using acrylic tubes (inner diameter 6.5 cm) which had pre-drilled holes for pore water extraction. Two sediment cores were sliced (1 cm thick) down to the first 2 cm of sediment depth for approaching the total standing stock of benthic foraminifera, since they live mostly in the top 2 cm of surface sediments in the Paracas Bay (Merma-Mora, 2020), and were preserved with Rose Bengal solution. A third sediment core was similarly sliced and then frozen for

determinations of sedimentary total organic carbon (TOC) and nitrogen (NT). Other two sediment cores were used for extracting pore water of the 0-2 cm sediment depth interval using syringes of 20 mL and rhizons (Seeberg-Elverfeldt *et al*., 2005). For free sulfides determination, pore water subsamples of 1.5 mL were immediately fixed with 0.5 mL of a 5% Zinc acetate solution for preventing oxidation and stored in plastic vials at 4°C, whereas the remaining volumes were used to measure pore water pH with the same pH sensor of bottom water samples.

3.2.3. Laboratory analyses

3.2.3.1. Chemical and geochemical determinations

Salinity was determined by a Portasal Wildline 8410 salinometer, whereas nitrates and phosphates concentrations, by the UV-visible spectrophotometric technique (Strickland and Parsons, 1972) with a Perkin Elmer LAMBDA 45 spectrophotometer. The sand, silt, and clay contents were determined through standard sieving of dry sediment samples (Ingram, 1971) and the pipette method (Galehouse, 1971). The total organic matter of sediments was determined by the loss of ignition (LOI) method (Dean, 1974). The content of total phytopigments (Chlorophyll a + Phaeopigments) in sediments, or phytodetritus quantity, termed as Chloroplastic Pigment Equivalents (CPE, Koho *et al*., 2008) was fluorometrically analyzed by using a method of double extraction with 90% acetone and fluorescent readings as detailed in Gutiérrez *et al*., (2000). The ratio of its components (C:P = Chlorophyll a / Phaeopigments) was used as an indicator of phytodetritus quality (Koho *et al*., 2008).

Concentrations of the dissolved hydrogen sulfide (H_2S) of pore waters were determined according to a standard methylene blue spectrophotometric method (Cline, 1969; Gieskes *et al*., 1991). The content in sediments of total organic carbon and total nitrogen were determined through oxidative decomposition, and corrected for carbonate content, by using a Perkin-Elmer Series II 2400 CHN Elemental Analyzer.

3.2.3.2. Foraminiferal analysis

After at least two weeks of storing for proper staining of foraminifera, the original volume of each sample was determined by subtracting the staining solution volume from the total volume contained in the jars. Each sample was wet-sieved into a 63 - 500 μm size fraction in order to separate the foraminifera from fine sediments and macrobenthic organisms (Schönfeld *et al*., 2012). The retained material was sorted in Petri dishes with water, and the foraminiferal specimens were hand-picked and counted under stereomicroscopy.

Some samples were previously wet split into manageable volumes (containing ca. 500 living individuals) using a Folsom splitter. Only hard-walled foraminifera such as calcareous and agglutinated ones were considered for the living assemblage characterization of the study area because of their potential to form dead and fossil assemblages that are useful for palaeoecological and palaeoceanographic applications (Murray, 2006). In samples of the monthly monitoring stations, living and dead (empty tests) foraminifera were counted for evaluating the general effects of early diagenesis of the organic matter on the general foraminiferal abundance.

3.2.4. Data analysis

3.2.4.1. Historical data

The spatiotemporal variability of the bottom water properties were analyzed through the examination of monthly percentiles of their data in the annual cycle. For temporal comparisons of each physicochemical variable (temperature, salinity, dissolved oxygen and pH), the monthly interquartile range (IQR = 75th – 25th percentiles) and interdecile range (IDR = 90th – 10th percentiles) were determined from data of all monitoring stations. For additional spatial comparisons, the median values between percentiles 55th and 45th were determined from data of each group of stations corresponding to the defined zones.

3.2.4.2. Environmental data of surveys

The environmental properties of bottom water and sediments recorded in the three field surveys were described for each sampling station and zone. Univariate permutation analysis of variance (Two-way crossed PERMANOVA based on Euclidean distance and 9999 permutations) was performed for every abiotic variable in order to find significant spatiotemporal (time and zone) differences. This analysis is semi-parametric and robust to non-normal data distribution and heterogeneous dispersions among groups (Anderson, 2017).

3.2.4.3. Analysis of the assemblage structure

Spatiotemporal variability of the living foraminiferal assemblage was explored by means of the PCA ordination. The dataset of the species abundances was transformed using a centered log-ratio (clr) transformation of their relative abundances for removing the effects of the constant-sum constraint, which occurs

when there is a low number of species in the assemblage (Murray, 2006), and for retaining the proper covariance structure of compositional data (Kucera and Malmgren, 1998). A zero replacement by 0.005 was made in this transformation as suggested by Alperin *et al*., (2008, 2011) and others cited therein. Furthermore, the total foraminiferal abundance (N) and the diversity indices such as the species richness (S), Shannon-Wiener's index (H'), and Simpson's index of dominance (D) were described and projected in the PCA ordination of the assemblage as passive (post hoc) explanation of the axes (Borcard *et al*., 2018).

A permutation analysis of variance (Two-way crossed PERMANOVA based on Euclidean distance and 9999 permutations) was performed univariate for every structure parameter (N, S, H' and D), and multivariate for the transformed assemblage data, in order to establish which spatiotemporal (time and zone) differences are significant.

3.2.4.4. Abiotic and biotic associations

To assess the relationships between environmental variables and foraminiferal species, a canonical Redundancy Analysis (RDA) was performed on datasets of the species abundances and all benthic biotope properties, as response and explanatory variables, respectively. This parametric constrained ordination allows to show a biplot in which the angle between arrows of response and explanatory variables reflect their correlations (Borcard *et al*., 2018).

Furthermore, the monthly changes of the benthic foraminiferal density, at station 3, were compared with those of the contents of TOC and TN of surface (0-2 cm)

sediments, as well as the average pH and hydrogen sulfide concentrations of the pore waters, in order to find similar temporal changes.

3.3. Results

3.3.1. Spatiotemporal variability of the benthic environment

3.3.1.1. Historical data of bottom water properties

In the 2010-2015 period, the bottom water temperature usually varied between 14 and 20 °C, the salinity between 34.9 and 35.2 ‰, the dissolved oxygen between 0 and 4 mlL-1, and the pH between 7.5 and 8.0 (Figure 3.2). In the annual cycle, temperature increased towards March (summer) and salinity increased towards July (early winter), and both parameters decreased towards December (late spring). Dissolved oxygen and pH kept low during December-April (late spring – summer – early autumn), with conditions of frequent hypoxia (BWDO 75th percentile < 1.4 mlL-1) and low pH (BWpH 75th percentile < 7.75), and both increased towards July. Except for salinity, the bottom water properties exhibited spatial differences, with median values (55th - 45th percentiles) being lower in the deeper zone, slightly higher in the bay and the eastern zone, and higher in the northern zone (Figure 3.2).

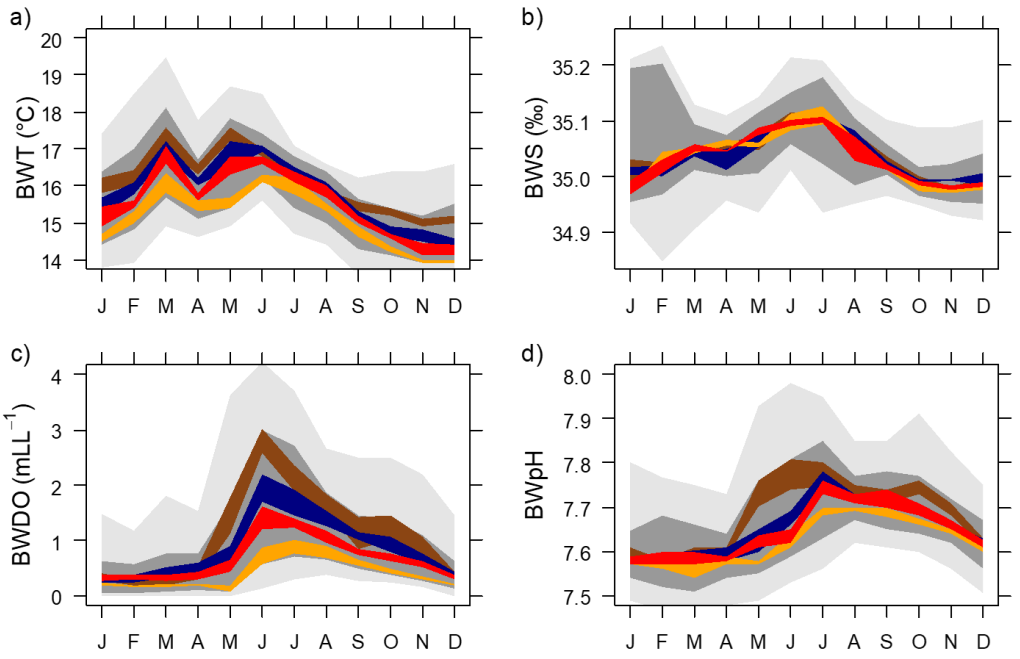

Figure 3.2. The annual cycle of variability, based on records of the 2010 – 2015 period, of the bottom water properties: a) temperature (BWT), b) salinity (BWS), c) dissolved oxygen (BWDO), and d) pH (BWpH). Interquartile range (75th - 25th percentiles) and interdecile range (90th - 10th percentiles) of all data are shown in dark gray and light gray polygons, respectively. Polygons in colors represent the median values (55th - 45th percentiles) of each data group by zone for spatial comparisons (bay, deep, east and north in red, orange, blue, and brown, respectively).

3.3.1.2. Environmental variability recorded in surveys

The bottom water properties mainly varied temporally (Figure 3.3). The temperature and salinity exhibited lower levels mostly in November 2014 and higher levels in July 2015, whereas the dissolved oxygen, pH and dissolved nitrates exhibited lower levels mostly in March 2015 (oxygen and nitrates almost depleted),

and higher levels in July 2015. On the other hand, phosphates exhibited higher levels mostly in March and lower levels in July. Permanova univariate results (Table A.B1) indicated that temporal differences of all these variables were significant, but only temperature and nitrates also exhibited significant spatial differences, with the deep zone exhibiting lower temperatures and higher nitrates, than the other zones.

The sedimentary properties that characterized the bottom substrate showed mainly spatial differences. Then, the clay content was greater mostly in the bay stations, whereas silt content was greater in all stations out of the bay. The sand content was minor in all stations and almost absent in the northern zone (Figure 3.4). The organic matter content (LOI) in sediments was mostly greater in the bay and smaller in the northern zone. Similarly, the content of phytodetritus (CPE) was greater mostly in the bay, whereas the C:P ratio did not show spatial patterns. Permanova univariate results (Table A.B2) indicated that spatial differences in the clay content, LOI, and CPE were significant, but only the LOI values also exhibited significant temporal differences, with greater values in March than November and July.

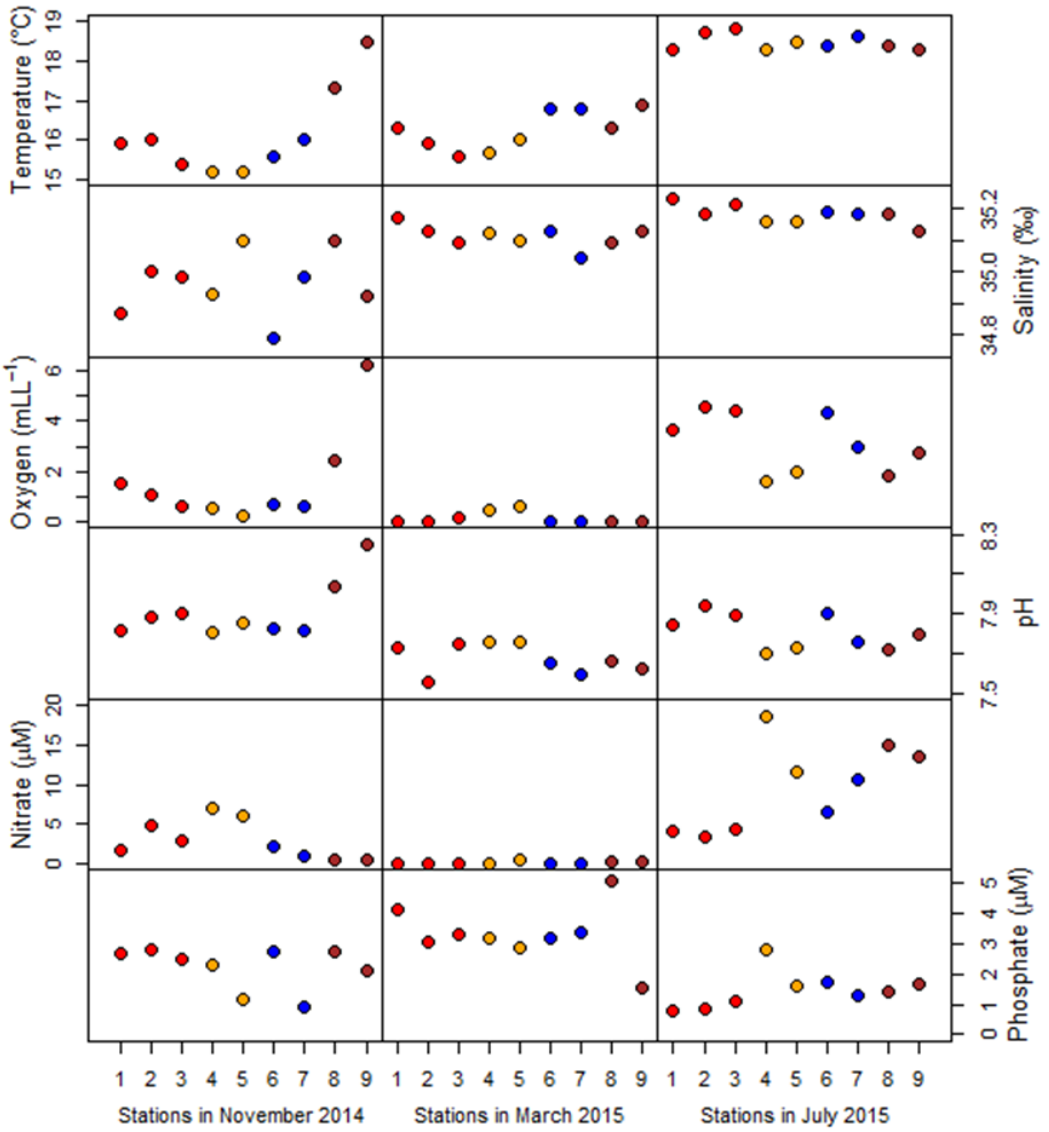

Figure 3.3. Records of bottom water properties (temperature, salinity, dissolved oxygen, pH, dissolved nitrates, and phosphates) at the monitoring stations in three field surveys between 2014 and 2015. Colors indicate data of each corresponding zone (bay, deep, east, and north in red, orange, blue, and brown, respectively).

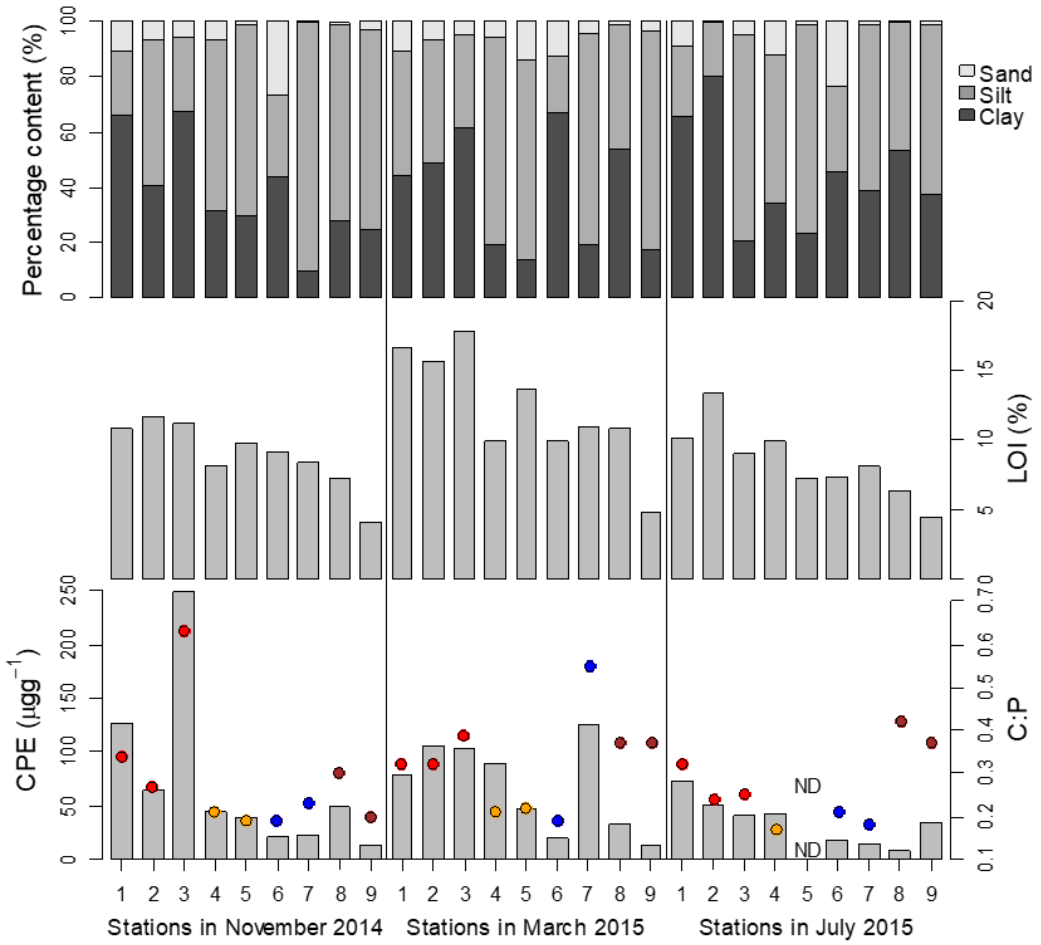

Figure 3.4. Bottom substrate properties (sedimentary texture, LOI and CPE) recorded at the monitoring stations in three field surveys between 2014 and 2015. Colored points correspond to data of C:P ratio of each zone (bay, deep, east and north in red, orange, blue, and brown, respectively).

3.3.2. The living assemblage of benthic foraminifera

The living assemblage of surface sediments was characterized almost entirely by calcareous species since agglutinated ones were less than 1% of the total abundance (Table 3.2). *Buliminella elegantissima* (d'Orbigny, 1839) was on average the most abundant species with about 56% of total, followed by *Bolivina costata* (d'Orbigny, 1839) with 27%, *Virgulinella fragilis* (Grindell & Collen, 1976) with 7%, and *Nonionella auris* (d'Orbigny, 1839) with 7%. The other calcareous species such as *Buccella peruviana* (d'Orbigny, 1839), *Discorbis* sp., and *Bulimina* sp., along with the agglutinated ones *Textularia* sp., and *Reophax* sp., together accounted for less than 3% (Table 3.2).

The PCA ordination of foraminiferal samples exhibited the same four zones as groups of samples, with those of the bay being consistently similar among them through time (Figure 3.5). Multivariate Permanova of the assemblage structure indicated that only spatial variations were significant (Table A.B3). The longer vectors of *B. costata*, *N. auris* and *V. fragilis* in the PCA biplot indicated that only the abundances of those species contributed the most to the variations of the assemblage structure in the study area.

The diversity indices overlapped along the PC1, exhibiting that dominance (D) was positively associated with the abundances of *B. costata*, mainly in the bay where *B. costata* dominated the assemblage (Figure 3.5), and along with *B. elegantissima* encompassed together almost 100% of the assemblage (Table 3.2). On the other hand, the species richness (S) and Shannon diversity (H') were positively associated with the abundances of *N. auris* and *V. fragilis* that were greater in the eastern and northern zones, respectively. Univariate Permanova indicated that only these spatial

variations of S, H’ and D, were significant, whereas the total foraminiferal abundance (N) significantly varied in time, with greater abundance in March than in November and July (Table A.B3).

The time-averaged abundance, at every station, of the four main species were plot in the map (Figure 3.6), exhibiting that *B. elegantissima* were well distributed in the entire study area, whereas *B. costata* was mainly abundant in the bay and secondarily in the deeper zone. *V. fragilis* was abundant mainly in the northern zone, and *N. auris* was abundant in the deep and eastern zones.

Table 3.2. Foraminiferal abundance and diversity per sample. N: Total density. S: Species richness. H': Shannon-Wiener index, D: Simpson's dominance index. B.ele.: *Buliminella elegantissima*. B.cos.: *Bolivina costata*. V.fra.: *Virgulinella fragilis*. N.aur.: *Nonionella auris*. B.per.: *Buccella peruviana*. Dis.sp.: *Discorbis* sp. Bul.sp.: *Bulimina* sp. Reo.sp.: *Reophax* sp. Tex.sp.: *Textularia* sp.

Zone	Sample	N	S	H'	D	B.ele.	B.cos.	V.fra.	N.aur.	B.per.	Dis.sp.	Bul.sp.	Reo.sp.	Tex.sp.
Bav	n1	92.5	3	0.57	0.66	78.3	20.3	0.0	0.0	1.4	0.0	0.0	0.0	0.0
Bay	n2	457.0	4	0.60	0.71	5.5	83.9	1.9	0.0	8.7	0.0	0.0	0.0	0.0
Bay	n3	2646.7	2	0.38	0.78	12.9	87.1	0.0	0.0	0.0	0.0	0.0	0.0	0.0
Deep	n4	308.8	4	0.76	0.55	25.6	69.5	0.0	0.4	4.5	0.0	0.0	0.0	0.0
Deep	n5	920.8	3	0.52	0.73	6.9	85.1	0.0	8.1	0.0	0.0	0.0	0.0	0.0
East	n6	696.5	5	0.66	0.67	80.7	14.1	0.8	2.9	1.6	0.0	0.0	0.0	0.0
East	n7	1792.6	5	1.25	0.35	52.0	6.4	21.0	17.6	3.0	0.0	0.0	0.0	0.0
North	n8	3641.7	7	1.10	0.42	57.1	7.0	28.3	6.3	0.1	0.0	0.1	1.0	0.0
North	n9	1944.0	5	1.29	0.30	30.9	25.1	37.9	0.0	0.0	0.0	0.0	1.6	4.5
Bay	m1	1273.0	2	0.49	0.69	80.4	19.6	0.0	0.0	0.0	0.0	0.0	0.0	0.0
Bay	m2	4612.6	6	0.74	0.51	38.5	60.1	0.8	0.0	0.2	0.3	0.0	0.0	0.0
Bay	m3	3592.2	3	0.68	0.51	43.0	57.0	0.0	0.0	0.0	0.0	0.0	0.0	0.0
Deep	m4	6528.3	4	0.87	0.51	67.5	18.6	0.0	13.5	0.0	0.3	0.0	0.0	0.0
Deep	m5	3402.3	3	0.72	0.53	63.8	34.6	0.0	1.6	0.0	0.0	0.0	0.0	0.0
East	m6	4181.4	6	0.98	0.56	73.6	4.3	5.2	4.4	2.9	9.5	0.0	0.0	0.0
East	m7	2014.0	6	1.30	0.38	58.1	10.1	7.0	16.4	4.7	3.7	0.0	0.0	0.0
North	m8	3669.1	6	0.79	0.61	76.8	12.8	5.0	5.2	0.0	0.1	0.0	0.2	0.0
North	m9	3150.1	6	0.95	0.49	65.7	14.7	18.0	0.9	0.0	0.0	0.0	0.2	0.6
Bay	j1	2286.4	5	0.54	0.73	84.7	12.0	1.2	0.4	1.8	0.0	0.0	0.0	0.0
Bay	j2	2227.1	4	0.73	0.49	49.4	49.9	0.6	0.1	0.0	0.0	0.0	0.0	0.0
Bay	j3	1121.1	3	0.62	0.58	30.1	69.8	0.0	0.1	0.0	0.0	0.0	0.0	0.0
Deep	j4	784.3	7	0.83	0.57	72.0	20.9	0.0	4.0	0.6	1.4	0.1	0.9	0.0
Deep	j5	3423.4	5	1.11	0.36	46.7	24.1	1.1	28.0	0.0	0.0	0.0	0.1	0.0
East	j6	3905.2	6	1.04	0.52	70.1	3.1	8.0	12.2	4.0	2.6	0.0	0.0	0.0
East	j7	2154.3	7	1.05	0.47	64.9	6.0	20.7	6.4	0.7	1.1	0.0	0.2	0.0
North	j8	3157.6	7	1.23	0.36	53.2	14.0	18.3	13.9	0.1	0.0	0.0	0.1	0.3
North	j9	915.0	6	1.25	0.34	42.1	38.5	8.1	9.0	0.0	1.0	0.0	0.0	1.4
	Total	62953.9	-	-	-	56.3	27.2	7.4	6.9	1.0	0.9	0.0	0.2	0.2

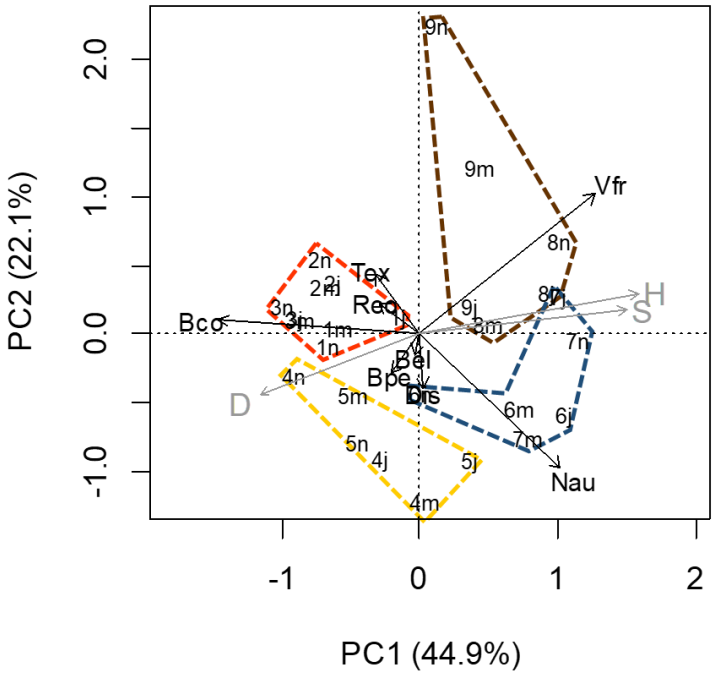

Figure 3.5. PCA biplot of the clr-transformed abundances of *Bolivina costata* (Bco), *Nonionella auris* (Nau), *Virgulinella fragilis* (Vfr), *Buliminella elegantissima* (Bel), *Buccella peruviana* (Bpe), *Discorbis* sp. (Dis), *Reophax* sp. (Reo), and *Textularia* sp. (Tex); and passive post hoc Species richness (S), Simpson's dominance (D), and Shannon Wiener's diversity (H). Each zone is in colored polygons (bay, deep, east, and north in red, orange, blue, and brown, respectively).

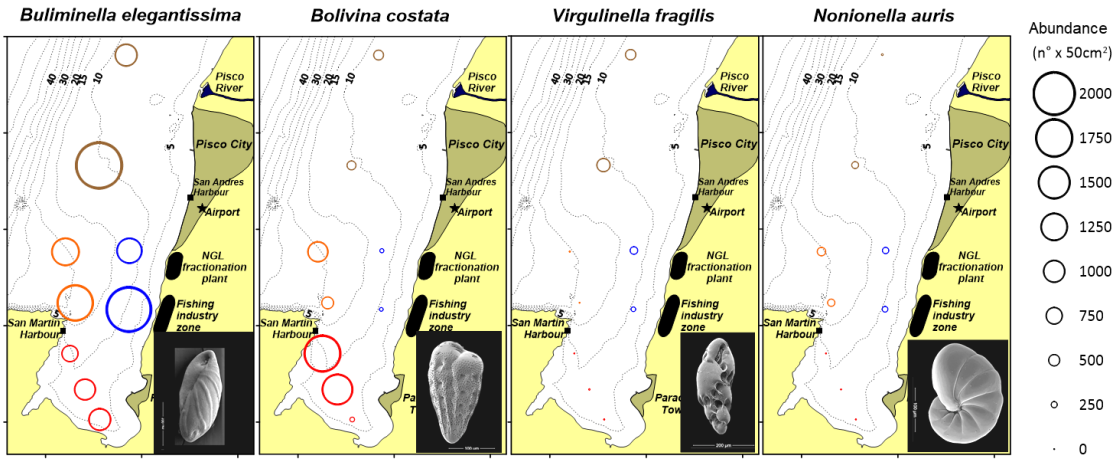

Figure 3.6. Time-average spatial distribution of the most abundant foraminiferal species in the Pisco-Paracas coastal area. Bubbles are proportional to their respective abundances in the surface sediments (top 1cm). Colors correspond to each zone (bay, deep, east, and north in red, orange, blue, and brown, respectively).

3.3.3. Relationships of environmental factors and foraminifera

A significant (p-value = 0.0311) model resulted from RDA, whose canonical axes (linear combinations of the benthic environmental factors) explain ~55% of variance of the foraminiferal assemblage structure. The first and second canonical axes (RDA1 and RDA2) accounted for 29% and 13% of that variance, respectively.

The R- and Q-mode biplots of RDA allowed to observe that higher contribution of *B. costata* in the assemblage was associated with more clayey and organic-rich (LOI) sediments with a greater content of phytodetritus (CPE) (Figure 3.7a), which mainly occurred in the bay (Figure 3.7b). On the other hand, the higher contribution of *V. fragilis* was associated with siltier sediments with lower organic matter (LOI), underlying slightly warmer bottom waters (Figure 3.7a), which mainly occurred in

the northern zone (Figure 3.7b). Furthermore, although its shorter projection, the higher contribution of *N. auris* in the assemblage was associated with higher salinity and dissolved nitrates of the bottom water (Figure 3.7a), which occurred in July and mainly at the deeper and eastern zones. The other species exhibited even shorter projections.

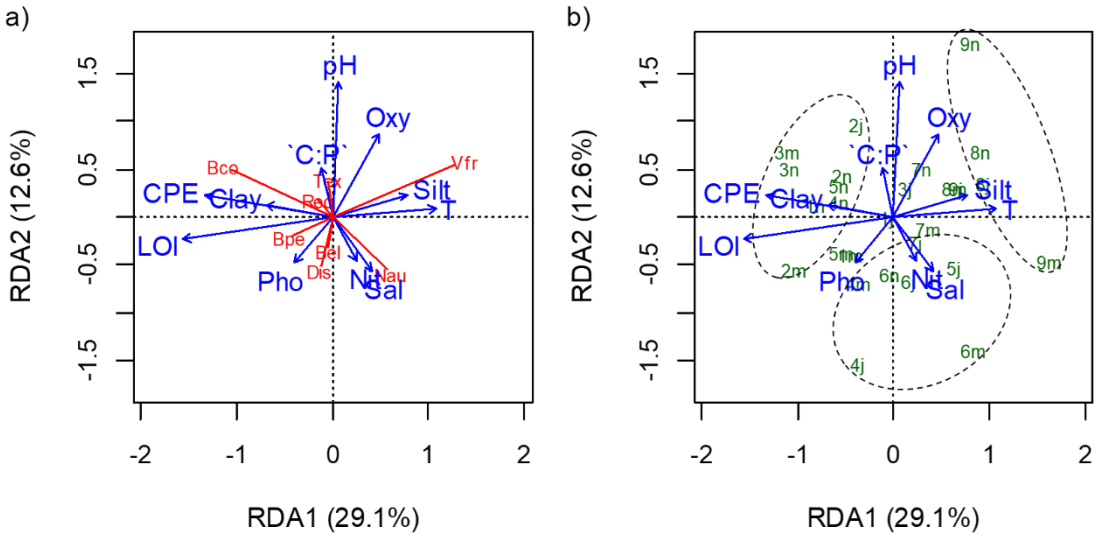

Figure 3.7. The Redundancy Analysis biplots in (a) R - and (b) Q - mode. R mode showing the relationships of the species *Bolivina costata* (Bco), *Nonionella auris* (Nau), *Virgulinella fragilis* (Vfr), *Buliminella elegantissima* (Bel), *Discorbis* sp. (Dis), *B. peruviana* (Bpe), *Reophax* sp. (Reo), and *Textularia* sp. (Tex); and environmental factors. Q mode shows the ordination of the samples constrained by factors.

3.3.4. Changes in the monthly monitoring station

Monthly changes in the TOC and TN contents of the 2 cm top surface sediments were observed at the monitoring station (3), from November 2014 to July 2015. The greatest concentration of TOC (37.9 µg/g) was registered in March and the second peak in July (32.9 µg/g), whereas the concentrations of TN in November, February, and June (>13 µg/g) were greater than the other months (<11 µg/g, Figure 3.8a). The hydrogen sulfide (H_2S) concentrations in the pore waters were greater in March (> 750 µM) and July (> 600 µM), and lower in the other months although it was always present (< 600 µM and > 0 µM) (Figure 3.8b). The measured values of pore water pH were also greater in March (> 7.50) and exhibited lower values in February and June (< 7.35) (Figure 3.8b). The H_2S concentrations changed according to the TOC content, whereas pH measurements changed in opposition to the TN content.

Density of living and dead (empty tests) benthic foraminifera in the 2 cm top sediments (2 cm x 50 cm^2 = 100 cm^3) also reached maximum values (8280 and 11202 in 100 cm^3, respectively) in March, although density of empty tests exhibited more drastic changes with its minimum (29 in 100 cm^3) in November 2014 (Figure 3.8c). *Bolivina costata* and *Buliminella elegantissima* dominated the assemblage all the period consistently, with no changes in the assemblage structure, and other species being together always less than 1% of the total abundance.

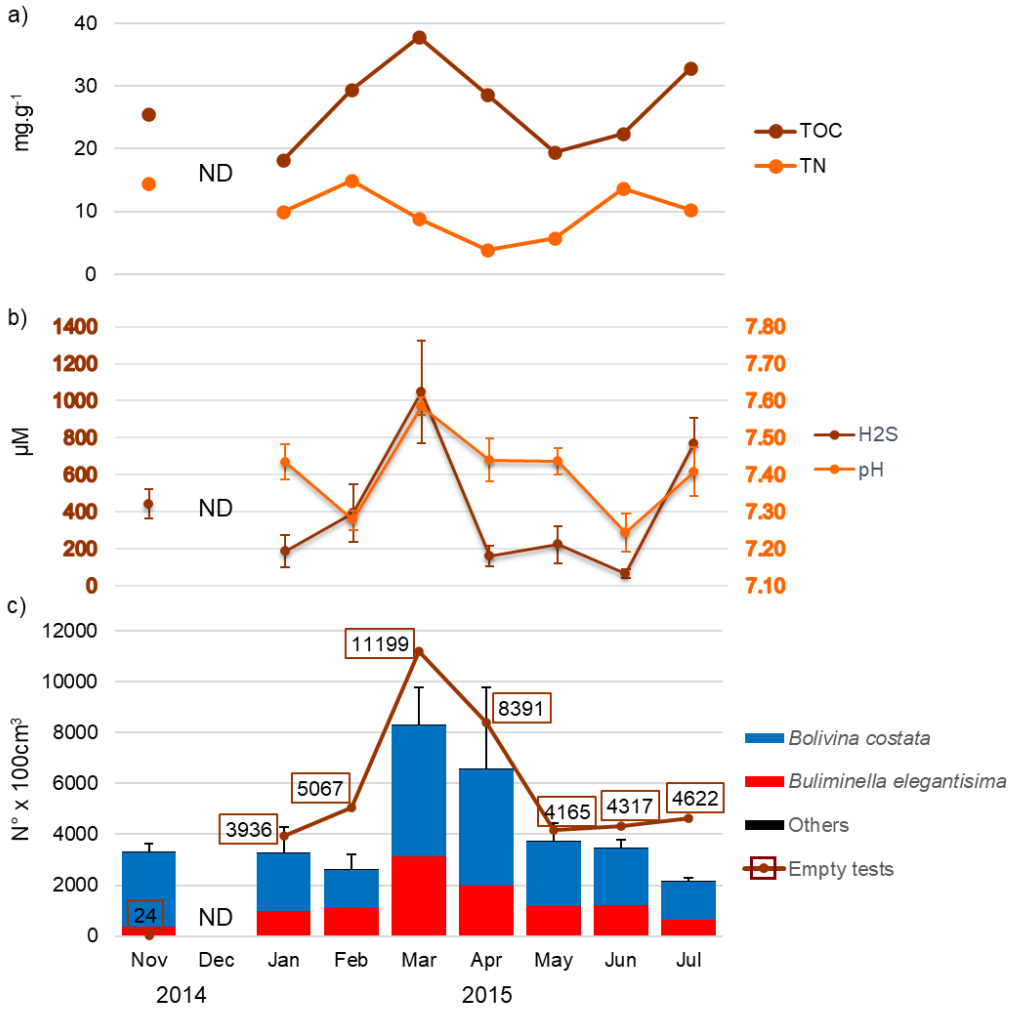

Figure 3.8. Monthly changes of sedimentary properties and foraminiferal fauna in monitoring station 3. a) Content of TOC and TN. b) H_2S and pH of sedimentary pore waters. c) Density of living and dead (tests) foraminifera (c). ND: not determined.

3.4. Discussion

3.4.1. The subtidal benthic habitat of the Pisco-Paracas coastal area

Seasonality of limiting factors for calcareous benthic fauna such as BWpH and BWDO, derived from historical data (2010-2015), indicated that conditions of low pH (BWpH < 7.75) and hypoxia (BWDO <1.4 mlL-1) can occur all year round, but they are more frequent towards summer and less frequent towards winter (Figure 3.2). This seasonal variability is likely related to the influence of the adjacent OMZ, which shoals and deepens in those seasons, respectively (Graco *et al*., 2017), becoming a hypoxic source for subsurface waters of the Pisco-Paracas coastal area (Merma-Mora *et al*., 2023, Arellano *et al*., 2023). Furthermore, the oxygen depletion in these coastal waters is usually accompanied by the depletion of dissolved nitrates, through denitrification, and by increase of phosphates as released from the sediments (Pitcher *et al*., 2021), that occurred in late summer (March 2015), whereas the opposite (higher oxygen and nitrates but lower phosphates) occurred in early winter (July 2015, Figure 3.3). Besides seasonality, the subtle but consistent spatial differences of the bottom water properties between the bay and the northern zone (Figure 3.2) suggest a closer connection of the deeper zone with the former, and a less connection with the latter.

The similar spatial distribution of the clay content and amount of organic matter in the sediments (Figure 3.4) revealed the occurrence of a spatial gradient of the benthic environments in shallower bottoms of the Pisco-Paracas coastal area. This distribution of sediment fractions and organic matter is persistent through time (Solís *et al*., 2022) and would be conditioned by the semi-enclosed geomorphology

of the bay that limits the effects of waves and currents on the bottom (Velazco and Solis, 2000), allowing the sedimentation of finer (inorganic and organic) particles, and by the Pisco River mouth in the northern zone, which is a source of terrigenous sediments that allows the settlement of coarser particles such as silt and sand in its surrounding area.

3.4.2. The foraminiferal assemblage and differences of species distribution

The dominance of a few calcareous species in the benthic foraminiferal assemblage observed in the Pisco-Paracas coastal area, as well as the negligible abundance of agglutinated species and absence of miliolid taxa, are typical features of the oxygen-depleted and organic-rich sedimentary environments that are impinged by the upper Peruvian OMZ (Levin, 2003; Cardich *et al.*, 2012, 2015; Mallon *et al.*, 2012). The dominant species found here were also described in those environments. A great density of *Bolivina costata* followed by *Nonionella auris* characterizes the living foraminiferal assemblage from sediments of the central Peruvian inner shelf (depth range of 50 – 100 m; Cardich *et al*., 2012, 2015). On the other hand, the species *Virgulinella fragilis* and *Buliminella elegantissima* were described as little abundant in shelf sediments, with the former being restricted to the inner shelf and the latter exhibiting a plastic distribution reaching depths down to the lower limit (~600 m) of the OMZ (Cardich *et al*., 2015).

The dominance of *B. elegantissima* in the living foraminiferal assemblage of the Pisco-Paracas coastal area is a feature that was observed in other sheltered shallow (<50 m) sedimentary environments of the coasts of southern Peru (Romero, 2021) and northern Chile (Tavera-Martínez *et al*., 2022). Several studies associate the

dominance of this cosmopolitan species with eutrophic conditions and organic enrichment in sediments of shallow environments (Eichler and Barker, 2020).

The observed preference of *V. fragilis* for the less frequently hypoxic northern zone (Figure 3.6), and its association with siltier sediments of lower organic matter content (Figure 3.7), are unexpected findings of this study. This species is thought to be restricted to organic-rich sediments undergoing oxygen depletion (Tsuchiya *et al*., 2009; Leiter and Altenbach, 2010), and tolerating sulfidic conditions due to some adaptations such as a peroxisome proliferation (Bernhard and Bowser, 2008), and the symbiosis with sulfide-oxidizing bacteria and kleptoplasts (Bernhard, 2003; Bernhard *et al*., 2018; Tsuchiya *et al*., 2015). However, the organic matter content of the northern zone (LOI > 4.1%) is still in a higher range than those of other shallow sedimentary environments on the central Peruvian coast (Merma-Mora, 2020). Furthermore, the bottom water oxygen measured ca. 1 m above the sediment-water interface is not likely a direct record of oxygenation of the benthic foraminiferal microhabitat, since dissolved oxygen can be depleted in the surficial first millimeters of coastal sediments (Fenchel and Finlay, 2008). Then, although hydrogen sulfide was not measured in surface sediments of the northern zone, it is likely that *V. fragilis* is reflecting anoxic/sulfidic conditions in there, maybe associated with less acidic pore waters than those in the bay that allow the occurrence of this very fragile calcareous species (Leiter and Altenbach, 2010).

N. auris has been reported as a subdominant species in the sediments of the central Peruvian inner shelf, which are sulfidic and rich in labile organic matter underlying severe hypoxic bottom waters (BWDO < 0.5mLL-1, Cardich *et al*., 2015). It is

capable of thriving in those conditions through the physiological adaptation of storing and utilizing nitrates for cellular respiration (Risgaard-Petersen *et al*., 2006; Høgslund *et al*., 2008; Glock *et al*., 2019). The association of this species with greater concentrations of nitrates and salinity (Figure 3.7) would be not only due to the conditions of early winter (July) in which those variables were greater (Figure 3.3), but also the preference of this species for the intermediate zones that are connected to the entrance path of the colder and nitrate-rich upwelling waters (Arellano *et al*., 2023). In shallow environments, this species could be benefited from frequent replenishments of nitrates in the bottom waters that prevent them from depletion (Cardich *et al*., 2015).

The relationship of *B. costata* with greater availability of phytodetritus (CPE) in more clayey organic-rich sediments (Figure 3.7), is in accordance with the observed preference of this species for muddy sediments rich in labile organic matter in the inner continental shelf (Cardich *et al*., 2015). Furthermore, *B. costata* can tolerate periodic anoxic/sulfidic pore-water conditions due to its capacity of switching from oxygen to nitrate respiration (Glock *et al*., 2019). Although the inner shelf sediments are a deeper and colder environment than the small bays of the Peruvian coast, it is likely that Paracas Bay fosters similar geochemical conditions and food availability to those of the inner shelf that *B. costata* is specialized to thrive on, unlike the other adjacent shallow zones.

3.4.3. The geochemically dynamic habitat of foraminifera in Paracas Bay

The muddy bottoms of about 10 m depth in Paracas Bay are a geochemically dynamic environment. The fluctuations of TOC content in the monitoring period reflect the organic matter accumulation, which is not restricted to summer months since also happened in early winter (July, Figure 3.8a). The decreases of TN content would indicate degradation of organic matter, since nitrogen of planktonic-derived detritus tends to decrease because net efflux (lost nitrogen) from the microbe/detritus complex exceeds influx via microbial biomass production (gained nitrogen) (Rice and Tenore 1981; Thornton and McManus 1994). Hydrogen sulfide (H_2S) is produced in the surface sediments enhanced by the accumulation of organic carbon (Figure 3.8b). The sulfate-reduction process was already described in sediments of the Peruvian margin (Fossing, 1990; Treude *et al*., 2021) and is also expected to occur in the Paracas Bay not only by the detection of H_2S, but also the other sulfide phases such as the amorphous Acid Volatile Sulfides (AVS) and Chromium Reducible Sulfur (CRS) in its sediments (Flores *et al*., 2023). The higher levels of pore water pH in March (Figure 3.8b) may be due to the high rates of sulfate reduction in predominant anoxic conditions, whereas in the other months there would be a mixture of oxygenated and reduced conditions in the surface sediments that lowered pH (Walter and Burton, 1990; Morse *et al*., 2007).

Under those changing geochemical conditions, *Bolivina costata* and *Buliminella elegantissima* thrive with high abundances in the living and dead assemblages (Figure 3.8c). While preferences and adaptations of the former species were already discussed, the latter was reported as tolerant to the presence of hydrogen sulfide and reactive oxygen species (such as H_2O_2), produced in sulfides chemical oxidation,

by having abundant presence of peroxisomes, associated with the smooth endoplasmic reticulum, that converts H_2O_2 into water and oxygen for respiration (Bernhard and Bowser, 2008). *B. elegantissima* was also described as associated with sedimentary organic matter accumulation under microxic conditions (DO < 0.1 mLL-1, Castillo *et al*., 2021), as well as under more oxygenated conditions (>1 mLL-1), in bays from the coasts of northern Chile and southern Peru (Castillo *et al*., 2021; Romero 2021, Tavera-Martínez *et al*., 2022). The positive response of *B. costata* and *B. elegantissima* abundances to the increase of TOC and H_2S in summer months reveals their capacity to take advantage of the available food under high sulfidic conditions. However, the concomitant increase of empty calcareous tests (Figure 3.8c) is likely reflecting the early reproduction and short life cycle of these species.

The decrease in the number of empty tests after summer suggests that, under more oxygenated conditions towards winter in the bay (Chapter 2), there is a partial dissolution of the calcareous material in the surface sediments due to the lowering of pH. Acidified conditions in the pore waters (pH usually < 7.5, Figure 3.8b) may explain not only the empty tests dissolution, but also the scarcity of other living calcareous species such as *Virgulinella fragilis* and *Nonionella auris* in the bay (Figure 3.8c), since the foraminiferal sensitivity and response to acidification and to calcite undersaturation is likely to be species specific (Haynert *et al*., 2012; Mcintyre-wressnig *et al*., 2014).

3.5. Conclusions

The subtidal sediments of the Pisco-Paracas coastal area are inhabited by a low diverse (9 taxa) foraminiferal assemblage, composed of calcareous species adapted to tolerate anoxic and sulfidic conditions. *Buliminella elegantissima* was the most abundant species during the period 2014 – 2015, and dominated throughout the coastal area except in the Paracas Bay, where *Bolivina costata* dominated.

The species *B. costata*, *Nonionella auris*, and *Virgulinella fragilis* were associated with geochemical gradients of the benthic habitat, suggesting their potential as indicators of different environmental conditions. Thus, the finer and phytodetritus-rich sediments of Paracas Bay seem to benefit *B. costata*, whereas the silty and slightly warmer sediments of the northern zone benefit *V. fragilis*. Furthermore, the colder and nitrate-rich bottom waters characterizing the intermediate zones likely benefit the nitrate-storing species *N. auris*.

B. costata and *B. elegantissima* can tolerate temporal hydrogen sulfide enrichment and lowering of pH (<7.5) in surface sediments of the bay, and take advantage of the available food in such inhospitable conditions. Monthly fluctuations in the number of empty calcareous tests in the bay revealed the quick reproduction and short life cycles of those species, but also suggest carbonate dissolution conditions.

IV. CHAPTER 4: A two-year monitoring of changes of the benthic foraminiferal assemblage and the sedimentary indicators of eutrophication in the Pisco-Paracas coastal area.

4.1. Introduction

Since the last decades of the 20th century, eutrophication has been considered as one of the main environmental threats to many coastal marine areas (Richardson and Jørgensen, 1996). Although eutrophication is usually referred to as the increasing entry of mineral nutrients of Nitrogen (N) and Phosphorus (P) into an aquatic environment, Nixon (1995) pointed out that these are not the only factors that determine the trophic state of a body of water, and proposed to define eutrophication as an increase in the rate of supply of organic matter to an ecosystem.

Eutrophication in the Pisco-Paracas coastal area, induced by the effluents of fishmeal industry, was notorious until 2004, when a treatment system was stablished and a pipeline that discharges those effluents outside this coastal area, was deployed. However, signs of eutrophic conditions are still observed in the bottom water such as a severe deficit of nitrates with respect to phosphates (N ratio: P << 16) in hypoxic conditions (Pitcher *et al*., 2021), and in the anoxic sediments that accumulate organic matter mainly in the Paracas Bay (Solís *et al*., 2022).

Mineralization (early diagenesis) of sedimentary organic matter, and nutrient fluxes between water and sediments, can change due to eutrophication, as increased organic flux to the bottom promotes oxygen depletion and stimulates sulfate reduction, which becomes the main respiration process of the sedimentary organic matter (Jørgensen, 1996a). These changes affect the benthic fauna mainly due to

deficient oxygen levels and the presence of hydrogen sulfide (H_2S) which is toxic to eukaryotic organisms. In this regard, benthic foraminifera can respond in different ways to eutrophication and organic enrichment of sediments, taking into account the natural environmental properties of a given area and the type of organic effluent that has generated eutrophication (Alve, 1995). Although foraminifera diversity is often affected by organic enrichment of sediments, some species can tolerate and even thrive in such conditions, making them potential indicators of eutrophication (Yanko *et al*., 1999).

The diversity and structure of the assemblage of benthic foraminifera in the Pisco-Paracas coastal area vary in accordance to the distribution of organic matter contained in the surface sediments, whose temporal fluctuations can also affect the number of accumulated calcareous tests of the dead assemblage (Chapter 3). However, the sedimentary geochemical processes associated with eutrophication that generate changes in the assemblage of benthic foraminifera are unknown. For this reason, the present study seeks to evaluate changes in the abundance and structure of living (biocoenosis) and dead (thanatocoenosis) assemblages of benthic foraminifera, associated with variations in the concentration and early diagenesis of organic matter in sediments, linked to the eutrophication process in the Pisco-Paracas coastal area.

4.2. Methods

4.2.1. Design of sampling

A monitoring of the assemblage of benthic foraminifera and the geochemistry of the subtidal sediments of the coastal zone of Pisco-Paracas was carried out between 2019 and 2021, in a north-south arrangement of 3 muddy substrate stations. Although the stations have similar depth (Table 4.1), their spatial arrangement corresponds to a gradient of organic matter content with higher concentrations towards the bay (Velazco and Solís, 2000; Solís *et al*., 2022). The origin of this gradient is associated with the different conditions, from the semi-enclosed and protected configuration of the bay towards the northern zone with greater exposure to the open ocean, as well as by the presence of the Pisco River and the industrial zone. Thus, P1 was located inside the bay, which is a buffer zone of the Paracas National Reserve, a protected natural area located to the south of the bay. P2 was located in front of the industrial zone, and P3 in front of the mouth of the Pisco River (Table 4.1).

Table 4.1. Features of monitoring stations in the Pisco-Paracas coastal area

Station	Latitude	Longitude	Zone	Substrate	Depth (m)
P1	-13.82239	-76.28164	Bahía Paracas	Muddy	10.0
P2	-13.77732	-76.25724	Industrial	Muddy	11.0
P3	-13.65986	-76.25758	North	Muddy	9.5

4.2.2. Collecting of samples

Sediment samples were collected manually in triplicate, using acrylic tubes (6.5 cm inner diameter) and PVC caps, by semi-autonomous compressor diving aboard an artisanal fishing vessel (approx. 6m in length). The first 2 cm of collected surface sediments were sectioned and stored in plastic vials with a Rose Bengal solution (2g/L of 70% methyl alcohol) to stain the cytoplasm of living foraminifera (Schonfeld *et al*., 2012). Surface sediments (0-2 cm) from a fourth tube were sectioned and stored in hermetically sealed plastic bags, and then frozen, to determine the total organic carbon (TOC) and total particulate nitrogen (TN) of the sediments, as well as the isotopic ratios of ^{13}C and ^{15}N.

Another two tubes with drilled holes were obtained at each station. Pore water were extracted from the same depth interval (0-2 cm), using 20 mL syringes and micro-porous rhizomes (Seeberg-Elverfeldt *et al*., 2005). Aliquots of 1.5 mL of interstitial water were immediately fixed with 0.5 mL of a 5 % zinc acetate solution and stored in vials at 4 °C for the determination of hydrogen sulfide (H_2S) concentration. The remaining volumes of interstitial water were kept in glass flasks at 4 °C to determine the concentration of phosphates and ammonium.

4.2.3. Determination of TOC, TN and stable isotopes

The sediment samples were dried in an oven at 50°C and then homogeneously ground in an agate mortar. Approximately 1g of dry sediment from each sample was treated with 10% HCl to remove inorganic carbon and measure total organic carbon (TOC) and total nitrogen (TN), and also the isotopic ratio of carbon ($\delta^{13}C$) and nitrogen ($\delta^{15}N$) (Lichtfouse and Budzinski, 1995; Kenedy *et al*., 2005). These

were performed with an elemental analyzer (ThermoFisher Flash HT type) coupled to an isotope mass spectrometer (Delta V Advantage type) with analytical precision of C: 0.05 %, N: 0.05 %, $\delta^{13}C$: 0.05 ‰ and $\delta^{15}N$: 0.1 ‰, at the Isotopic Analysis Laboratory (ALYSES) of the Institute for Development Research (IRD) in France.

4.2.4. Determination of sulfide, phosphate, ammonium from pore water

The pore water H_2S concentrations were determined by the standard methylene blue formation method (Cline, 1969), which mixes the 5% zinc acetate-fixed sample with solutions of p-phenylonediamine hydrochloride and ferric chloride, to take absorbance readings of each sample at 670 nm wavelength. To determine the concentration of dissolved phosphates, 2 mL aliquots of the pore water were mixed with solutions of hexamolybdate and ascorbic acid to form a blue-colored phosphomolybdate solution, and the absorbance of each sample was measured at 885 nm wavelength (Strickland and Parsons, 1972). To determine the dissolved ammonium concentration, 2 mL aliquots of the pore water were mixed with solutions of phenol and sodium nitroprusside, to form the 'indophenol blue' solution, and the absorbance of each sample at 634 nm wavelength was measured (Strickland and Parsons, 1972). The absorbances were measured by the spectrophotometric technique, with a Perkin Elmer LAMBDA 45 spectrophotometer, in the IMARPE Hydrochemistry laboratory.

4.2.5. Determination of abundance and diversity of benthic foraminifera

After two weeks of fixation with alcohol and Rose Bengal, the samples were washed with tap water through a 63 µm mesh sieve. The retained material was transferred wet to Petri dishes. This material was observed by stereomicroscopy and

the foraminifera tests were manipulated with fine brushes, distinguishing and separating stained (biocoenosis) from dead (thanatocoenosis) individuals. Taxa to the lowest possible category were identified, and abundances per taxon and total abundance were counted, in biocoenosis and thanatocoenosis separately. The total number of living and dead foraminifera in each sample was then standardized as the number of tests per 50 cm^2 (# tests / 50 cm^2).

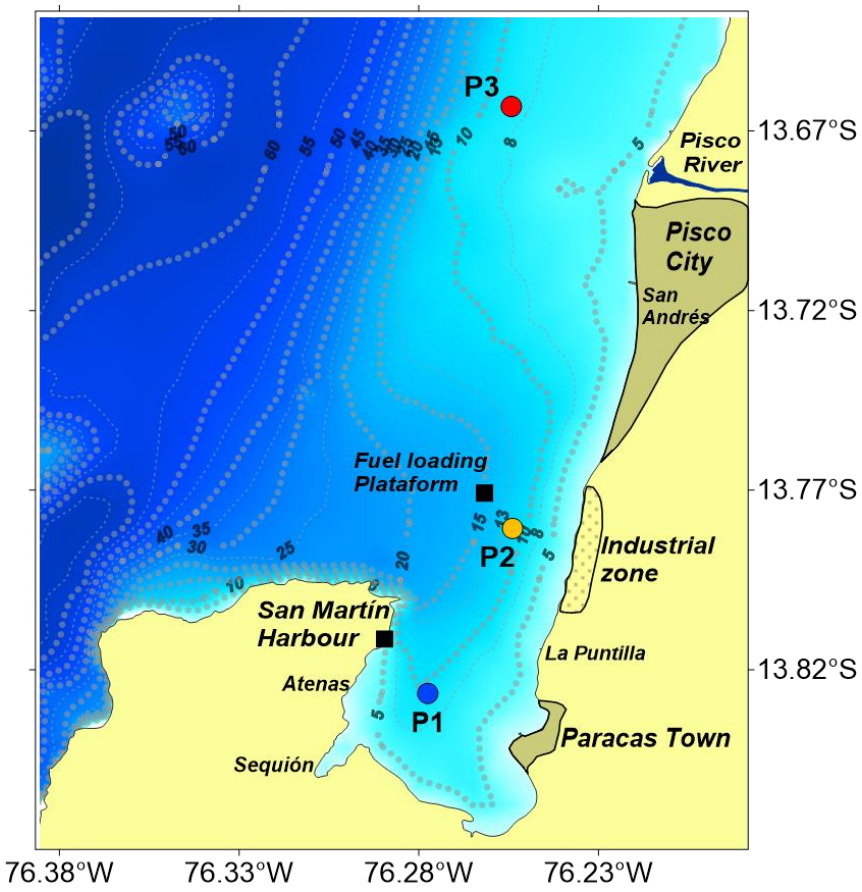

Figure 4.1. Monitoring stations in the Pisco-Paracas coastal area from 2019 to 2021. Bathymetry is depicted in contours and blue color scale.

4.3. Results

4.3.1. Variability of sediment geochemistry

The organic matter indicators exhibited a spatial gradient, from north to south, and a temporal trend between 2019 and 2021 (Figure 4.2a and 4.2b). Thus, the total organic carbon content (%TOC) was higher in P1 (between 5.5% and 6.0%), moderate in P2 (between 2.9% and 4.3%), and lower in P3 (between 0.8% and 1.8 %). Similarly, the total nitrogen content (%TN) was higher in P1 (between 0.7% and 0.9%), moderate in P2 (between 0.4% and 0.6%), and lower in P3 (between 0.1% and 0.2%). The highest values of both indicators occurred in December 2019 and February 2020, and progressively decreased afterwards. The C:N ratio was higher than 7.5 in P3, and between 7.0 and 7.5 in P1, with an increasing trend in both stations (Figure 4.2c). No trend of C:N occurred in P2 (between 6.8 and 7.2).

The $\delta^{13}C$ exhibited higher values in P1 (between -19.2 and -19.9), slightly lower in P2 (between -19.8 and -20.2), and much lower in P3 (between -21.2 and -22.6). In the three stations, $\delta^{13}C$ exhibited a slight decreasing trend towards the end of the monitoring (Figure 4.2d). On the other hand, $\delta^{15}N$ was higher in P2 (between 8.9 and 10.1) with no apparent trend; it was slightly lower (8.5 and 9.3) in P1 with an increasing trend, and it was notoriously lower in P3 (between 5.7 and 8.0) also with an increasing trend, except for its minimum value in August 2021 (Figure 4.2e).

Regarding the solute concentrations in pore waters, phosphates varied between 1 and 35 µM in P1, between 37 and 221 µM in P2, and between 41 and 376 µM in P3 (Figure 4.2f). Sulfides varied between 4 and 184 µM in P1, between 31 and 684 µM in P2, and between 0 and 147 µM in P3 (Figure 4.2g). Ammonium varied

between 27 and 603 µM in P1, between 59 and 1500 µM in P2, and between 126 and 941 µM in P3 (Figure 4.2h). While the lowest concentrations of the three solutes occurred in P1, the highest concentrations of phosphates (>50 µM) and ammonium (>200 µM) occurred in P3, and those of H_2S (>100 µM) in P2.

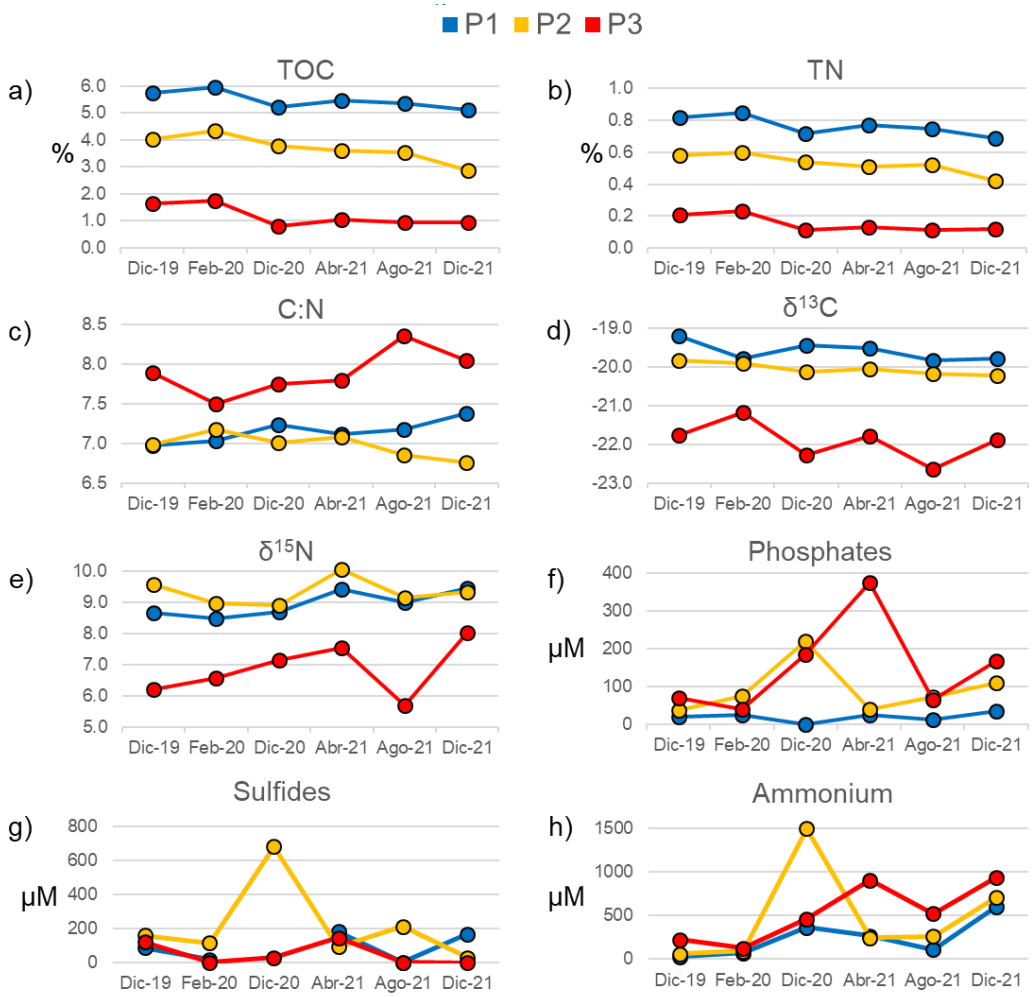

Figure 4.2. Geochemical variables of sediments (0-2 cm). Percentage content of Total Organic Carbon (a), and Total Nitrogen (b), and C:N ratio (c). $\delta^{13}C$ (d). $\delta^{15}N$ (e). Pore water dissolved phosphates (f), sulfides (g), and ammonium (h).

4.3.2. Abundance of biocoenosis and thanatocoenosis of benthic foraminifera

The abundance of biocoenosis and thanatocoenosis, in the accumulated 2 cm of surface sediments (2 cm x 50 cm^2 = 100 cm^3), varied in space and time (Figure 4.3a). The spatial comparison revealed that the abundances between sampling stations differ in order of magnitude, such that the biocoenosis was usually more abundant in P1 (between 1000 and 7000 foraminifera in 100 cm^3 of sediment), slightly less abundant in P2 (between 1000 and 5000 foraminifera in 100 cm^3 of sediment), except in December 2020 and December 2021, while in P3 the abundances were the lowest ones (between 100 and 1000 foraminifera in 100 cm^3 of sediment). On the contrary, the thanatocoenosis was much more abundant in P2 (between 70000 and 150000 tests in 100 cm^3 of sediment), less abundant in P1 (between 1000 and 8000 tests in 100 cm^3 of sediment), and even lower in P3 (between 100 and 2000 tests in 100 cm^3 of sediment).

At each sampling station it was also possible to observe temporal differences in the biocoenosis and thanatocoenosis (Figure 4.3a). Thus, the abundance of living foraminifera in P1 was on average higher in December 2019 and February 2020 (more than 6200 foraminifera in 100 cm^3 of sediment) and lower in December 2020 and December 2021 (less than 1600 foraminifera in 100 cm^3 of sediment). In P2, the abundance was higher in February 2020 and December 2021 (more than 3800 foraminifera in 100 cm^3 of sediment) and lower in December 2020 and August 2021 (less than 1900 foraminifera in 100 cm^3 of sediment). In P3 the abundance was higher in February 2020 (more than 1000 foraminifera in 100 cm^3 of sediment) and lower in August and December 2021 (less than 200 foraminifera in 100 cm^3 of sediment). Regarding thanatocoenosis, a decreasing trend in the number of tests

was observed in P1 and P3, which was not the case of P2. The number of tests at P2 was one or more orders of magnitude higher than the other stations, and remained around 100000 in 100 cm^3 of sediment throughout the monitoring.

In addition, it was observed that the abundances at 0-1 cm and 1-2 cm, of the biocoenosis and the thanatocoenosis, exhibited the same spatiotemporal patterns observed in the accumulated two centimeters (Figure 4.3b and 4.3c).

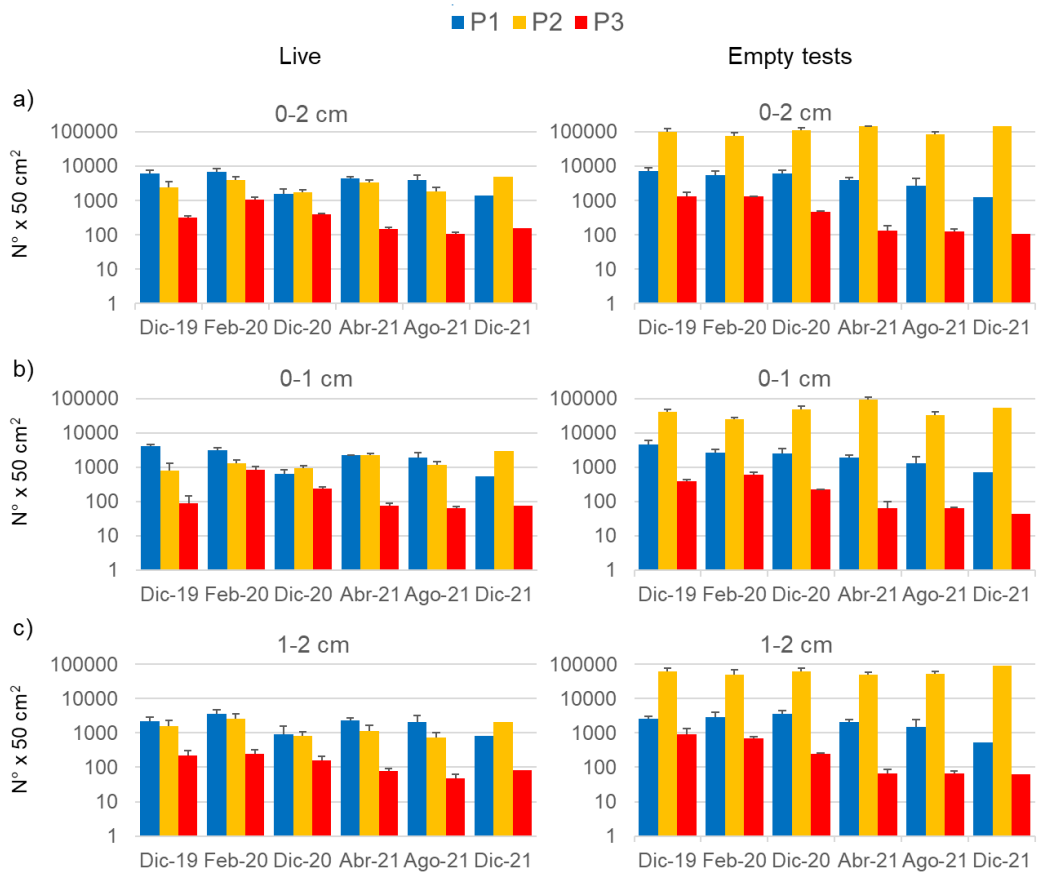

Figure 4.3. Total abundance of the biocoenosis and thanatocoenosis of benthic foraminifera in the first (b, 0-1 cm) and second (c, 1-2 cm) level of surface sediments (50 cm^2), and the sum of both or accumulated (a, 0-2 cm), for each station and sampling time. Vertical axes in logarithmic scale.

4.3.3. Species composition and structure of biocoenosis

The percentage composition of the species in the living assemblage or biocoenosis revealed that *Buliminella elegantissima*, *Bolivina costata*, *Nonionella auris*, and *Virgulinella fragilis* were the species that together made up between 98% and 100% of the total abundance of foraminifera that inhabit the study area, of which *B. elegantissima* and *B. costata* represent more than 70% (Figure 4.4a). These four species composed the total biocoenosis in P3, similar in P1 but additionally with *Buccella peruviana*, and similar in P2 but additionally with *B. peruviana*, *Discorbis* sp., and *Bulimina* sp. (Figure 4.5, Table A.C1).

In P1, *B. elegantissima* was always the dominant species, accounting for between 60% and 80% of the total abundance of the assemblage, followed by *B. costata* between 15% and 25% of the abundance, and the rest of the species (*N. auris*, *V. fragilis* and *B. peruviana*) were usually less than 5% (Figure 4.5c). In P2, *B. elegantissima* was also always the dominant species with 60% to 80% of the total, followed by *B. costata* between 5% and 20%, *N. auris* between 5% and 15%, *V. fragilis* usually less than 10%, and the other species (*B. peruviana*, *Discorbis* sp. and *Bulimina* sp.) were always less than 2% (Figure 4.5b). However, in P3 the living assemblage changed markedly between 2019 and 2021. It went from having *B. elegantissima* as the dominant species in 2019, comprising more than 50% of the abundance and followed by *B. costata* with less than 45%, to have *B. costata* as the dominant species by the end of 2021 with more than 70%, and *B. elegantissima* with less than 10% (Figure 4.5a). The species *N. auris* and *V. fragilis* fluctuated between 5 and 20% throughout the period.

4.3.4. Species composition and structure of thanatocoenosis

The dead assemblage or thanatocoenosis was also mostly composed (between 75% and 100%) of tests of *B. elegantissima*, *B. costata*, *N. auris* and *V. fragilis*, and smaller amounts (between 0% and 25%) of *B. peruviana*, *Discorbis* sp. and *Bulimina* sp (Figure 4.4b). Other rare species, not observed in the biocoenosis, were grouped into "other hyaline, miliolid and agglutinated" taxa (Table A.C1).

The percentage composition of species of the thanatocoenosis had almost no changes in P1, and was characterized by the dominance of *B. elegantissima* tests with 45% to 75% of the total, followed by those of *B. costata*, with 15% to 45%, while the other species (*N. auris*, *V. fragilis*, *B. peruviana*, *Discorbis* sp., *Bulimina* sp.) were together less than 10% (Figure 4.5c). Thanatocoenosis did not change significantly either in P2, and it was dominated by *B. elegantissima* tests with more than 50 % of the total. This was followed by similar contributions of *B. costata*, *N. auris*, *B. peruviana* and *Discorbis* sp., each between 5% to 10 %, a contribution of *V. fragilis* of less than 5%, and even lower contribution of *Bulimina* sp., which together with the other hyaline, miliolid and agglutinated taxa, were less than 1% (Figure 4.5b). On the other hand, the thanatocoenosis in P3 exhibited a notorious change in the monitoring period, from being dominated by *V. fragilis*, with more than 70% of the total in 2019, to be dominated by *B. costata*, with more than 60 %, at the end of 2021. The *B. elegantissima* tests fluctuated between 10% and 20% and those of *N. auris*, between 0% and 5% throughout the period, whereas the contribution of the other hyaline, miliolid and agglutinated taxa, varied from 5% to 20% between 2020 and 2021 (Figure 4.5a).

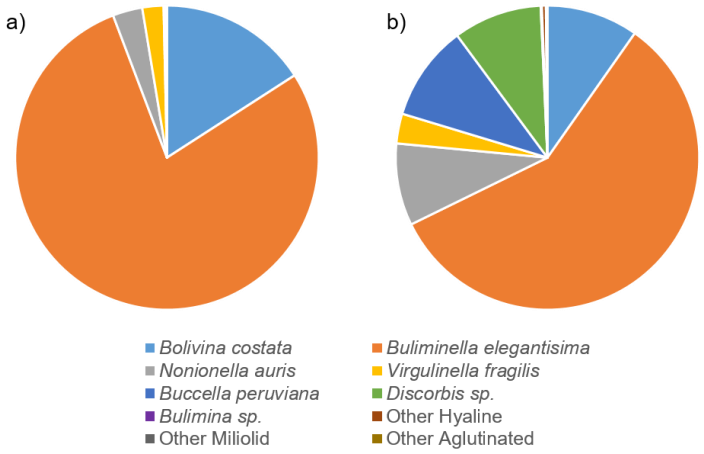

Figure 4.4. Percentage composition of foraminiferal species of the biocoenosis (a), and thanatocoenosis (b), in the accumulated surface sediment (50 cm^2 x 2 cm).

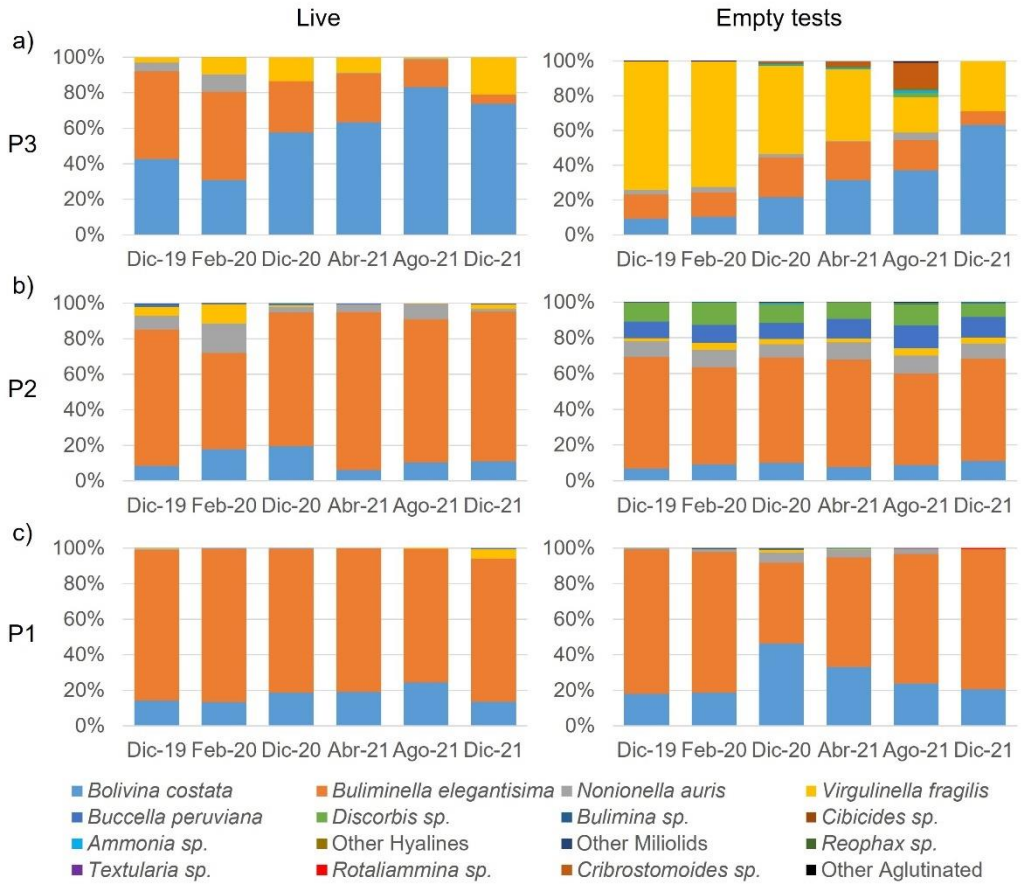

Figure 4.5. Percentage composition of foraminiferal species of the biocoenosis and thanatocoenosis, in the accumulated surface sediment (50 cm^2 x 2 cm), for sampling time, and each station: P3 (a), P2 (b), and P1 (c).

4.3.5. Species abundances

In the biocoenosis, the abundance of *B. elegantissima* exhibited maximum values in P1, and minimum values in P3. Apart from temporal fluctuations, its abundance exhibited a notorious decreasing trend only in P3 (Figure 4.6). The abundance of *B. costata* had similar spatial and temporal patterns, although with much subtler differences and fluctuations. On the other hand, the abundances of *N. auris*, *V. fragilis* and *B. peruviana* were higher in station P2 and in December 2019 and February 2020. From there, the abundance of *N. auris* decreased drastically until disappearing in P1 and P3, but remaining in P2. *V. fragilis* exhibited irregular fluctuations in its abundance, although with minimum values in P1 and maximum in P2. *B. peruviana* that inhabited only P1 and P2, and *Discorbis* sp. and *Bulimina* sp., which inhabited only P2, tended to disappear towards the end of monitoring.

In the case of the thanatocoenosis, all species had higher abundances at station P2 (one or more higher degrees of magnitude) and with no variation trend. *B. elegantissima* was the species with the highest abundance of tests, and exhibited a decreasing trend in P1 and P3. Similar was the case for *B. costata*, although with subtler differences. *N. auris* tests tended to disappear in P1 and P3 towards the end of monitoring, but remained at similar abundances in P2. *V. fragilis* tests tended to increase in P2, decrease in P3, and disappear in P1. The tests of *B. peruviana*, *Discorbis* sp., and *Bulimina* sp., disappeared from stations P1 and P3 towards the end of the monitoring, but remained with minor variations at P2.

Figure 4.6. Abundances of the main species of foraminifera of the biocoenosis and thanatocoenosis, in the accumulated surface sediment (50cm^2 x 2cm), for each station and sampling time. Vertical axes in logarithmic scale.

4.3.6. Biotope and biocoenosis association

A correlation matrix revealed the degree of association between benthic foraminiferal abundances and the environmental variables of their sedimentary habitat (Figure 4.7). The species best associated with the organic matter indicators was *B. elegantissima*, being positively correlated with the content of TOC ($r = 0.82$, $p<0.01$), TN ($r = 0.81$, $p<0.01$), $\delta^{13}C$ ($r = 0.72$, $p<0.01$), and $\delta^{15}N$ ($r = 0.59$, $p<0.01$), but negatively correlated with C:N ($r = -0.84$, $p<0.01$). *B. costata* exhibited a lower degree of association with these variables, being positively correlated with the content of TOC ($r = 0.79$, $p<0.01$), TN ($r = 0.79$, $p<0.01$), $\delta^{13}C$ ($r = 0.65$, $p<0.01$), but negatively correlated with C:N ($r = -0.64$, $p<0.01$). *N. auris* was only negatively correlated with C:N ($r = -0.61$, $p<0.01$). On the other hand, the tests abundance of thanatocoenosis was also negatively correlated with C:N ($r = -0.82$, $p<0.01$) and positively with $\delta^{15}N$ ($r = 0.71$, $p<0.01$).

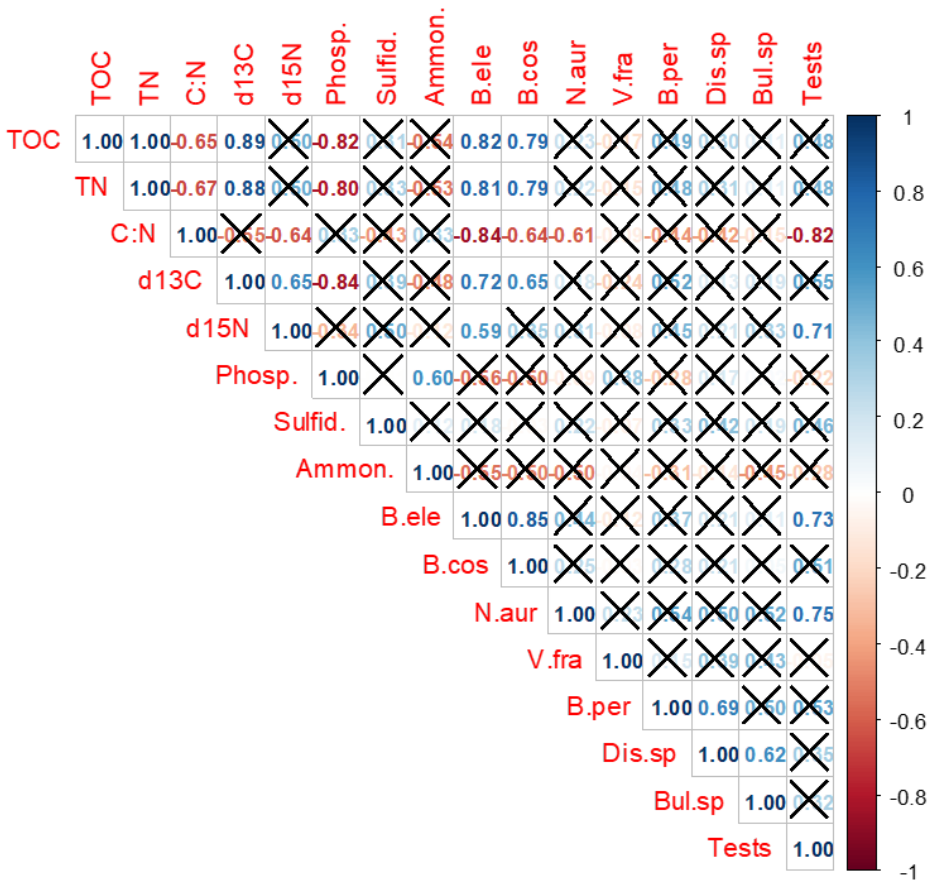

Figure 4.7. Spearman's correlation matrix of the abiotic variables and the abundances of benthic foraminifera (species of the biocoenosis and the number of tests of the thanatocoenosis). Non-significant correlations ($p > 0.01$) are marked as null. More positive correlations tend to blue and more negative tend to red.

4.4. Discussion

4.4.1. Geochemical variability of the sedimentary habitat

The general variation range of the C:N ratio (6.8 to 8.4, Figure 4.2c) reflected the predominance of the phytoplankton origin of organic matter, mainly in the bay (P1) and the industrial zone (P2), as they exhibited very close values to the typical C:N of marine phytoplankton (C:N ~ 6.63; Lamb *et al*., 2006). This origin was reaffirmed by the ranges of variation of $\delta^{13}C$ (-23.0 to -19.0) and $\delta^{15}N$ (5.5 to 10.0) that are typical of sedimentary phytodetritus (Cifuentes *et al*., 1996). On the other hand, the higher values of C:N (> 7.5), and lower values of $\delta^{13}C$ (< -21.0), in the northern zone (P3, Figure 4.2c and 4.2d), reflect a higher degree of mixing of phytodetritus with organic components of terrestrial origin such as cellulose and lignin (Silva and Prego, 2002; Lamb *et al*., 2006), which would enter this area due to its proximity to the Pisco River.

Although the monitoring of the present study had an irregular frequency, the clear decreasing trend of TOC and TN, in sediments of the three zones (Figure 4.2a and b), suggests a general alleviation of eutrophic conditions between 2019 and 2021, which were particularly severe in the bay (TOC > 5%). Since $\delta^{13}C$ of sedimentary organic matter can reflect the recent trophic evolution of aquatic environments (Lehmann *et al*., 2004), the observed decrease in $\delta^{13}C$ (more negative values) in all stations would be reflecting a decreasing primary productivity and less amounts of phytodetritus.

With an ongoing less predominance of phytodetritus in the bulk organic matter, it is expected to observe an increasing trend of C:N, which was the case for P1 and

P3, but not for P2 (Figure 4.2c). This different pattern might be related to other processes in the sediments such as distinct early diagenesis of the organic matter. Thus, the increasing C:N during the study period suggests an increasing degradation of nitrogenous particles due to more oxidative (in presence of oxygen) mineralization of the sedimentary organic matter (Jørgensen 1996a, 1996b). The nitrogen released by mineralization is preferentially ^{14}N, which leaves the organic substrate enriched in ^{15}N (increased $\delta^{15}N$, Thornton and McManus, 1994), as occurred in P1 and P3 (Figure 4.2e). On the other hand, the lack of trend in C:N and $\delta^{15}N$, observed in P2, suggest a particular retention (relative minor loss) of nitrogen throughout the study period.

The usual higher concentrations of interstitial sulfides in P2 indicate more frequent anoxic conditions than in the other stations (Figure 4.2g). Those conditions inhibit or slow down processes of nitrogen loss from the sediment matrix such as nitrification and denitrification. (Joye and Anderson, 2008), which supports the nitrogen retention previously suggested. Furthermore, nitrogen retention usually occurs when dissolved ammonium released by the nitrogen mineralization, that was increasingly available in pore waters of the three stations (Figure 4.2h), is adsorbed to the sedimentary particles under anoxic conditions (Morse and Morin, 2005).

The increase in dissolved phosphate also reflects an increase in the mineralization of organic matter (Sundby *et al*., 1992), and its accumulation in pore water occurs under anoxic conditions (Rozan *et al*., 2002), as was observed in P2 and P3 (Figure 4.2f). However, the phosphate concentrations were always lower in pore waters of the bay (P1), despite containing the highest values of sedimentary organic matter

(TOC and TN). This indicates a greater frequency of oxygenation, and consequently redox oscillations (Aller, 1994), in the surficial sediments of P1 that promotes the rapid adsorption of phosphates to the sedimentary particles, leaving low concentrations in the pore water (Sundby *et al*., 1992).

Starting from severe eutrophic conditions in 2019, the continuous decrease in sediment organic matter until 2021 was likely associated with changes in the redox conditions of the sedimentary microhabitat. From all of the above, and considering that bottom hypoxic conditions are frequent in the Pisco-Paracas coastal area (Chapter 2), the spatiotemporal pattern of the redox conditions of the surface sediments of the 3 stations can be described for the monitoring period 2019-2021. The sediments in P2 underwent predominant anoxic conditions. In P3, the anoxic sediments experienced an increasing coexistence of reductive and oxidative processes. In contrast, the sediments in P1 exhibited more intense redox oscillations associated with an increasing predominance of oxidative processes and greater contents of organic matter.

4.4.2. Variability in the living assemblage of foraminifera

The main species identified were previously described as the same species that inhabit and dominate the sediments of the upper continental shelf, tolerating anoxic and sulfidic conditions through physiological adaptations such as anaerobic respiration and the incorporation of bacterial symbionts that oxidize sulfides (Chapter 3). The overwhelming dominance (>70%) of very few species (*B. elegantissima* and *B. costata* in this study) in the foraminifera biocoenosis is usually characteristic of areas affected by eutrophication or organic contamination of

sediments (Bandy *et al*., 1964; Stott *et al*., 1996). The most abundant, *B. elegantissima*, is a cosmopolitan species that was identified as tolerant to various sources of pollution in coastal areas (Yanko *et al*., 1999), to anoxia, and to the presence of sulfide (Bernhard and Bowser, 2008). In addition, it is known that *B. elegantissima* particularly benefits from organic enrichment in sediments, exhibiting a direct association with sedimentary carbon and nitrogen content (McGann, 2009), and increasing its relative abundance in the assemblage (Eichler and Barker, 2020).

B. elegantissima particularly dominated the biocoenosis of Paracas Bay (P1), where it was always more than 75% of the total (Figure 4.4), contrasting with what was observed between 2014 and 2015, in which *B. costata* was the dominant species in the bay (Chapter 3). In the present study, there was a progressive decrease in the abundance of *B. elegantissima* in the northern zone (P3, Figure 4.5) that left *B. costata* as the dominant species since December 2020 (Figure 4.4). Given the greater positive correlation of *B. elegantissima* with TOC and TN ($r > 0.8$, Figure 4.7), the observed changes in P3 would be responding to the downward trend of sedimentary TOC and TN, which reached their lowest values around 2021 (Figure 4.2). Conversely, the change in the dominant species in the bay between the previous study of 2014-2015 (*B. costata*) and the current one of 2019-2021 (*B. elegantissima*), could have been generated by the increase in TOC that occurred between these periods, going from ~3.5% in 2015 (Chapter 3) to ~5.8% in 2019 (Figure 4.2a).

These changes in the dominant species in coastal areas can respond not only to changes in the quantity (TOC and TN) but also in the type of predominant organic matter in the sediments: phytodetritus, algal structures and bacteria, due to the differences in the feeding adaptations of the foraminiferal species (Loubere and Fariduddin, 1999). The species *B. costata* is known to dominate in the sediments of the upper continental shelf underlying active coastal upwelling cells off Peru (Cardich *et al*., 2015), in which diatom species dominate the phytoplankton community (Rojas de Mendiola, 1981; Ochoa *et al*., 1999), and their remains characterize the surface sediments (Schrader and Sorknes, 1991). Thus, the dominance of *B. costata* in the Paracas Bay observed between 2014 and 2015 (Chapter 3) is consistent with the dominance of diatoms in the phytoplankton of the bay, reported in several field surveys in the same years (Sánchez *et al*., 2019).

On the other hand, the dominance of *B. elegantissima* in the bay observed in the present study may also be related to some nutritional benefit that this species obtains from a phytodetritus that comes mainly from dinoflagellate blooms, which increased in frequency in the bay after 2016 (*e.g.*, Cuellar *et al*., 2021; Romero *et al*., 2022; Tenorio *et al*., 2022). Similar changes in the foraminiferal assemblage, due to changes in the predominant phytoplankton, were observed in other coastal environments that experienced eutrophication such as Long Island Sound (Thomas *et al*., 2004) and Osaka Bay (Tsujimoto *et al*., 2006).

Although *V. fragilis* was more abundant in percentage in P3 (Figure 4.5), the highest densities of this and the other species of the biocoenosis were in P2 (Figure 4.6). The frequently anoxic sediments of P2 also harbored the tolerant species *V. fragilis*,

N. auris, *B. peruviana*, *Discorbis* sp., and *Bulimina* sp., although these last three were disappearing towards the end of the monitoring. It was not possible to find an explanation for this disappearance since no correlation of these species with any environmental variable was observed (Figure 4.7).

4.4.3. Inferences from the dead assemblage of foraminifera

The thanatocoenosis represents an average contribution of the biocoenosis and the processes that modify them after death, such as transport and destruction of tests by dissolution (Murray and Alve, 1999a). The identification of these taphonomic processes is achieved by comparing the thanatocoenosis with the biocoenosis (Murray and Alve, 1999b). Particularly, the dissolution of calcareous layers is a very common seasonal process in coastal sediments of temperate regions. A greater penetration of oxygen into surface sediments in winter generates the oxidation of organic matter and reduced solids (FeS and FeS_2) and dissolved metabolites (H_2S, Mn^{2+} and NH_4^+), which are accumulated in anoxic conditions in the previous summer (Green and Aller, 1998). Of these, the oxidation of the reduced metabolites, and the neutralization of the strong acids that this produces, are coupled to the dissolution of calcium carbonate ($CaCO_3$) minerals from the sediments, such as the tests of dead foraminifera (Green and Aller, 2001).

In this sense, good conditions for the preservation of foraminiferal tests of thanatocoenosis only occurred in P2, since they were more abundant, by one or more orders of magnitude, than the tests numbers in P1 and P3, throughout the monitoring period (Figure 4.3). On the other hand, conditions for tests dissolution occurred in P1 and P3 by exhibiting progressively lower numbers of

thanatocoenosis' tests in the same period (Figure 4.3). The correlations of the thanatocoenosis' tests number with C:N (r = -0.82) and with $\delta^{15}N$ (r = 0.71, Figure 4.7), suggests the influence of an oxidative diagenesis of organic matter on the reducing number of tests by carbonate dissolution. Considering the presence of dissolved reduced metabolites such as H_2S and NH_4^+ in pore waters (Figure 4.2), and the potential accumulation of solid reduced metabolites in sediments of this coastal area (Flores *et al*., 2023), it is very likely that the oxidation of reduced metabolites has also occurred, promoting the active dissolution of carbonates.

Empty tests of *V. fragilis* are particularly susceptible to dissolution due to their characteristic brittleness (Haman, 1993) and have very low preservation potential in Peruvian coastal sediments (Cardich *et al.,* 2014). Considering the tests of *V. fragilis* as a more sensitive indicator of the dissolution conditions of biogenic carbonates, the degree of such conditions can be distinguished between P1 and P3. Thus, the progressive decrease of these tests in P3, compared to their disappearance in P1, after December 2020 (Figure 4.6), indicates that the dissolution was more intense in P1. On the other hand, the slight and continuous increase of these tests in P2, suggests that the preservation conditions were maintained throughout the monitoring in that station. This is consistent with the increasing predominance of oxidative processes in P1, the coexistence of anoxic conditions and oxidative processes in P3, and the predominance of anoxic conditions in P2, discussed previously.

4.5. Conclusions

The two-year monitoring of sediments revealed changing geochemical conditions of the benthic habitat in the Pisco-Paracas coastal area, associated to eutrophication, that impact on living and dead foraminiferal assemblages.

The species *Buliminella elegantissima* notoriously responded to changes in the amount of sedimentary organic matter. This study proposes this species as an indicator of eutrophication in shallow marine environments of the Peruvian coast.

Spatial differences in early diagenesis of organic matter and carbonates were identified in sediments of the three zones of this area. Off the industrial zone (P2), the reductive processes and carbonate preservation predominated. Off the Pisco River mouth (P3), there was a coexistence of reductive and oxidative processes increasing diagenesis of organic matter and carbonates. In the Paracas Bay (P1), there was an increasing predominance of oxidative processes promoting diagenesis of organic matter and carbonates. These differences were reflected in the large spatial variability of preservation of all the dead assemblage, as well as empty tests of *Virgulinella fragilis*, among the three zones confirming more redox dynamics in P1 and P3, and more stable in P2.

V. CHAPTER 5: Historical evaluation of the benthic foraminiferal diversity of the last 100 years in the Paracas Bay.

5.1. Introduction

Industrial production of anchovy meal was established on the Pisco coast in the mid-1960s, but only since the end of that decade the plants processed considerable volumes of caught anchovy (around 10% of the total catch of the entire Peruvian coast; Vásquez, 1969). Since then, the wastewater from this production has been discharged directly into the marine environment, in front of the industrialized zone of Pisco, adjacent to the Paracas Bay (Figure 5.1). In 2004, a new waste treatment system was started and a pipeline was deployed to discharge the effluents outside the coastal zone, 14 km to the northwest, and at a depth of 50 meters (Figure 5.1).

Mortality events of marine fauna occurred quite frequently during the 1990s (Cabrera Carranza, 1999) and early 2000s (Jacinto, 2014), which raised awareness on the anthropogenic eutrophication that the Pisco-Paracas coastal area was subjected. These mortality cases were associated with events of anoxia and bottom organic enrichment (Cabello *et al*., 2002), a finding that later promoted the establishment of a monitoring system of environmental conditions by the Peruvian Marine Research Institute (IMARPE). Despite this, it is not known how the development of eutrophication of the marine environment was during the period of greatest influence (1960s -2004) of organic pollution by the fishmeal industry, nor of the direct and indirect effects on the bottom water oxygen content and on the diversity of benthic organisms of the area (Pitcher *et al*., 2021).

Considering that eutrophication causes changes in the phytoplankton composition and productivity, the sedimentation of these altered organic carbon can generate changes in the ecological structure of the benthic fauna (Howarth and Marino, 2006). Thus, the objective of this chapter is to reconstruct the eutrophication process in the Paracas Bay through the analysis of changes in the organic matter content in sediments, and its accumulation rates, as well as to determine the effects of this process on the diversity of the benthic foraminiferal assemblage throughout the last 100 years.

5.2. Methods

The sediment core was collected at 11 m depth inside the Paracas Bay, within a topographic depression that crosses the bay from the northwest to the southeast (Figure 1). Sediments in the central and deepest part of the bay (> 8m) are mainly clay-silty (Solís *et al*., 2022). Circulation studies suggest that the bay is an environment of slow flows (Yzocupe, 2005; Carbonel, 2013; Arellano et al., 2023) enabling the accumulation of particulate organic matter (Velazco & Solís, 2000; Solís et al., 2022), which makes it suitable for obtaining sedimentary cores.

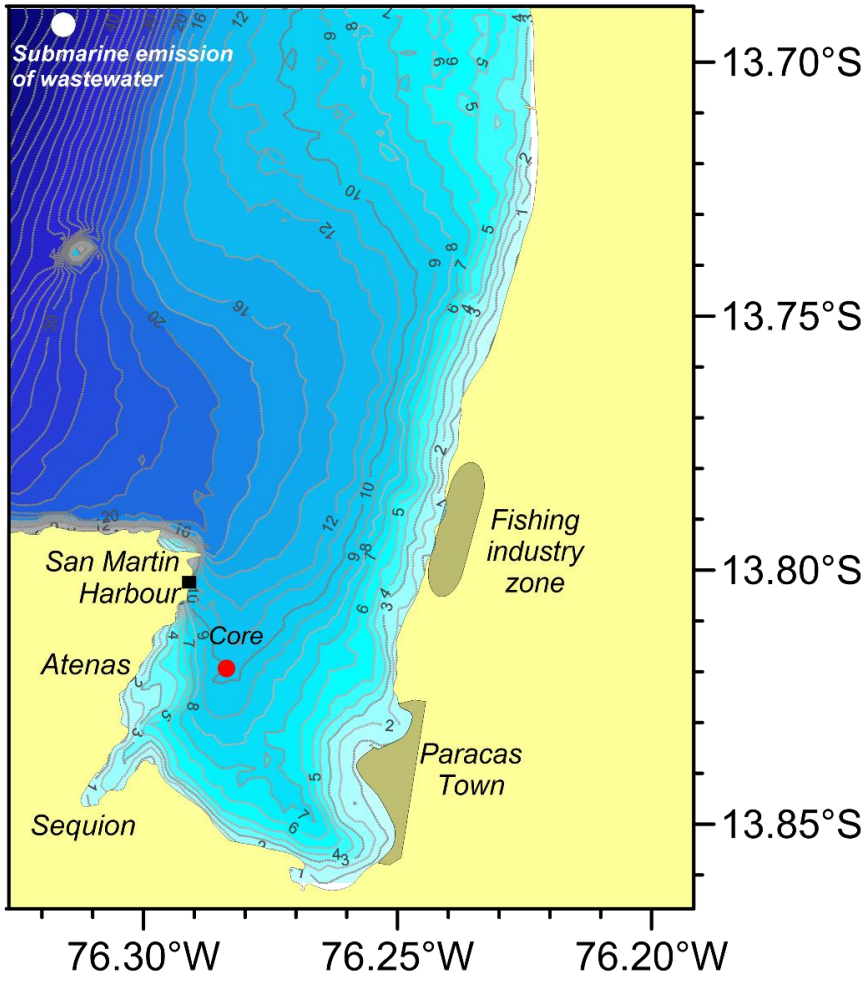

Figure 5.1. Sampling site of the sedimentary core in the Paracas Bay (in red). The site of discharge of fishmeal industry wastewater is indicated (in white). Bathymetry is represented in contours and blue color scale.

5.2.1. Collection and preparation of the sediment core

A 70 cm long PVC tube with 8 cm of internal diameter was used for collecting the sediment core. Prior to field work, the tube was cut lengthwise into two equal parts and glued in its original shape with duct tape.

The sediment core was manually collected by semi-autonomous compressor diving aboard a small artisanal fishing vessel in December 2020. Then on board, the core was kept upright to preserve its sedimentary structure, and the water excess overlying the sediments was extracted using a syringe with hose, until it was transferred to a laboratory.

The core was transported to the IMARPE – Pisco laboratory, located in Paracas town. Once there, the tube was stripped of the duct tape and then laid flat for slitting. A nylon thread was passed between the two halves of the PVC tube to cut the core lengthwise, and immediately separate the two halves. Each of these was covered with packaging film and protected by PVC caps at the ends, for transport to Lima.

5.2.2. Description and subsampling of the core

The core halves were kept refrigerated (~4°C) in the Laboratory of Marine Sciences at UPCH until their visual description. The core was also photographed and X-radiographed in order to identify sedimentary structures as sequences of laminae or bands along the core.

Subsequently, the two halves of the core were sectioned every 1 cm, starting from the surficial sediments. A subsample of known volume (1 cm x 6.03 cm^2) was extracted from each section to determine the dry bulk density (DBD) and humidity (%), for which the subsamples were wet weighed and weighed again after being dried in an oven at 50°C. The remaining sediments of each section were also dried for the analysis of the activity of the radionuclides ^{210}Pb, ^{241}Am and ^{137}Cs, as well as for total organic carbon (TOC) and total nitrogen (TN) concentrations, isotopic ratios of C and N, and the preserved foraminiferal assemblage.

5.2.3. Determination of radionuclide activities

Approximately 10 g from dry subsamples were ground in an agate mortar and used for the determination of the natural radionuclide ^{210}Pb and the artificial radionuclides ^{241}Am and ^{137}Cs activities. The total and excess activity of ^{210}Pb was determined by gamma ray measurements using coaxial high purity Germanium detectors (CANBERRA BE3830P) at the University of Kiel, Germany. The activity of the excess ^{210}Pb (^{210}Pbex) was estimated by subtracting the ^{226}Ra activity from the total ^{210}Pb activity (Moore, 1984).

5.2.4. Treatment and analysis of the organic matter indicators

Approximately 1g from dry subsamples was treated with 10% HCl to remove inorganic carbon and measure total organic carbon (TOC), total nitrogen (TN), and also the isotopic ratio of carbon (δ^{13}C) and nitrogen (δ^{15}N). These were performed with an elemental analyzer (ThermoFisher Flash HT type) coupled to an isotope mass spectrometer (Delta V Advantage type) with analytical precision of C: 0.05 %, N: 0.05 %, δ^{13}C: 0.05 ‰ and δ^{15}N: 0.1 ‰, at the Isotopic Analysis Laboratory (ALYSES) of the Institute for Development Research (IRD) in France.

5.2.5. Treatment and analysis of the preserved benthic foraminifera

Dry subsamples of about 1-2 g of the sections were treated with distilled water and 6 ml of a solution composed of 500 ml of distilled water, 400 ml of 35% hydrogen peroxide and 10 g of sodium pyrophosphate, in a water bath, for 10 minutes to remove organic matter (Machado de Almeida, 2013).

The treated subsamples were washed through a 63 μm mesh size sieve, retaining all particles greater than that size (≥ 63 μm). The retained material was transferred wet to a Whatman (No. 1) filter paper and dried in an oven at 50°C. Then, this material was observed by stereo-microscopy and the foraminifera tests were manipulated with fine brushes. Taxa to the lowest possible category were identified and abundances per taxon and total abundance were counted. The total number of the foraminiferal tests in each subsample was then standardized as the number of tests per gram of sediment (# tests g^{-1}).

5.2.6. Age model

The Constant Flux Constant Sedimentation (CFCS) and Constant Rate Supply (CRS) age models were computed from a downcore profile of ^{210}Pbex activity, using the SERAC R-package (Bruel and Sabatier, 2020), that allows the reproducibility and comparison of the models with independent markers such as the artificial radionuclides fallout and historical sedimentation events. The CFCS and CRS models both assume constant fluxes of ^{210}Pbex, but a constant and variable sedimentation rate, respectively (Appleby & Oldfield, 1992).

In order to take into account both natural and coring compactions of the sediment column, the age models were computed as a function of mass depth (g cm^{-2}) instead of just depth (cm); then sedimentation rates were expressed as mass accumulation rates (MAR) in g cm^{-2} y^{-1} (Bruel and Sabatier, 2020). Since the CRS model always generates a “too-old” age error for deeper core sections due to underestimation of ^{210}Pbex (Bruel and Sabatier, 2020), a piecewise version of CRS (CRS-pw) was also computed by using independent time markers.

5.2.7. Calculation of TOC and TN fluxes

The estimation of the flux or accumulation rate of organic particles (of TOC or TN) has the advantage of providing information on the inputs of these constituents into the system, regardless of their relative dilution in the sediment matrix (Sifeddine *et al*., 2008). Then, the flux was calculated using the following equation for every core depth interval (cm):

TOC_{acc} (kg m^{-2} y^{-1}) = [MAR; g cm^{-2} y^{-1}] x [TOC; g g^{-1}] x 10

TN_{acc} (kg m^{-2} y^{-1}) = [MAR; g cm^{-2} y^{-1}] x [TN; g g^{-1}] x 10

Where MAR is the mass accumulation rate, TOC and TN are the total organic carbon and nitrogen contents, and the factor 10 that converts g cm^{-2} to kg m^{-2}.

5.2.8. Calculation of the foraminiferal tests' accumulation

The benthic foraminiferal accumulation rate (BFAR) was also calculated for every interval based on the number of total tests per gram (# tests g-1), according to Herguera (1992):

BFAR (# tests cm^{-2} y^{-1}) = [MAR; g cm^{-2} y^{-1}] x [# tests g^{-1}]

Where MAR is the mass accumulation rate.

5.2.9. Calculation of the effective diversity of foraminifera

Using the species abundances of the preserved foraminifera, a modified version of the Shannon-Wiener diversity index (H') was calculated in each interval since H' has a significant bias when the number of species of the assemblage is

underestimated by the insufficient sample sizes (Bouchet *et al*., 2012). The corrected version (H'_{bc}) is an estimate of the Shannon entropy, developed by Chao and Shen (2003), which was calculated with the ENTROPY package in R (Hausser and Streamer, 2009). Since the Shannon entropy is not precisely an indicator of the species number, the exponential function ($\exp(H'_{bc})$) was applied (Hill, 1973), to generate an "effective number" of species that would, if they were equally abundant, produce the same H'_{bc} as the sample (Bouchet *et al*., 2012).

5.3. Results

5.3.1. Description of the core properties and dating

The sediment core was 61.5 cm long, with a general olive-green color of silty-clay sediments. Subtle color changes (from olive green to slightly greyer tones) were observed in layers between 16 and 18 cm, 24 and 36 cm, 45 and 52 cm, and between 56 and 61 cm (Figure 5.2). The X-radiography only revealed a sequence of clearer and darker banded sediments corresponding to those layers. The DBD and humidity also exhibited relative increases and decreases (between 0.20 and 0.55 g cm^{-3}, and between 65% and 80%, respectively) in the same layers mentioned above.

The TOC varied between 2.5% and 6% with an increasing trend upwards in the upper 10 cm, a drop from 4% to 2.5% between 16 and 18 cm (very similar to that of humidity and ^{210}Pbex), and smaller variations in deeper sections (Figure 5.2). The activity of ^{210}Pbex (>0) was detected downcore until 50 cm, decreasing exponentially with depth, but with pronounced non-monotonic variations between 10 and 20 cm.

The computation of the ^{210}Pbex activities with respect to mass-depth, in semi-logarithmic diagram (Figure 5.3a), exhibited a good linear relationship (r = 0.942) for a CFCS model with a constant MAR of 0.173 g cm^{-2} y^{-1}. The sediment sections of consistent variability in all the sedimentary properties, between 16 and 18 cm, correspond to the mid-1990s in this age model (Table A.D1). Due to the non-monotonic variations of the ^{210}Pbex activities, a CRS age model was also computed, producing a MAR that varied between 0.09 and 0.23 g cm^{-2} y^{-1} (Table A.D2), and exhibiting older years for deeper sediment sections (> 30 cm) than the CFCS model (Figure 5.3c).

Although the ^{137}Cs and ^{241}Am profiles exhibited low activities, and degraded signals without notorious peaks (Figure 5.3b), the ^{137}Cs first fallout (1955) can be used as an independent marker for a piecewise CRS (CRS-pw). Along with that, the age range resulting from the CFCS model, and the El Niño 1997-1998 event, which triggered the maximum recorded levels of the Pisco River flow (INRENA, 1999), were also considered for computing a CRS-pw model, using these known ages for the sections 38, 50 and 18 cm, respectively. Then, the CRS-pw model reconstructed the last 100 years within the upper 50 cm of the core (Figure 5.3c), with a MAR that varied between 0.02 and 0.29 g cm^{-2} y^{-1} (Table A.D3).

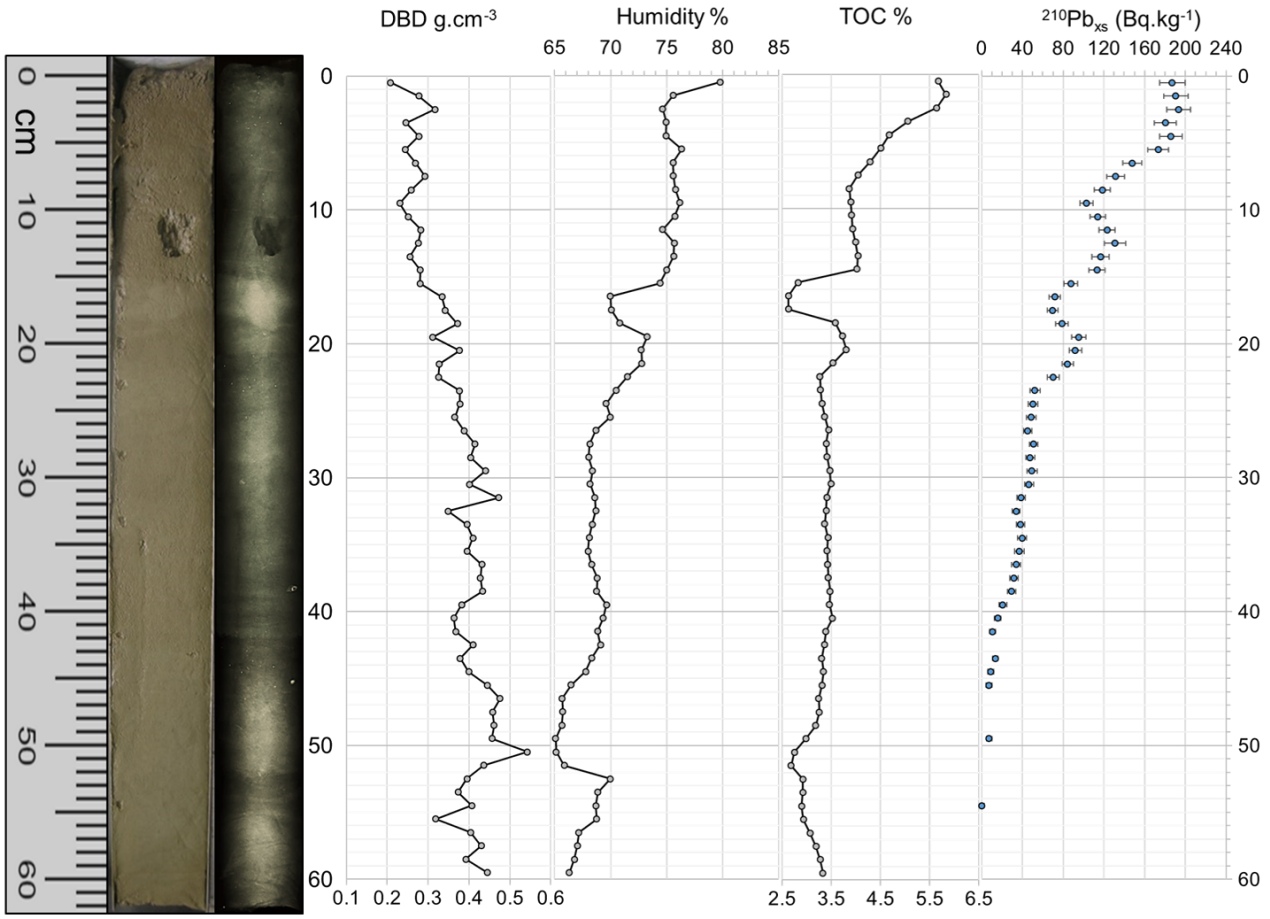

Figure 5.2. Sediment core properties: (a) Photography and X-ray radiography in a length scale in centimeters, and (b) profiles of dry bulk density (DBD), percentage humidity, percentage of Total Organic Carbon (TOC %), and activity of radionuclide Pb (^{210}Pbxs).

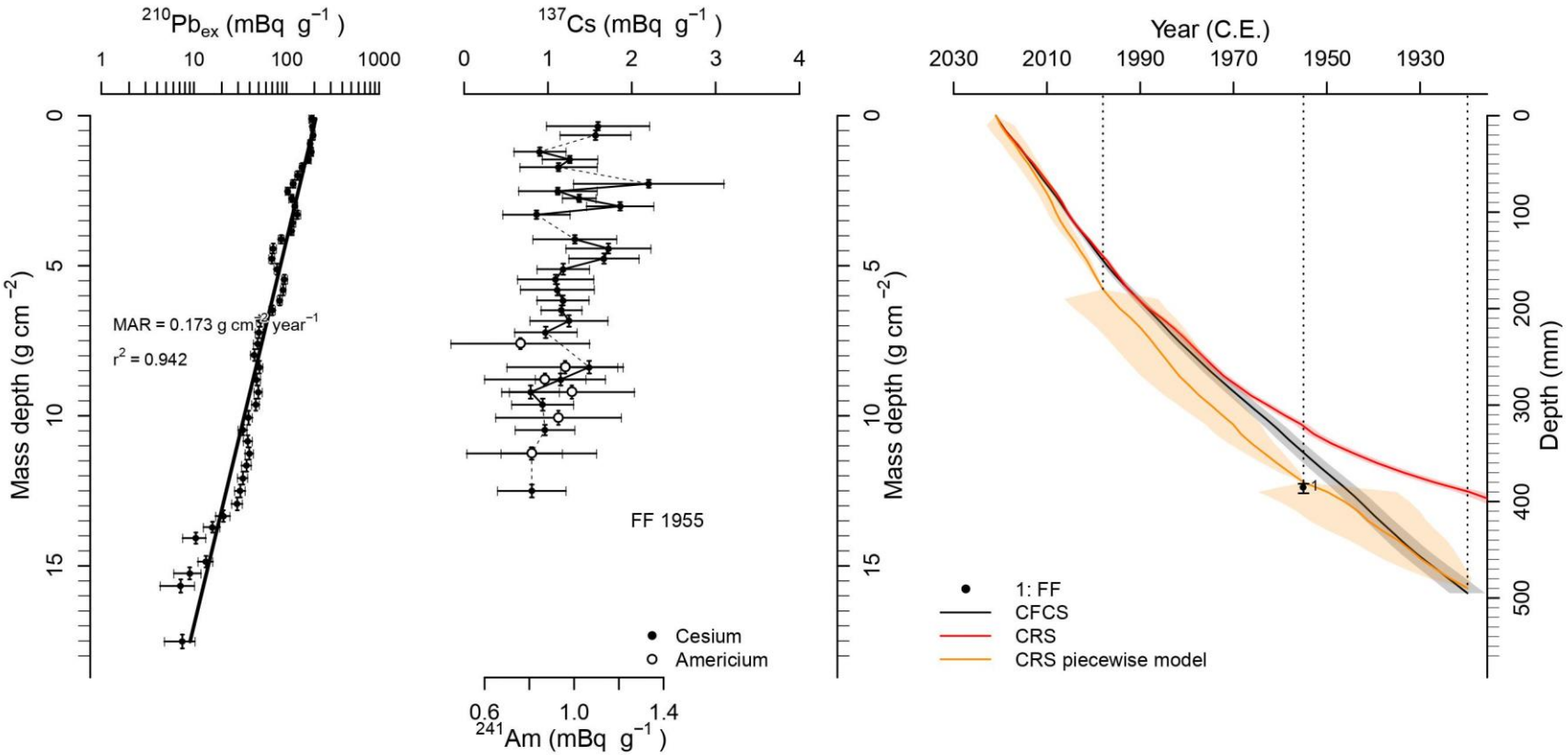

Figure 5.3. Profile of the activity of (a) ^{210}Pb in excess (^{210}Pbex), and of (b) ^{137}Cs and ^{241}Am, in relation to the mass depth (g cm^{-2}) of the core. (c) Age models in relation to the core depth: Constant flux constant supply (CFCS), Constant rate of supply (CRS), and CRS piecewise.

5.3.2. Development of organic matter content in sediments

Between the 1950s and the early 1980s, the total organic carbon (TOC) and total nitrogen (TN) content of the sediments varied very little, with 3.40 ± 0.06 % and 0.41 ± 0.003 %, respectively (Figure 5.4a). Since the early-1990s until about 19997, both indicators were higher (3.67 ± 0.13 % and 0.45 ± 0.01 %, respectively), followed by the drastic fall in El Niño 1997-1998 event (2.70 ± 0.11 % and 0.34 ± 0.02 %, respectively), and then again, the increase in their values in the 2000s (3.97 ± 0.07 % and 0.50 ± 0.01 %, respectively). Subsequently, in the 2010s, TOC and TN exhibited an increase trend, with the maximum values between 2018 and 2020 (5.72 ± 0.10% and 0.84 ± 0.02%, respectively).

The C:N ratio exhibited differences in three main periods (Figure 5.4a): the values between the 1950s and the 1970s, were the highest of all the core (8.37 ± 0.08), then slightly lower values until the end of the 2000s (7.99 ± 0.09), and subsequently a progressive decrease to its minimum values between 2018 and 2020 (6.79 ± 0.09). Since TOC and TN varied in a very similar way throughout the core, the decrease in the C:N ratio indicated a higher increase of TN relative to TOC.

Unlike the percentage content of TOC and TN, the calculated accumulation rates of TOC and TN exhibited a notorious increasing trend throughout the period 1950-2020 (from 2.5 to 10.6 kg m^{-2} y^{-1}, and from 0.3 to 1.5 kg m^{-2} y^{-1}, respectively), with accumulation peaks about 1970, in the mid-1980s, and in the second half of the 2000s (Figure 5.4b). The highest increasing trend and accumulation rates of TOC and TN occurred in the most recent period, between 2016 and 2020.

5.3.3. Stable isotope ratios of C and N

The $\delta^{13}C$ had a short range of variation (from -18.8 to -19.9 ‰), with a decreasing trend from the 1950s towards the end of the 1990s (Figure 5.4c), and an abrupt decrease (more negative values) corresponding to El Niño 1997-1998 event (-19.84 ± 0.05 ‰). After this, $\delta^{13}C$ was higher (-19.53 ± 0.05 ‰) until the mid-2010s and then progressively increased until 2020 (from -19.52 to -19.09 ‰). On the other hand, $\delta^{15}N$ varied in a wide range (from 7.6 to 9.7 ‰). It exhibited minimum values during the El Niño 1997-1998 event (7.89 ± 0.29 ‰), whereas peaks of maximum values (9.38 ± 0.18 ‰) occurred about 1970, the late-1980s, and mid-2000s.

5.3.4. Abundance and diversity of preserved foraminifera

The microfossil samples revealed notorious changes in the benthic foraminiferal accumulation rate (BFAR, Figure 5.4d) in the period 1950-2020, with very low values (21.4 ± 11.1 tests cm^{-2} y^{-1}) in the 1950s, as well as in the 2010s. On the other hand, a greater accumulation (114.4 ± 19.8 tests cm^{-2} y^{-1}) was observed in a short period about the late-1960s, and a longer period from early 1980s to early 1990s.

Twelve taxa of benthic foraminifera were identified among all the samples. However, the effective number of species ($exp(H'_{bc})$), calculated for each sample, exhibited lower values (3.6 ± 0.6) between the 1950s and the late 1960s, and from the mid-2000s to 2020 (Figure 5.4d), whereas its highest values (6.5 ± 1.5) occurred from the early-1980s to early 2000s.

5.3.5. Species of the benthic foraminiferal assemblage

The foraminiferal taxa identified were *Bolivina costata*, *Buliminella elegantissima*, *Nonionella auris*, *Virgulinella fragilis*, *Buccella peruviana*, *Discorbis* sp., *Bulimina* sp., *Ammonia* sp., *Rotaliammina* sp., *Cibicides* sp., *Fursenkoina* sp., and *Bolivina* sp. However, only *B. costata*, *B. elegantissima*, *N. auris*, and *Bulimina* sp., exceeded 1% of the total abundance (Table A.D4).

B. costata was the dominant species of the preserved assemblage throughout the reconstructed period (usually > 50%), except in a short period in the mid-1980s when it was surpassed by *N. auris*, and in the recent period between 2016 and 2020 when it was surpassed by *B. elegantissima*, which was historically a subdominant species in the assemblage (usually > 20%, Figure 5.4e).

Apart from its peak abundance in the mid-1980s, *N. auris* exhibited abundances generally greater than about 5% from the late 1960s to the early 2000s, and subsequently exhibited abundances less than 5% until 2020. The abundance of *Bulimina* sp., was always less than 4%, however it was consistently lower between 2010 and 2020, ranging from 1.2% at the beginning of the 2010s to 0% towards 2020 (Figure 5.4e; Table A.D4).

The tests of rare species (*V. fragilis*, *Discorbis* sp., *Cibicides* sp., *B. peruviana*, *Ammonia* sp., *Rotaliammina* sp., and *Fursenkoina* sp.) accumulated more during the mid-1980s and late 1990s (Figure 5.4f). Moreover, the species *V. fragilis*, *Discorbis* sp., and *Cibicides* sp., were only present in those periods.

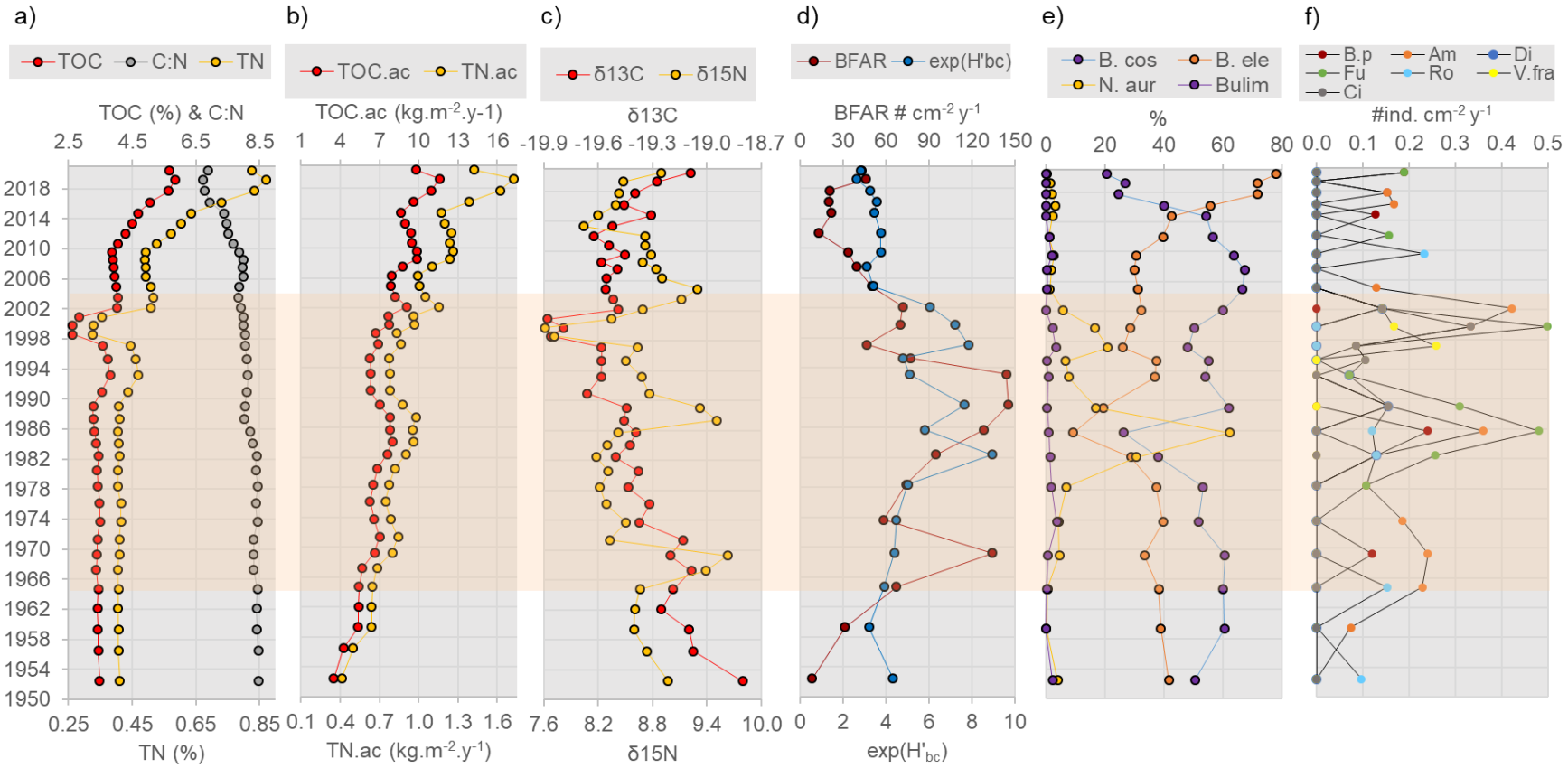

Figure 5.4. Age distribution of geochemical and palaeoecological indicators in the Paracas Bay. (a) % of TOC, TN, and the C:N ratio. (b) Accumulation rates of TOC and TN. (c) Isotopic ratios of ^{13}C and ^{15}N. (d) Accumulation rate of tests (BFAR) and diversity of foraminifera. (e) Abundance of main foraminiferal species. (f) Accumulation rate of rare species' tests. The light red band represents the fishmeal-induced eutrophication period.

5.4. Discussion

5.4.1. Scope of the age model and historical changes

The piecewise CRS age-depth model provided a geochronology and sedimentation rates for the last 100 years, a period long enough for assessing the variability of sediment geochemistry of the Paracas Bay associated with the fishmeal industrial activity. The use of the CRS-pw method was justified by the non-monotonic variations of the ^{210}Pbxs profile (Figure 5.3a), which revealed irregularities in sedimentation associated with a changing MAR (Table A.D3) that is typical of coastal environments exposed to anthropogenic processes (Lubis, 2006).

The observed degraded signal of the artificial radionuclides ^{137}Cs and ^{241}Am is quite common for coastal marine sediments, and can be caused by the physical or biological disturbance that mix surface sediments (Appleby, 2002, 2008), which is very likely in shallow environments such as the Paracas Bay. In fact, even in a sediment core from deeper and more stable environments of the Peruvian continental shelf, a low and constant activity of ^{241}Am was observed with respect to the depth of the sediments (Koide and Goldberg, 1982).

A probable mixing of the upper (surficial) sediments could generate some error in the ages estimated by the CRS model. In this regard, Appleby (2002) pointed out that a mixing zone that covers up to 10 years of accumulation would generate a maximum error of around two years in this model. This magnitude of error may not be a problem when considering processes and changes on a decadal scale, as in this study, but it would be significant under an interannual scale approach.

In particular, the El Niño 1997-1998 event, which produced the maximum recorded flow of the Pisco River in the summer of 1998 (INRENA, 1999), would have caused the drastic change observed of minimum elemental and isotopic values of C and N (Figure 5.4). The CFCS and CRS models marked these minimum values in the mid-1990s (Table A.D1 and A.D2), but there was no other stronger environmental event in that decade. This mismatch between the modelled ages and the El Niño event might be due to enhanced biological mixing associated with increased benthic oxygenation in the Peruvian shallow and sublittoral environments (Tarazona and Arntz, 2001; Gutiérrez et al, 2008). Then, the layers of minimum elemental and isotopic values were considered as a historical sedimentation event in 1998 for computing the piecewise version of the CRS model (CRS-pw).

5.4.2. Origin of the sedimentary organic matter

The main sources of organic matter in coastal environments have distinctive $\delta^{13}C$ and C:N signals, which can be preserved for a long time despite diagenetic modifications (Meyers, 1994). The short range of variation of these indicators since the 1940s (C:N from 6.7 to 8.5, and $\delta^{13}C$ from -19.9 to -18.8) evidenced a predominantly marine origin of the organic matter (Lamb *et al*., 2006).

However, the short period of minimum values of TOC and TN, and of isotopic ratios of C and N, around 1998 (Figures 5.4a and 5.4c) suggests an unusual mixing of phytodetritus with other type of organic material in the bay, which would be of terrestrial origin due to its typically lower isotopic ratios compared to those of phytodetritus (Lamb *et al*., 2006; Montoya, 2008). A significant amount of this

terrestrial material may have been delivered by the extreme discharge of the Pisco River in 1998, and then deposited in Paracas Bay.

5.4.3. Eutrophication signs in the bay's sediments

When transforming the percentage values of TOC and TN to their accumulation rates, it was possible to observe a notorious increase trend of C and N flux to the sediments starting in the 1960s (Figure 5.4b). However, the highest accumulation rates of C and N (> 10 kg m^{-2} y^{-1} and > 1.3 kg m^{-2} y^{-1}, respectively) did not occur in the period of fishmeal-induced eutrophication but in the late 2010s, reflecting a recent and intense eutrophication of the bay, with accumulation rates of one degree of magnitude greater than those of other eutrophic ecosystems on the Peruvian coast such as mangroves (Pérez *et al*., 2020) and marshes (Pérez *et al*., 2022).

Another sign of eutrophication is the decrease in the C:N ratio, due to the greater increase of TN relative to TOC, especially in the last two decades when the strong decrease of C:N coincides with an increase of $\delta^{13}C$ of organic matter, trends that are usually associated with higher primary productivity of phytoplankton (Meyers, 2002). The increase in phytoplankton productivity may be linked to a changing species composition due to an increase in the abundance of eutrophic taxa (Augustinus *et al*., 2006), suggested by the observed increasing trend in the number of dinoflagellate cysts throughout this same sediment core (Alvarado *et al*., 2022).

The $\delta^{15}N$ of sediments increases by a preferential removal of ^{14}N during the bacterial decomposition of organic matter (Thornton and McManus, 1994). This is magnified by eutrophication and oxygen depletion as they produce denitrification, which leads to the preferential loss of ^{14}N nitrates, not only in the sediments but

also in the water column, leaving the isotopically heavier nitrates available for the phytoplankton, generating a phytodetritus with a more enriched $\delta^{15}N$ (Bratton *et al*., 2003). Given the eutrophication trend since the 1960s, the $\delta^{15}N$ enrichment peaks would indicate periods of intense anoxic conditions. Although surface sediments could have experienced seasonal oxygenation, the isotopic impact of intense denitrification on the substrate is usually much greater than that of prolonged aerobic decomposition (Bratton *et al*., 2003). The enrichment of $\delta^{15}N$ at the end of the period of fishmeal-induced eutrophication (Figure 5.4c), coincides with the frequent anoxic conditions in the area between 2000 and 2003 recorded in an environmental monitoring program established since 1999 (Jacinto 2014).

5.4.4. Variations of the foraminiferal preserved assemblage

Throughout the first 40 cm of the core, the assemblage of benthic foraminifera was dominated by *B. costata* and *B. elegantissima*, which also characterizes the living assemblages of the Pisco-Paracas coastal area (Chapter 3). The dominance of these species throughout the core, as well as the abundance of *N. auris* (Figure 5.4e), suggest that benthic conditions in the bay were similar to those of the inner shelf bottoms even before the fishmeal-induced eutrophication. A high organic load, oxygen depletion in the first millimeters of surficial sediments, and the presence of sulfide in pore waters are typical characteristics of these bottoms (Cardich *et al*., 2015), although they would be more exposed to oxygenation events in the bay (at least seasonally), given its shallow depth (<15 m).

The four most abundant species along the core (*B. costata*, *B. elegantissima*, *N. auris*, *Bulimina* sp.) are known to be infaunal and dominant under conditions of

oxygen depletion (Bernhard and Sen Gupta, 1999; Cardich *et al*., 2015), and have adaptations to tolerate even sulfidic conditions (Bernhard and Bowser, 2008; Glock *et al*., 2019). The observed increase of species number in the period of fishmeal-induced eutrophication, the peak of *N. auris* in the mid-1980s, and the change of dominant species from *B. costata* to *B. elegantissima* in the 2010s, are only variations of the same characteristic structure of the foraminiferal assemblage from shallow environments of the central Peruvian coast (Merma, 2020).

5.4.5. Effect of the fish meal – induced eutrophication on foraminifera

The period of greater accumulation of foraminiferal tests (BFAR > 100 tests $cm^{-2}.y^{-1}$), and of greater effective diversity ($exp(H'_{bc}) > 5$), occurred within the fishmeal-induced eutrophication period (Figure 5.4d), whereas the changing trend of the dominant species occurred recently in the 2010s (Figure 5.4e). This initial apparent positive effect of fishmeal-induced eutrophication on the tests' accumulation, and on species diversity, was not expressed in changes of the community structure, but rather in the increase of all foraminiferal abundance and the accumulation of rare taxa (Figure 5.4f). Therefore, the preservation potential of the calcareous tests would have improved in that period, especially in lapses around 1970 and 1994, which were years of greater fishmeal production due to maximum anchovy landings in the Pisco Harbor (Figure 5.5).

The great accumulation of the calcareous tests is likely to happen in persistent anoxic conditions since they promote a reducing environment that allows a greater preservation of biogenic carbonates, as it occurred in the sediments of the industrial zone in the monitoring study (Chapter 4). In that sense, enriched $\delta^{15}N$ values in the

core, indicating anoxic conditions, occurred in lapses in which there were also BFAR peaks (Figure 5.4c and 5.4d), giving more support to that argument.

The rare species *Ammonia* sp., *V. fragilis*, *Discorbis* sp., *Cibicides* sp., and *Fursenkoina* sp., which showed up in the preserved assemblage in the period of fishmeal-induced eutrophication, are also known to tolerate low-oxygen or anoxia conditions (Leiter and Altenbach, 2010; Bernhard and Sen Gupta, 1999). In addition, the occurrence of *V. fragilis* tests only in the samples corresponding to this period is another sign of better preservation conditions in the sediments associated with persistent anoxia, considering their low preservation potential in the sediments of the Peruvian coast (Cardich *et al*., 2014). It is likely that the persistent anoxic (and sulfidic) conditions currently observed in the sediments of the industrial zone (Chapter 4), expanded to the center of the bay in the period of fishmeal-induced eutrophication, improving the preservation capacity of the foraminiferal tests and allowing that even rare species left tests in the preserved assemblage.

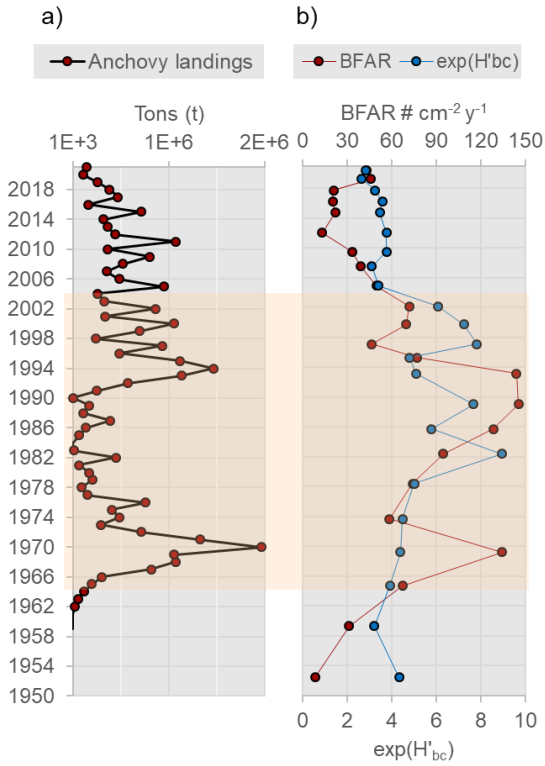

Figure 5.5. Similar variability of the (a) anchovy landings in the Pisco Harbor, and the (b) accumulation rate of foraminiferal tests (BFAR). Anchovy landings data came from the official records of IMARPE.

5.4.6. Change in the dominance

An interesting finding was the coincidence of the increasing accumulation rates of C and N in the 2010s (Figure 5.4b) and the change of the dominant species in the preserved foraminiferal assemblage: from *B. costata* (endemic to the southeast Pacific) until about 2015, to *B. elegantissima* (cosmopolitan species) up to the present (Figure 5.4e), which was also noticed when comparing the living assemblages of the bay in Chapter 3 and 4. Several studies found that the dominance of *B. elegantissima* in living assemblages was associated with anthropogenic processes of eutrophication and organic enrichment in sediments of coastal

environments (Bandy *et al*., 1964; Eichler and Barker, 2020), since this species tends to exhibit a direct relationship with the organic carbon and nitrogen content in the sediments (McGann, 2009).

In coastal sediments, benthic foraminifera populations are strongly influenced not only by the amount but also the type of organic matter (Loubere and Fariduddin, 1999). Although the organic matter found downcore was predominantly marine, its composition may have changed according to the predominant taxonomic group of the phytoplankton community (*e.g.*, diatoms or dinoflagellates), triggering potential changes of the foraminiferal assemblage (Gooday *et al*., 2009). For instance, it was reported that decadal changes in the type of dominant phytoplankton group in the water column (from diatoms to dinoflagellates), responding to the increase of nitrogen-rich effluents and Nitrogen/Silicon ratio, gave rise to changes of the dominant foraminiferal species in sediments of coastal environments such as the Long Island Sound (Thomas *et al*., 2004) and Osaka Bay (Tsujimoto *et al*., 2008).

Several field surveys between 2013 and 2015 observed that diatoms were the dominant group of phytoplankton abundance in the Paracas Bay (Sánchez *et al*., 2019). Nevertheless, in recent decades, an increasing frequency of harmful algal bloom (HAB), mainly caused by dinoflagellate species and associated with mortality of marine fauna, have been recorded on the Peruvian coast (Cabello *et al*., 2002; Sánchez *et al*., 2017, 2021). Specifically, shallow embayments (<30 m depth) of the Peruvian coast are likely to be hotbeds for dinoflagellate resistance cysts, since these areas exhibit a larger number of HABs (Sánchez *et al*., 2021). In Paracas Bay, since the 1990s many HABs originated by dinoflagellate species have been

increasingly reported, which were mostly concentrated outside the bay, in the adjacent coast of Pisco (Jacinto *et al*., 1996; Guzmán *et al*., 1997). A particular case was a HAB that occurred in June 2000, caused by the dinoflagellate *Prorocentrum micans*, which produced anoxic conditions at the bottoms of Pisco and Paracas, causing mortality of benthic fauna (Cabello *et al*., 2002). Since 2017, the species *Prorocentrum cordatum* increased its densities inside the bay compared to previous periods, which was related to its mixotrophic strategy that is capable of modifying the phytoplankton community (Tenorio *et al*., 2022). Blooms of another dinoflagellate, *Alexandrium ostenfeldii*, also increased in abundance and frequency around 2017-2018, which may have benefited from recurrent stratified conditions in the water column of the bay (Cuellar *et al*., 2021).

The greater water column mixing and less frequent stratification observed in in the bay (chapter 2) would have been able to maintain a phytoplankton community more dominated by diatoms until 2016-2017. On the other hand, the conditions of higher temperatures and longer stratification outside the bay (Arellano *et al*., 2023; Chapter 2) might favor a higher frequency of dinoflagellate blooms, modifying the phytoplankton community, and in turn, the phytodetritus composition, long before than within the bay.

5.5. Conclusions

The organic matter indicators in the sediment core (TOCac, TNac, C:N, $\delta^{13}C$ and $\delta^{15}N$) evidenced a process of eutrophication of the Paracas Bay that increased in the period of direct influence of fishmeal wastewater (1964-2004), although it reached a maximum organic enrichment recently, between 2010 and 2020.

Eutrophication in the period of industrial influence generated the highest rates of foraminiferal test accumulation in the bay, including rare species with low preservation potential, due to the improvement of the bio-carbonates preservation in the sediments associated with more persistent anoxic conditions in the bottom.

Although changes in tests preservation, the structure of the benthic foraminiferal assemblage had little variations during the last 100 years, suggesting that hypoxia and organic-rich sediments were natural features of the Paracas Bay bottom prior to the fishmeal industry establishment in the adjacent area. However, the change of dominant foraminiferal species in the assemblage, from *Bolivina costata* to *Buliminella elegantissima*, can be an indicator of induced and severe eutrophic conditions, associated with a change in the dominant group of phytoplankton community and, in turn, in the phytodetritus composition.

The switch of the dominant species of the benthic foraminiferal assemblage in the Paracas Bay, from *B. costata* to *B. elegantissima*, just recently between 2016 and 2017, can be reflecting a greater capacity of the bay of mitigating the eutrophication effects than the adjacent coastal zone, by exhibiting less persistent stratified conditions that hindered a rapid change of the phytodetritus composition.

VI. DISCUSSION

While Pisco-Paracas is a small coastal area without prominent environmental gradients, it is susceptible to both natural hypoxia and human-induced stress. The interaction of these factors poses a potential threat to its ecological integrity. Therefore, it is essential to identify organisms that serve as sentinels of environmental changes and indicators of the ecological quality of this coastal area.

This study presented evidence of the relationship between environmental conditions and the assemblages of both live and dead benthic foraminifera in chapters 3 and 4, highlighting the environmental preferences of certain species, such as *Buliminella elegantissima* for the sedimentary organic matter.

However, the lack of major alterations in the preserved assemblage of benthic foraminifera of the Paracas Bay, between 1950 and 2010, with changes mainly in test accumulation rates observed in chapter 5, reflects good ecological quality conditions in the bay throughout those decades, including the period of fishmeal-induced eutrophication.

Despite the continuous eutrophication of the entire Pisco-Paracas coastal area since the 1960s, *B. elegantissima* dominated the living assemblage in most zones, but except in the Paracas Bay, in which *Bolivina costata* did, just until 2016-2017. This is maybe reflecting a greater capacity of the bay of mitigating the effects of eutrophication rather than the adjacent coastal zones, likely related to greater water column mixing and less frequent stratification observed in in the bay (chapter 2).

While the dominance of *B. costata* indicated favorable ecological conditions in the bay, the current dominance of *B. elegantissima* is indicative of severe eutrophication. The origins of this condition still require further research, but it may be linked to processes associated with climate change, such as increased water stratification and the proliferation of harmful algal blooms. This idea is supported from paleo-ecological studies in other coastal areas, revealing preserved assemblages dominated by *B. elegantissima* under varying climatic conditions over the past 5 000 years (Vilela *et al*., 2014).

VII. CONCLUSIONS

According to the general objective and stated hypothesis, this study concludes:

The fishmeal-induced eutrophication (from 1964 to 2004), in the Pisco-Paracas coastal area, did not affect the structure of the benthic foraminiferal assemblage of the Paracas Bay, which rejects the proposed hypothesis. The ecological quality of Paracas Bay, in turn, was not degraded in that period.

Nevertheless, the bay sediments increasingly accumulated phytoplankton-derived organic matter, which, along with changes associated with other natural or anthropogenic processes, would have led a recent change of the dominant foraminiferal species (from *Bolivina costata* to *Buliminella elegantissima*) that reflects current severe eutrophic conditions.

VIII. REFERENCES

Aguirre-Velarde, A., Jean, F., Thouzeau, G., & Flye-sainte-marie, J. 2016. Effects of progressive hypoxia on oxygen uptake in juveniles of the Peruvian scallop, *Argopecten purpuratus* (Lamarck, 1819). Aquaculture, 451, 385–389.

Aguirre-Velarde, A., Jean, F., Thouzeau, G., & Flye-sainte-marie, J. (2016). Effects of progressive hypoxia on oxygen uptake in juveniles of the Peruvian scallop, Argopecten purpuratus (Lamarck, 1819). Aquaculture, 451, 385–389.

Aguirre-Velarde, A., Thouzeau, G., Jean, F., Mendo, J., Cueto-vega, R., Kawazo-delgado, M., Vásquez-spencer, J., Herrera-sanchez, D., Vega-espinoza, A., & Flye-sainte-marie, J. (2019). Chronic and severe hypoxic conditions in Paracas Bay, Pisco, Peru: Consequences on scallop growth, reproduction, and survival. Aquaculture, 512(June), 734259. https://doi.org/10.1016/j.aquaculture.2019.734259

Aller, R. C. (1994). Bioturbation and remineralization of sedimentary organic matter: effects of redox oscillation. Chemical Geology, 114(3–4), 331–345. https://doi.org/10.1016/0009-2541(94)90062-0

Alperin, M., Bernasconi, E., & Cusminsky, G. C. (2008). Asociaciones de foraminíferos bentónicos recientes de la Plataforma Continental Argentina (39°-43° S y 58°- 65° O) analizadas con métodos estadísticos para datos composicionales. Ameghiniana, 45(2).

Alperin, M. I., Cusminsky, G. C., & Bernasconi, E. (2011). Benthic foraminiferal morphogroups on the Argentine continental shelf. Journal of Foraminiferal Research, 41(2). https://doi.org/10.2113/gsjfr.41.2.155

Alvarado, A., Gutiérrez, D., & Cuéllar-Martínez, T. (2022, September 21). Changes in productivity in the Paracas Bay through the study of dinoflagellate cysts. *Open Science Conference on Eastern Boundary Upwelling Systems (EBUS): Past, Present and Future & Second International Conference on the Humboldt Current System*.

Alve, E. (1995). Benthic foraminiferal responses to estuarine pollution: a review. Journal of Foraminiferal Research, 25(3), 190–203. https://doi.org/10.2113/gsjfr.25.3.190

Alve, E., Lepland, A., Magnusson, J., & Backer-Owe, K. (2009). Monitoring strategies for re-establishment of ecological reference conditions: Possibilities and limitations. Marine Pollution Bulletin, 59(8–12). https://doi.org/10.1016/j.marpolbul.2009.08.011

Anderson, M. J. (2017). Permutational Multivariate Analysis of Variance (PERMANOVA). In Wiley StatsRef: Statistics Reference Online. https://doi.org/10.1002/9781118445112.stat07841

Appleby, P. G. (2002). Chronostratigraphic techniques in recent sediments. In W. L. Last & J. P. Smol (Eds.), Tracking environmental change using lake sediments. Volume 1: Basin analysis, coring, and chronological techniques (pp. 171–203). Kluwer Academic Publishers.

Appleby, P. G. (2008). Three decades of dating recent sediments by fallout radionuclides: a review. The Holocene, 18(1), 83–93.

Appleby, P. G., & Oldfield, F. (1992). Application of lead-210 to sedimentation studies. In Uranium Series Desiquilibrium: Application to Earth, Marine and Environmental Science.

Arellano, C., Echevin, V., Merma-Mora, L., Chamorro, A., Gutiérrez, D., Aguirre-Velarde, A., Tam, J., & Colas, F. (2023). Circulation and stratification drivers during the summer season in the upwelling bay of Paracas (Peru): A modelling study. Continental Shelf Research, 254, 104923. https://doi.org/10.1016/j.csr.2022.104923

Arntz, W. E., Gallardo, V. A., Gutiérrez, D., Isla, E., Levin, L. A., Mendo, J., Neira, C., Rowe, G. T., Tarazona, J., & Wolff, M. (2006). El niño and similar perturbation effects on the benthos of the Humboldt, California and Benguela Current upwelling ecosystems. Advances in Geosciences, 6, 243–265. https://doi.org/10.5194/adgeo-6-243-2006

Augustinus, P., Reid, M., Andersson, S., Deng, Y., & Horrocks, M. (2006). Biological and geochemical record of anthropogenic impacts in recent sediments from Lake Pupuke, Auckland City, New Zealand. Journal of Paleolimnology, 35(4). https://doi.org/10.1007/s10933-005-5306-8

Bakun, A., & Weeks, S. J. (2008). The marine ecosystem off Peru: What are the secrets of its fishery productivity and what might its future hold? Progress in Oceanography, 79(2–4). https://doi.org/10.1016/j.pocean.2008.10.027

Bandy, O. L., Ingle, J. C., & Resig, J. M. (1964). Foraminifera, Los Angeles County outfall area, California. Limnology and Oceanography, 9(1), 124–137. https://doi.org/10.4319/lo.1964.9.1.0124

Bernhard, J. M. (2003). Potential symbionts in bathyal foraminifera. Science, 299(5608). https://doi.org/10.1126/science.1077314

Bernhard, J. M., & Bowser, S. S. (2008). Peroxisome proliferation in foraminifera inhabiting the chemocline: An adaptation to reactive oxygen species exposure? The Journal of Eukaryotic Microbiology. https://doi.org/10.1111/j.1550-7408.2008.00318.x

Bernhard, J. M., & sen Gupta, B. K. (1999). Foraminifera of oxygen-depleted environments. In B. K. sen Gupta (Ed.), Modern Foraminifera (pp. 201–216). Kluwer Academic Publishers. https://doi.org/10.1007/0-306-48104-9_12

Bernhard, J. M., Tsuchiya, M., & Nomaki, H. (2018). Ultrastructural observations on prokaryotic associates of benthic foraminifera: Food, mutualistic symbionts, or parasites? Marine Micropaleontology, 138. https://doi.org/10.1016/j.marmicro.2017.09.001

Bertrand, A., Ballón, M., & Chaigneau, A. (2010). Acoustic observation of living organisms reveals the upper limit of the Oxygen Minimum Zone. Plos One, 5(4), e10330–e10330. https://doi.org/10.1371/journal.pone.0010330

Borcard, D., Gillet, F., & Legendre, P. (2018). Numerical Ecology with R (2nd ed.). Springer International Publishing.

Bouchet, V. M. P., Alve, E., Rygg, B., & Telford, R. J. (2012). Benthic foraminifera provide a promising tool for ecological quality assessment of marine waters. Ecological Indicators, 23(2012), 66–75. https://doi.org/10.1016/j.ecolind.2012.03.011

Bouchon, M., Ñiquen, M., & Ttito, H. (2018). Estadísticas de la pesquería pelágica en la costa peruana (1959- 2015). Inf Inst Mar Perú, 45(4), 397–562. https://hdl.handle.net/20.500.12958/3302

Bratton, J. F., Colman, S. M., & Seal, R. R. (2003). Eutrophication and carbon sources in Chesapeake Bay over the last 2700 yr: Human impacts in context. Geochimica et Cosmochimica Acta, 67(18). https://doi.org/10.1016/S0016-7037(03)00131-5

Breitburg, D., Levin, L. A., Oschlies, A., Grégoire, M., Chavez, F. P., Conley, D. J., Garçon, V., Gilbert, D., Gutiérrez, D., Isensee, K., Jacinto, G. S., Limburg, K. E., Montes, I., Naqvi, S. W. A., Pitcher, G. C., Rabalais, N. N., Roman, M. R., Rose, K. A., Seibel, B. A., … Zhang, J. (2018). Declining oxygen in the global ocean and coastal waters. Science, 359(eaam7240). https://doi.org/10.1126/science.aam7240

Bruel, R., & Sabatier, P. (2020). serac: A R package for ShortlivEd RAdionuclide chronology of recent sediment cores. Journal of Environmental Radioactivity, 225. https://doi.org/10.1016/j.jenvrad.2020.106449

Cabello, R., Tam, J., & Jacinto, M. E. (2002). Procesos naturales y antropogénicos asociados al evento de mortalidad de conchas de abanico ocurrido en la bahía de Paracas (Pisco, Perú) en junio del 2000. Revista Peruana de Biología, 9(2), 49–65. https://doi.org/10.15381/rpb.v9i2.2528

Cabrera Carranza, C. F. (1999). Compatibilidad ambiental de la industria de harina de pescado en Paracas-Pisco. Revista Del Instituto de Investigación de La Facultad de Minas, Metalurgia y Ciencias Geográficas, 2(3), 119–134. https://doi.org/https://doi.org/10.15381/iigeo.v2i3.2115

Carbonel, C. A. A. (2013). Un modelo de gravedad reducida de la hidrodinámica y termodinámica en zona costera. Caso de estudio: Bahías de Pisco y Paracas. Revista de Investigación de Física, 16(01), 1–9.

Cardich, J., Gutiérrez, D., Romero, D., Pérez, A., Quipúzcoa, L., Marquina, R., Yupanqui, W., Solís, J., Carhuapoma, W., Sifeddine, A., & Rathburn, A. E. (2015). Calcareous benthic foraminifera from the upper central peruvian margin: Control of the assemblage by pore water redox and sedimentary organic matter. Marine Ecology Progress Series, 535, 63–87. https://doi.org/10.3354/meps11409

Cardich, J., Morales, M., Quipúzcoa, L., Sifeddine, A., & Gutiérrez, D. (2012). Benthic foraminiferal communities and microhabitat selection on the continental shelf off central Peru. In A. v Altenbach, J. M. Bernhard, & J. Seckbach (Eds.), Anoxia. Evidence for Eukaryote Survival and Paleontological Strategies (Vol. 21, pp. 323–340). Springer Science & Business Media. https://doi.org/10.1007/978-94-007-1896-8_17

Cardich, J., Rathburn, A., Sifeddine, A., & Gutiérrez, D. (2014). On the taphonomy of benthic foraminifera: Comparison of living and dead assemblages in central Peruvian upper margin sediments. FORAMS 2014, International Symposium on Foraminifera.

Castillo, A., Hromic, T., Uribe, R. A., Valdés, J., Sifeddine, A., Quezada, L., Vega, S. E., Arencibia, A., Díaz-Ochoa, J., & Guiñez, M. (2021). Living (stained) calcareous benthic foraminiferal assemblages (>125μm) in a coastal upwelling zone of the Humboldt Current System, Northern Chile (~27∘S). Regional Studies in Marine Science, 44. https://doi.org/10.1016/j.rsma.2021.101725

Chamorro, A., Echevin, V., Dutheil, C., Tam, J., Gutiérrez, D., & Colas, F. (2021). Projection of upwelling-favorable winds in the Peruvian upwelling system under the RCP8.5 scenario using a high-resolution regional model. Climate Dynamics, 57(1–2). https://doi.org/10.1007/s00382-021-05689-w

Chan, F., Barth, J. A., Lubchenco, J., Kirincich, A., Weeks, H., Peterson, W. T., & Menge, B. A. (2008). Emergence of anoxia in the California current large marine ecosystem. In Science (Vol. 319, Issue 5865). https://doi.org/10.1126/science.1149016

Chao, A., & Shen, T. J. (2003). Nonparametric estimation of Shannon's index of diversity when there are unseen species in sample. Environmental and Ecological Statistics, 10(4). https://doi.org/10.1023/A:1026096204727

Cifuentes, L. A., Coffin, R. B., Solorzano, L., Cardenas, W., Espinoza, J., & Twilley, R. R. (1996). Isotopic and elemental variations of carbon and nitrogen in a mangrove estuary. Estuarine, Coastal and Shelf Science, 43(6). https://doi.org/10.1006/ecss.1996.0103

Cline, J. D. (1969). Spectrophotometric Determination of Hydrogen Sulfide in Natural Waters. Limnology and Oceanography, 14(3), 454–458.

Correa, D., Tam, J. and Chamorro, A. (2020). Pentadal classification of wind off Peruvian coast. Revista de investigación de física 23 (3), 61–65. https://doi.org/10.15381/rif.v23i3.20315.

Cuellar-Martinez, T., Huanca Ochoa, A. del R., Sánchez, S., Aguirre Velarde, A., Correa, D., Egoavil Gallardo, K. A., Luján Monja, H. F., Ipanaqué Zapata, J. M., Colas, F., Tam, J., & Gutiérrez, D. (2021). Paralytic shellfish toxins in Peruvian scallops associated with blooms of Alexandrium ostenfeldii (Paulsen) Balech & Tangen in Paracas Bay, Peru. Marine Pollution Bulletin, 173, 112988. https://doi.org/10.1016/j.marpolbul.2021.112988

Cueto-Vega, R., Flye-Sainte-Marie, J., Aguirre-Velarde, A., Jean, F., Gil-Kodaka, P., & Thouzeau, G. (2021). Size-based survival of cultured Argopecten purpuratus (L, 1819) under severe hypoxia. Journal of the World Aquaculture Society. https://doi.org/10.1111/jwas.12777

Dean, W. E. Jr. (1974). Determination of carbonate and organic matter in calcareous sediments and sedimentary rocks by Loss on Ignition: Comparison with other methods. Journal of Sedimentary Research, 44(1), 242–248. https://doi.org/10.1306/74D729D2-2B21-11D7-8648000102C1865D

Diaz, R. J., & Rosenberg, R. (2008). Spreading dead zones and consequences for marine ecosystems. Science, 321(5891), 926–929.

Dolven, J. K., Alve, E., Rygg, B., & Magnusson, J. (2013). Defining past ecological status and in situ reference conditions using benthic foraminifera: A case study from the Oslofjord, Norway. Ecological Indicators, 29, 219–233.

Eichler, P. P. B., & Barker, C. P. (2020). Benthic Foraminiferal Ecology: Indicators of Environmental Impacts. In Benthic Foraminiferal Ecology. Springer Nature. https://doi.org/10.1007/978-3-030-61463-8

Espinoza-Morriberón, D., Echevin, V., Colas, F., Tam, J., Gutiérrez, D., Graco, M., Ledesma, J., & Quispe-Ccalluari, C. (2019). Oxygen variability during ENSO in the Tropical South Eastern Pacific. Frontiers in Marine Science, 5(JAN). https://doi.org/10.3389/fmars.2018.00526

Fenchel, T., & Finlay, B. (2008). Oxygen and the spatial structure of microbial communities. In Biological Reviews (Vol. 83, Issue 4). https://doi.org/10.1111/j.1469-185X.2008.00054.x

Fennel, K., & Testa, J. M. (2019). Biogeochemical Controls on Coastal Hypoxia. Annual Review of Marine Sciences, 11, 105–130.

Flores, E., Mendoza, U., Callbeck, C. M., Díaz, R., Aguirre-Velarde, A., Böttcher, M. E., Merma-Mora, L., Moreira, M., Saldarriaga, M. S., Silva-Filho, E. v., Albuquerque, A. L., Pizarro-Koch, M., & Graco, M. (2023). Attenuation of wind intensities exacerbates anoxic conditions leading to sulfur plume development off the coast of Peru. PLoS ONE, 18(8 August). https://doi.org/10.1371/journal.pone.0287914

Fossing, H. (1990). Sulfate reduction in shelf sediments in the upwelling region off Central Peru. Continental Shelf Research, 10(4), 355–367.

Francescangeli, F., Armynot du Châtelet, E., Billon, G., Trentesaux, A., & Bouchet, V. M. P. (2016). Palaeo-ecological quality status based on foraminifera of Boulogne- sur-Mer harbour (Pas-de-Calais , Northeastern France) over the last 200

years. Marine Environmental Research, 117, 32–43. https://doi.org/10.1016/j.marenvres.2016.04.002

Fuenzalida, R., Schneider, W., Garcés-Vargas, J., Bravo, L., & Lange, C. (2009). Vertical and horizontal extension of the oxygen minimum zone in the eastern South Pacific Ocean. Deep-Sea Research II, 56, 992–1003. https://doi.org/10.1016/j.dsr2.2008.11.001

Galehouse. (1971). Sedimentation analysis. In R. Carver (Ed.), Procedures in sedimentary petrology (pp. 69–94). John Wiley & Sons, Ltd.

Gieskes, J., Gamo, T., & Brumsack, H. (1991). Chemical Methods for Interstitial Water Analysis aboard JOIDES Resolution. In Chemical Methods for Interstitial Water Analysis aboard JOIDES Resolution. https://doi.org/10.2973/odp.tn.15.1991

Glock, N., Roy, A. S., Romero, D., Wein, T., Weissenbach, J., Revsbech, N. P., Høgslund, S., Clemens, D., Sommer, S., & Dagan, T. (2019). Metabolic preference of nitrate over oxygen as an electron acceptor in foraminifera from the Peruvian oxygen minimum zone. Proceedings of the National Academy of Sciences of the United States of America, 116(8), 2860–2865. https://doi.org/10.1073/pnas.1813887116

Gooday, A. J., Jorissen, F., Levin, L. A., Middelburg, J. J., Naqvi, S. W. A., Rabalais, N. N., Scranton, M., & Zhang, J. (2009). Historical records of coastal eutrophication-induced hypoxia. In Biogeosciences (Vol. 6, Issue 8). https://doi.org/10.5194/bg-6-1707-2009

Goubanova, K., Echevin, V., Dewitte, B., Codron, F., Takahashi, K., Terray, P., & Vrac, M. (2010). Statistical downscaling of sea-surface wind over the Peru-Chile

upwelling region: diagnosing the impact of climate change from the IPSL-CM4 model. Climate Dynamics, 36(7), 1365–1378.

Graco, M. I., Purca, S., Dewitte, B., Castro, C. G., Morón, O., Ledesma, J., Flores, G., & Gutiérrez, D. (2017). The OMZ and nutrient features as a signature of interannual and low-frequency variability in the Peruvian upwelling system. Biogeosciences, 14, 4601–4617. https://doi.org/10.5194/bg-14-4601-2017

Grantham, B. A., Chan, F., Nielsen, K. J., Fox, D. S., Barth, J. A., Huyer, A., Lubchenco, J., & Menge, B. A. (2004). Upwelling-driven nearshore hypoxia signals ecosystem and ocenographic changes in the northeast Pacific. Nature, 429(June), 749–754.

Green, M. A., & Aller, R. C. (1998). Seasonal patterns of carbonate diagenesis in nearshore terrigenous muds: Relation to spring phytoplankton bloom and temperature. Journal of Marine Research, 56, 1097–1123.

Green, M. A., & Aller, R. C. (2001). Early diagenesis of calcium carbonate in Long Island Sound sediments: Benthic fluxes of Ca2+ and minor elements during seasonal periods of net dissolution. Journal of Marine Research, 59(5). https://doi.org/10.1357/002224001762674935

Grillo, J., Gozzer, R., Sueiro, J. C., & Riveros, J. C. (2018). Producción ilegal de harina de pescado en Perú a partir de anchoveta extraída por la flota artesanal y de menor escala.

Gutiérrez, D., Akester, M., & Naranjo, L. (2016). Productivity and sustainable management of the Humboldt Current Large Marine Ecosystem under climate change. Environmental Development, 17, 126–144.

Gutiérrez, D., Bouloubassi, I., Sifeddine, A., Purca, S., Goubanova, K., Graco, M., Field, D., Méjanelle, L., Velazco, F., Lorre, A., Salvatteci, R., Quispe, D., Vargas, G., Dewitte, B., & Ortlieb, L. (2011). Coastal cooling and increased productivity in the main upwelling zone off Peru since the mid-twentieth century. Geophysical Research Letters, 38(7), 1–6. https://doi.org/10.1029/2010GL046324

Gutiérrez, D., Enríquez, E., Purca, S., Quipúzcoa, L., Marquina, R., Flores, G., & Graco, M. (2008). Oxygenation episodes on the continental shelf of central Peru: Remote forcing and benthic ecosystem response. Progress in Oceanography, 79(2–4), 177–189.

Gutiérrez, D., Gallardo, V., Mayor, S., Neira, C., Vasquez, C., Sellanes, J., Rivas, M., Soto, A., Carrasco, F., & Baltazar, M. (2000). Effects of dissolved oxygen and fresh organic matter on the bioturbation potential of macrofauna in sublittoral sediments off Central Chile during the 1997/1998 El Nino. Marine Ecology Progress Series, 202, 81–99.

Guzmán, M., Chávez, J., Morón, O., Sánchez, S., & Flores, G. (1997). Evaluación de la calidad del medio ambiente marino en la bahía de Pisco - Paracas, 22 a 24 de mayo 1996. Informe Progresivo Instituto Del Mar Del Perú, 54, 3–29. https://hdl.handle.net/20.500.12958/1443

Haman, D., Baker, M. B., & Seiglie, G. A. (1993). Virgulinella ossamagnifica n.sp., from the miocene of Cabinda, Equatorial West Africa. Journal of Foraminiferal Research, 23(3), 205–208.

Hausser, J., & Strimmer, K. (2009). Entropy inference and the james-stein estimator, with application to nonlinear gene association networks. Journal of Machine Learning Research, 10.

Haynert, K., Schönfeld, J., Polovodova-Asteman, I., & Thomsen, J. (2012). The benthic foraminiferal community in a naturally CO2-rich coastal habitat of the southwestern Baltic Sea. Biogeosciences, 9, 4421–4440.

Helly, J. J., & Levin, L. A. (2004). Global distribution of naturally occurring marine hypoxia on continental margins. Deep Sea Research Part I: Oceanographic Research Papers, 51(9), 1159–1168.

Herguera, J. C. (1992). Deep-sea benthic foraminifera and biogenic opal: Glacial to postglacial productivity changes in the western equatorial Pacific. Marine Micropaleontology, 19(1–2), 79–98. https://doi.org/10.1016/0377-8398(92)90022-C

Hernandez-Ayon, J. M., Paulmier, A., Garcon, V., Sudre, J., Montes, I., Chapa-Balcorta, C., Durante, G., Dewitte, B., Maes, C., & Bretagnon, M. (2019). Dynamics of the Carbonate System Across the Peruvian Oxygen Minimum Zone. Frontiers in Marine Science, 6. https://doi.org/10.3389/fmars.2019.00617

Hill, M. O. (1973). Diversity and Evenness: A Unifying Notation and Its Consequences. Ecology, 54(2). https://doi.org/10.2307/1934352

Høgslund, S., Revsbech, N. P., Cedhagen, T., Nielsen, L. P., & a Gallardo, V. (2008). Denitrification, nitrate turnover, and aerobic respiration by benthic foraminiferans in the oxygen minimum zone off Chile. Journal of Experimental

Marine Biology and Ecology, 359(2), 85–91. https://doi.org/10.1016/j.jembe.2008.02.015

Howarth, R. W., & Marino, R. (2006). Nitrogen as the limiting nutrient for eutrophication in coastal marine ecosystems: Evolving views over three decades. Limnology and Oceanography, 51(1part2), 364–376. https://doi.org/10.4319/lo.2006.51.1_part_2.0364

Ibarra, A. A. (2015). Variabilidad temporal en la estructura y composición de la macrofauna bentónica en Playa Atenas, Pisco. Tesis Ing. Pesquero. [Universidad Nacional Agraria La Molina]. https://hdl.handle.net/20.500.12996/1913

IMARPE. (2015). Anuario Científico Tecnológico IMARPE (Vol. 15). Instituto del Mar del Perú.

Ingram, R. (1971). Sieve analysis. In R. E. Carver (Ed.), Procedures in sedimentary petrology (pp. 49–67). John Wiley & Sons, Ltd.

INRENA. (1999). Delimitación de la faja marginal del río Pisco: Resumen ejecutivo. https://repositorio.ana.gob.pe/handle/20.500.12543/1567

Jacinto, M. E. (2014). Propuesta de un sistema de indicadores ambientales y socioeconómicos en la zona marino costera de Pisco - Paracas (p. 109).

Jacinto, M. E., Martínez, C., Sánchez, S., Flores, G., & Pizarro, L. (1996). Evaluación de la varazón y contaminación en la Bahía de Paracas - Pisco. Informe Progresivo Instituto Del Mar Del Perú, 29, 3–46.

Jessen, C., Bednarz, V. N., Rix, L., Teichberg, M., & Wild, C. (2015). Marine Eutrophication. In Environmental Indicators (pp. 177–203). Springer Netherlands. https://doi.org/10.1007/978-94-017-9499-2_11

Jørgensen, B. B. (1996a). Case study — Aarhus Bay. In B. B. Jørgensen & K. Richardson (Eds.), Eutrophication in Coastal Marine Ecosystems (Vol. 52, pp. 137–154). American Geophysical Union. https://doi.org/10.1029/ce052p0137

Jørgensen, B. B. (1996b). Material flux in the sediment. In B. B. Jørgensen & K. Richardson (Eds.), Eutrophication in Coastal Marine Ecosystems (Vol. 52, pp. 115–135). American Geophysical Union. https://doi.org/10.1029/ce052p0115

Joye, S. B., & Anderson, I. C. (2008). Nitrogen Cycling in Coastal Sediments. In D. G. Capone, D. A. Bronk, M. R. Mulholland, & E. J. Carpenter (Eds.), Nitrogen in the Marine Environment (2nd ed., pp. 867–915). Academic Press. https://doi.org/10.1016/B978-0-12-372522-6.00019-0

Kanneworff, E., & Nicolaisen, W. (1972). The “Haps” a frame-supported bottom corer. Ophelia, 10(2), 119–129. https://doi.org/10.1080/00785326.1972.10430108

Kennedy, P., Kennedy, H., & Papadimitriou, S. (2005). The effect of acidification on the determination of organic carbon, total nitrogen and their stable isotopic composition in algae and marine sediment. Rapid Communications in Mass Spectrometry, 19(8). https://doi.org/10.1002/rcm.1889

Koho, K. A., García, R., de Stigter, H. C., Epping, E., Koning, E., Kouwenhoven, T. J., & van der Zwaan, G. J. (2008). Sedimentary labile organic carbon and pore water redox control on species distribution of benthic foraminifera: A case study

from Lisbon-Setúbal Canyon (southern Portugal). Progress in Oceanography, 79(1), 55–82. https://doi.org/10.1016/j.pocean.2008.07.004

Koide, M., & Goldberg, E. D. (1982). Transuranic nuclides in two coastal marine sediments off Peru. Earth and Planetary Science Letters, 57(2). https://doi.org/10.1016/0012-821X(82)90149-2

Kucera, M., & Malmgren, B. A. (1998). Logratio transformation of compositional data - A resolution of the constant sum constraint. Marine Micropaleontology, 34(1–2). https://doi.org/10.1016/S0377-8398(97)00047-9

Lamb, A. L., Wilson, G. P., & Leng, M. J. (2006). A review of coastal palaeoclimate and relative sea-level reconstructions using δ13C and C/N ratios in organic material. Earth-Science Reviews, 75(1–4). https://doi.org/10.1016/j.earscirev.2005.10.003

Largier, J. L. (2020). Upwelling Bays: How Coastal Upwelling Controls Circulation, habitat, and productivity in bays. Annual Review of Marine Science, 12(1), 415–447. https://doi.org/10.1146/annurev-marine-010419-011020

Lehmann, M. F., Bernasconi, S. M., Barbieri, A., Simona, M., & McKenzie, J. A. (2004). Interannual variation of the isotopic composition of sedimenting organic carbon and nitrogen in Lake Lugano: A long-term sediment trap study. Limnology and Oceanography, 49(3). https://doi.org/10.4319/lo.2004.49.3.0839

Leiter, C., & Altenbach, A. v. (2010). Benthic Foraminifera from the Diatomaceous Mud Belt Off Namibia: Characteristic Species for Severe Anoxia. Palaeontologia Electronica, 13(2), 11A:19p. http://palaeo-electronica.org/2010_2/188/index.html

Levin, L. A. (2003). Oxygen minimum zone benthos: Adaptation and community response to hypoxia. Oceanography and Marine Biology: An Annual Review, 41, 1–45.

Levin, L. A., Ekau, W., Gooday, A. J., Jorissen, F. J., Middelburg, J. J., Naqvi, S. W. A., Neira, C., Rabalais, N. N., & Zhang, J. (2009). Effects of natural and human-induced hypoxia on coastal benthos. Biogeosciences, 6(10), 2063–2098.

Levin, L. A., Gutiérrez, D., Rathburn, A. E., Neira, C., Sellanes, J., Muñoz, P., Gallardo, V. A., & Salamanca, M. (2002). Benthic processes on the Peru margin: A transect across the oxygen minimum zone during the 1997 – 98 El Niño. Progress in Oceanography, 53, 1–27. https://doi.org/10.1016/S0079-6611(02)00022-8

Li, W. K. W. (2002). Macroecological patterns of phytoplankton in the northwestern North Atlantic Ocean. Nature, 419(6903), 154–157. https://doi.org/10.1038/nature00994

Lichtfouse, E., & Budzinski, H. (1995). 13C analysis of molecular organic substances, a novel breakthrough in analytical sciences. Analusis, 23(8). https://doi.org/10.1016/0365-4877(96)84515-3

Lomovasky, B. J., Firstater, F. N., Gamarra Salazar, A., Mendo, J., & Iribarne, O. O. (2011). Macro benthic community assemblage before and after the 2007 tsunami and earthquake at Paracas Bay, Peru. Journal of Sea Research, 65(2), 205–212. https://doi.org/10.1016/j.seares.2010.10.002

Loubere, P., & Fariduddin, M. (1999). Benthic Foraminifera and the flux of organic carbon to the seabed. In B. K. sen Gupta (Ed.), Modern Foraminifera (pp. 181–199). Kluwer Academic Publishers. https://doi.org/10.1007/0-306-48104-9_11

Lubis, A. A. (2006). Constant Rate of Supply (CRS) Model for Determining the Sediment Accumulation Rates in the Coastal Area Using 210 Pb. Journal of Coastal Development, 10(1).

Machado de Almeida, C. (2013). Condições paleoredox na plataforma central do Peru inferidas através de foraminíferos bentônicos para os últimos 1000 anos. Tese de doutorado. [Universidade Federal Fluminense]. https://app.uff.br/riuff/handle/1/1536

Mallon, J., Glock, N., & Schönfeld, J. (2012). The response of benthic foraminifera to low-oxygen conditions of the Peruvian Oxygen Minimum Zone. In A. v Altenbach, J. M. Bernhard, & J. Seckbach (Eds.), Anoxia. Evidence for Eukaryote Survival and Paleontological Strategies (pp. 305–321). Springer Science & Business Media. https://doi.org/10.1007/978-94-007-1896-8

Mcgann, M. (2009). Review of impacts of contaminated sediment on microfaunal communities in the Southern California Bight. Special Paper of the Geological Society of America, 454, 413–455. https://doi.org/10.1130/2009.2454(6.3).

McIntyre-Wressnig, A., Bernhard, J. M., Wit, J. C., & McCorkle, D. C. (2014). Ocean acidification not likely to affect the survival and fitness of two temperate benthic foraminiferal species: Results from culture experiments. Journal of Foraminiferal Research, 44(4). https://doi.org/10.2113/gsjfr.44.4.341

Merma-Mora, L. (2016). Foraminíferos bentónicos asociados a condiciones de hipoxia costera y bajo pH en la Bahía de Paracas. Tesis de Maestría. [Universidad Peruana Cayetano Heredia]. https://hdl.handle.net/20.500.12866/240

Merma Mora, L. (2020). Estructura comunitaria de foraminíferos bentónicos en relación a factores ambientales en sedimentos marinos someros de la costa central del Perú. Tesis Biólogo. [Universidad Nacional Agraria La Molina]. https://hdl.handle.net/20.500.12996/4513.

Meyers, P. A. (1994). Preservation of elemental and isotopic source identification of sedimentary organic matter. Chemical Geology, 114(3–4). https://doi.org/10.1016/0009-2541(94)90059-0

Meyers, P. A. (2002). Evidence of mid-Holocene climate instability from variations in carbon burial in Seneca Lake, New York. Journal of Paleolimnology, 28(2). https://doi.org/10.1023/A:1021662222452

Montoya, J. P. (2008). Nitrogen Stable Isotopes in Marine Environments. In Nitrogen in the Marine Environment (2nd ed., pp. 1277–1302). Academic Press. https://doi.org/10.1016/B978-0-12-372522-6.00029-3

Moore, W. S. (1984). Radium isotope measurements using germanium detectors. Nuclear Instruments and Methods In Physics Research, 223(2–3). https://doi.org/10.1016/0167-5087(84)90683-5

Morón, O., Quispe, J., Lorenzo, A., Flores, G., Sánchez, S., Aronés, K., Solís, J., & Quipuzcoa, L. (2017). Caracterización de los procesos físicos, químicos, biológicos y sedimentológicos en las Islas Ballestas y Chincha 2013. Informe Instituto Del Mar Del Perú, 44(4), 472–506.

Morse, J. W., Arvidson, R. S., & Lüttge, A. (2007). Calcium Carbonate Formation and Dissolution. Chemical Reviews, 107(2), 342–381.

Morse, J. W., & Morin, J. (2005). Ammonium interaction with coastal marine sediments: Influence of redox conditions on K. Marine Chemistry, 95(1–2). https://doi.org/10.1016/j.marchem.2004.08.008

Murray, J. W. (1991). Ecology and palaeoecology of benthic foraminifera. In Ecology and Palaeoecology of Benthic Foraminifera. Routledge. https://doi.org/10.4324/9781315846101

Murray, J. W. (2006). Ecology and applications of benthic foraminifera. Cambridge University Press.

Murray, J. W., & Alve, E. (1999a). Natural dissolution of modern shallow water benthic foraminifera: taphonomic effects on the palaeoecological record. Palaeogeography, Palaeoclimatology, Palaeoecology, 146, 195–209.

Murray, J. W., & Alve, E. (1999b). Taphonomic experiments on marginal marine foraminiferal assemblages: How much ecological information is preserved? Palaeogeography, Palaeoclimatology, Palaeoecology, 149(1–4). https://doi.org/10.1016/S0031-0182(98)00200-4

Ni, X., Huang, D., Zeng, D., Zhang, T., Li, H., & Chen, J. (2016). The impact of wind mixing on the variation of bottom dissolved oxygen off the Changjiang Estuary during summer. Journal of Marine Systems, 154, 122–130. https://doi.org/10.1016/j.jmarsys.2014.11.010

Nixon, S. W. (1995). Coastal marine eutrophication: A definition, social causes, and future concerns. Ophelia, 41, 199–220. https://doi.org/10.1080/00785236.1995.10422044

Nixon, S. W. (2009). Eutrophication and the macroscope. Hydrobiologia, 629, 5–19. https://doi.org/10.1007/s10750-009-9759-z

Nomaki, H., Ogawa, N. O., Ohkouchi, N., Suga, H., Toyofuku, T., Shimanaga, M., Nakatsuka, T., & Kitazato, H. (2008). Benthic foraminifera as trophic links between phytodetritus and benthic metazoans: Carbon and nitrogen isotopic evidence. Marine Ecology Progress Series, 357, 153–164. https://doi.org/10.3354/meps07309

Ochoa, N., Gómez Caballero, O., Sánchez Ramírez, S., & Delgado Loayza, E. (1999). Diversidad de diatomeas y dinoflagelados marinos del Perú. Boletín IMARPE, 18(1–2), 1–14.

Paerl, H. W., & Piehler, M. F. (2008). Nitrogen and Marine Eutrophication. In D. G. Capone, D. A. Bronk, M. R. Mulholland, & E. J. Carpenter (Eds.), Nitrogen in the Marine Environment (2nd ed.). Elsevier Inc. https://doi.org/10.1016/B978-0-12-372522-6.00011-6

Paulmier, A., & Ruiz-Pino, D. (2009). Oxygen minimum zones (OMZs) in the modern ocean. Progress in Oceanography, 80(3–4), 113–128.

Pennington, J. T., Mahoney, K. L., Kuwahara, V. S., Kolber, D. D., Calienes, R., & Chavez, F. P. (2006). Primary production in the eastern tropical Pacific: A review. Progress in Oceanography, 69(2–4). https://doi.org/10.1016/j.pocean.2006.03.012

Pérez, A., Escobedo, R., Castro, R., Jesus, R., Cardich, J., Romero, P. E., Salas-Gismondi, R., Ochoa, D., Aponte, H., Sanders, C. J., & Carré, M. (2022). Carbon and nutrient burial within Peruvian coastal marsh driven by anthropogenic activities. Marine Pollution Bulletin, 181, 113948. https://doi.org/10.1016/j.marpolbul.2022.113948

Pérez, A., Machado, W., Gutiérrez, D., Saldarriaga, M. S., & Sanders, C. J. (2020). Shrimp farming influence on carbon and nutrient accumulation within Peruvian mangroves sediments. Estuarine, Coastal and Shelf Science, 243. https://doi.org/10.1016/j.ecss.2020.106879

Pitcher, G. C., Aguirre-Velarde, A., Breitburg, D., Cardich, J., Carstensen, J., Conley, D. J., Dewitte, B., Engel, A., Espinoza-Morriberón, D., Flores, G., Garçon, V., Graco, M., Grégoire, M., Gutiérrez, D., Hernandez-Ayon, J. M., Huang, H. H. M., Isensee, K., Jacinto, M. E., Levin, L., … Zhu, Z. Y. (2021). System controls of coastal and open ocean oxygen depletion. Progress in Oceanography, 102613. https://doi.org/10.1016/j.pocean.2021.102613

Pitcher, G. C., Probyn, T. A., Randt, A. du, Lucas, A. J., Bernard, S., Evers-king, H., Lamont, T., & Hutchings, L. (2014). Dynamics of oxygen depletion in the nearshore of a coastal embayment of the southern Benguela upwelling system. Journal of Geophysical Research: Oceans, 119, 2183–2200. https://doi.org/10.1002/2013JC009443.Received

Pizarro, O., Hormazabal, S., Gonzalez, A., & Yañez, E. (1994). Coastal wind, sea level and temperature variability in the north of Chile. Investigaciones Marinas, 22, 85–101. https://doi.org/10.4067/s0717-71781994002200007

Quispe-Ccalluari, C., Tam, J., Demarcq, H., Chamorro, A., Espinoza-Morriberón, D., Romero, C., Dominguez, N., Ramos, J., & Oliveros-Ramos, R. (2018). An index of coastal thermal effects of El Niño Southern Oscillation on the Peruvian Upwelling Ecosystem. International Journal of Climatology, 38(7). https://doi.org/10.1002/joc.5493

R core Team. 2020. R: A language and environment for statistical computing. In R foundation for Statistical Computing. http://www.r-project.org/

Rabalais, N. N., Díaz, R. J., Levin, L. A., Turner, R. E., Gilbert, D., & Zhang, J. (2010). Dynamics and distribution of natural and human-caused coastal hypoxia. Biogeosciences, 7, 585–619.

Rice, D. L., & Tenore, K. R. (1981). Dynamics of carbon and nitrogen during the decomposition of detritus derived from estuarine macrophytes. Estuarine, Coastal and Shelf Science, 13(6). https://doi.org/10.1016/S0302-3524(81)80049-7

Richardson, K., & Jørgensen, B. B. (1996). Eutrophication: Definition, history and effects. In B. B. Jørgensen & K. Richardson (Eds.), Eutrophication in Coastal Marine Ecosystems (Vol. 52, pp. 1–19). https://doi.org/10.1029/ce052p0001

Risgaard-Petersen, N., Langezaal, A. M., Ingvardsen, S., Schmid, M. C., Jetten, M. S. M., den Camp, H. J. M. O., Derksen, J. W. M., Piña-Ochoa, E., Eriksson, S. P., Nielsen, L. P., Revsbech, N. P., Cedhagen, T., & der Zwaan, G. J. van. (2006). Evidence for complete denitrification in a benthic foraminifer. Nature, 443(7107), 93–96. https://doi.org/10.1038/nature05070

Rojas de Mendiola, B. (1981). Seasonal phytoplankton distribution along the Peruvian coast. In F. A. Richards (Ed.), Coastal Upwelling (Vol. 1). https://doi.org/10.1029/co001p0348

Romero, D. (2021). Distribution of benthic foraminiferas in surface sediments off San Juan de Marcona (15°21’S). Inf. Inst. Mar Peru, 48(2), 186–194.

Romero, L., Huamaní, A., Sánchez, S., & Hernández-Becerril, D. U. (2022). Floración algal nociva del dinoflagelado Blixaea quinquecornis en el Perú. Revista Peruana de Biología, 29(1), e19348. https://doi.org/10.15381/rpb.v29i1.19348

Roughan, M., Mace, A. J., Largier, J. L., Morgan, S. G., Fisher, J. L., & Carter, M. L. (2005). Subsurface recirculation and larval retention in the lee of a small headland: A variation on the upwelling shadow theme. Journal of Geophysical Research, 110(C10027). https://doi.org/10.1029/2005JC002898

Rozan, T. F., Taillefert, M., Trouwborst, R. E., Glazer, B. T., Ma, S., Herszage, J., Valdes, L. M., Price, K. S., & Luther, G. W. (2002). Iron-sulfur-phosphorus cycling in the sediments of a shallow coastal bay: Implications for sediment nutrient release and benthic macroalgal blooms. Limnology and Oceanography, 47(5). https://doi.org/10.4319/lo.2002.47.5.1346

Sánchez, S., Bernales, A., Delgado, E., Carmen Chang, F. del, Jacobo, N., & Quispe, J. (2017). Variability and Biogeographical Distribution of Harmful Algal Blooms in Bays of High Productivity off Peruvian Coast (2012-2015). Journal of Environmental & Analytical Toxicology, 07(06), 530. https://doi.org/10.4172/2161-0525.1000530

Sánchez, S., Delgado, E., Bernales, A., Jacobo, N., Franco, A., & Correa, D. (2021). Floraciones algales nocivas en la costa peruana durante El Niño Costero 2017 y su relación con las condiciones ambientales. Boletin Instituto Del Mar Del Perú, 36(2), 452–462. https://doi.org/10.53554/boletin.v36i2.347

Sánchez, S., Jacobo, N., Bernales, A., Franco, A., Quispe, J., & Flores, G. (2019). Seasonal Variability in the Distribution of Phytoplankton in Paracas Bay/Peru, as a

Response to Environmental Conditions. Journal of Environmental Science and Engineering B, 7(10). https://doi.org/10.17265/2162-5263/2018.10.002

Schönfeld, J., Alve, E., Geslin, E., Jorissen, F., Korsun, S., Spezzaferri, S., Abramovich, S., Almogi-Labin, A., du Chatelet, E. A., Barras, C., Bergamin, L., Bicchi, E., Bouchet, V., Cearreta, A., Bella, L. di, Dijkstra, N., Disaro, S. T., Ferraro, L., Frontalini, F., … Tsujimoto, A. (2012). The FOBIMO (FOraminiferal BIo-MOnitoring) initiative-Towards a standardised protocol for soft-bottom benthic foraminiferal monitoring studies. Marine Micropaleontology, 94–95, 1–13.

Schrader, H., & Sorknes, R. (1991). Peruvian coastal upwelling: Late Quaternary productivity changes revealed by diatoms. Marine Geology, 97(3–4). https://doi.org/10.1016/0025-3227(91)90118-N

Seeberg-Elverfeldt, J., Schlüter, M., Feseker, T., & Kölling, M. (2005). Rhizon sampling of porewaters near the sediment-water interface of aquatic systems. Limnology and Oceanography: Methods, 3(8). https://doi.org/10.4319/lom.2005.3.361

Sifeddine, A., Gutiérrez, D., Ortlieb, L., Boucher, H., Velazco, F., Field, D., Vargas, G., Boussafir, M., Salvatteci, R., Ferreira, V., García, M., Valdés, J., Caquineau, S., Yogo, M. M., Cetin, F., Solis, J., Soler, P., & Baumgartner, T. (2008). Laminated sediments from the central Peruvian continental slope: A 500 year record of upwelling system productivity, terrestrial runoff and redox conditions. Progress in Oceanography, 79, 190–197. https://doi.org/10.1016/j.pocean.2008.10.024

Silva, N., & Prego, R. (2002). Carbon and nitrogen spatial segregation and stoichiometry in the surface sediments of southern Chilean inlets (41°-56°S).

Estuarine, Coastal and Shelf Science, 55(5). https://doi.org/10.1006/ecss.2001.0938

Solís, J., Velazco, F., Moron, O., Sanchéz, S., Calderon, A., Fernández, J. C., Luciano, L., & Vítor, J. (2022). Características sedimentológicas y geoquímicas de sedimentos recientes de la bahía de Paracas, Pisco, durante los años 2013, 2014 y 2015. Boletin Instituto Del Mar Del Perú, 37(2), 348–360. https://doi.org/10.53554/boletin.v37i2.377

Stanley, D. W., & Nixon, S. W. (1992). Stratification and bottom-water hypoxia in the Pamlico River Estuary. Estuaries, 15(3), 270–281.

Stott, L. D., Hayden, T. P., & Griffith, J. (1996). Benthic foraminifera at the Los Angeles County whites point outfall revisited. Journal of Foraminiferal Research, 26(4), 357–368. https://doi.org/10.2113/gsjfr.26.4.357

Strickland, J. D. H., & Parsons, T. R. (1972). A practical handbook of seawater analysis (2nd ed.). Fisheries Research Board of Canada.

Sundby, B., Gobeil, C., Silverberg, N., & Alfonso, M. (1992). The phosphorus cycle in coastal marine sediments. Limnology and Oceanography, 37(6). https://doi.org/10.4319/lo.1992.37.6.1129

Tarazona, J., & Arntz, W. (2001). The Peruvian Coastal Upwelling System. In U. Seeliger & B. Kjerfve (Eds.), Coastal Marine Ecosystems of Latin America (1st ed., pp. 229–244). Springer-Verlag Berlin Heidelberg.

Tarazona, J., Canahuire, E., Salzwedel, H., Jeri, T., Arntz, W. E., & Cid, L. (1991). Macrozoobenthos in two shallow areas of the Peruvian upwelling ecosystem. In M.

Elliot & J.-P. Ducrotoy (Eds.), Eastuaries and coasts spatial and temporal intercomparisons (pp. 251–258). Olsen & Olsen.

Tarazona, J., Gutiérrez, D., Paredes, C., & Indacochea, A. (2003). Overview and challenges of Marine Biodiversity Research in Peru. Gayana (Concepción), 67(2). https://doi.org/10.4067/s0717-65382003000200009

Tarazona, J., Salzwedel, H., & Arntz, W. (1988). Oscillations of macrobenthos in shallow waters of the Peruvian central coast induced by El Niño 1982-83. Journal of Marine Research, 46(3), 593–611.

Tavera Martínez, L., Marchant, M., Muñoz, P., & Abdala Díaz, R. T. (2022). Spatial and Vertical Benthic Foraminifera Diversity in the Oxygen Minimum Zone of Mejillones Bay, Northern Chile. Frontiers in Marine Science, 9. https://doi.org/10.3389/fmars.2022.821564

Tenorio, C., Álvarez, G., Perez-Alania, M., Blanco, J. L., Paulino, C., Blanco, J., & Uribe, E. (2022). Bloom of Prorocentrum cordatum in Paracas Bay, Peru. Diversity, 14(10), 844. https://doi.org/10.3390/d14100844

Testa, J. M., & Kemp, W. M. (2011). Oxygen – Dynamics and Biogeochemical Consequences. In E. Wolansky & D. McLusky (Eds.), Treatise on Estuarine and Coastal Science (Vol. 5, pp. 163–200). Academic Press. https://doi.org/10.1016/B978-0-12-374711-2.00505-2

Thomas, E., Abramson, I., Varekamp, J. C., & Buchholtz ten Brink, M. R. (2004). Eutrophication of Long Island Sound as traced by benthic foraminifera. Sixth Biennual LIS Research Conference Proceedings, 87–91.

Thomsen, S., Kanzow, T., Colas, F., Echevin, V., Krahmann, G., & Engel, A. (2016). Do submesoscale frontal processes ventilate the oxygen minimum zone off Peru? Geophysical Research Letters, 43(15), 8133–8142. https://doi.org/10.1002/2016GL070548

Thornton, S. F., & McManus, J. (1994). Application of organic carbon and nitrogen stable isotope and C/N ratios as source indicators of organic matter provenance in estuarine systems: evidence from the Tay estuary, Scotland. Estuarine, Coastal and Shelf Science, 38, 219–233.

Treude, T., Hamdan, L. J., Lemieux, S., Dale, A. W., & Sommer, S. (2021). Rapid sulfur cycling in sediments from the Peruvian oxygen minimum zone featuring simultaneous sulfate reduction and sulfide oxidation. Limnology and Oceanography, 66(7). https://doi.org/10.1002/lno.11779

Tsuchiya, M., Grimm, G. W., Heinz, P., Stögere, K., Ertan, K. T., Collen, J., Brüchert, V., Hemleben, C., Hemleben, V., & Kitazato, H. (2009). Ribosomal DNA shows extremely low genetic divergence in a world-wide distributed, but disjunct and highly adapted marine protozoan (Virgulinella fragilis, Foraminiferida). Marine Micropaleontology, 70(1–2), 8–19. https://doi.org/10.1016/j.marmicro.2008.10.001

Tsuchiya, M., Toyofuku, T., Uematsu, K., Brüchert, V., Collen, J., Yamamoto, H., & Kitazato, H. (2015). Cytologic and Genetic Characteristics of Endobiotic Bacteria and Kleptoplasts of Virgulinella fragilis (Foraminifera). Journal of Eukaryotic Microbiology, 62(4). https://doi.org/10.1111/jeu.12200

Tsujimoto, A., Nomura, R., Yasuhara, M., Yamazaki, H., & Yoshikawa, S. (2006). Impact of eutrophication on shallow marine benthic foraminifers over the last 150 years in Osaka Bay, Japan. Marine Micropaleontology, 60(4). https://doi.org/10.1016/j.marmicro.2006.06.001

Tsujimoto, A., Yasuhara, M., Nomura, R., Yamazaki, H., Sampei, Y., Hirose, K., & Yoshikawa, S. (2008). Development of modern benthic ecosystems in eutrophic coastal oceans: The foraminiferal record over the last 200 years, Osaka Bay, Japan. Marine Micropaleontology, 69(2), 225–239. https://doi.org/10.1016/j.marmicro.2008.08.001

Vaquer-Sunyer, R., & Duarte, C. M. (2008). Thresholds of hypoxia for marine biodiversity. Proceedings of the National Academy of Sciences of the United States of America, 105(40), 15452–15457. https://doi.org/10.1073/pnas.0803833105

Vaquer-Sunyer, R., & Duarte, C. M. (2011). Temperature effects on oxygen thresholds for hypoxia in marine benthic organisms. Global Change Biology, 17, 1788–1797. https://doi.org/10.1111/j.1365-2486.2010.02343.x

Vásquez, I. (1970). Resumen general de la pesquería de anchoveta durante el año 1969. Inf. Esp. Inst. Mar Perú , 57(Informe Especial). https://hdl.handle.net/20.500.12958/1625

Velazco, F., & Solís, J. (2000). Estudio Sedimentológico de la Bahía de Paracas. Informe Progresivo Instituto Del Mar Del Perú, 133, 3–22.

Vilela, C. G., Figueira, B. O., Macedo, M. C., & Baptista Neto, J. A. (2014). Late Holocene evolution and increasing pollution in Guanabara Bay, Rio de Janeiro, SE

Brazil. Marine Pollution Bulletin, 79(1–2). https://doi.org/10.1016/j.marpolbul.2013.12.020

Walter, L. M., & Burton, E. A. (1990). Dissolution of recent platform carbonate sediments in marin pore fluids. American Journal of Science, 290, 601–643.

Wilkerson, F., & Dugdale, R. C. (2008). Coastal Upwelling. In D. G. Capone, D. A. Bronk, M. R. Mulholland, & E. J. Carpenter (Eds.), Nitrogen in the Marine Environment (2nd ed., pp. 771–807). Elsevier Inc. https://doi.org/10.1016/B978-0-12-372522-6.00017-7

Yanko, V., Arnold, A. J., & Parker, W. C. (1999). Effects of marine pollution on benthic foraminifera. In B. K. sen Gupta (Ed.), Modern Foraminifera (pp. 217–235). Kluwer Academic Publishers.

Yzocupe, V. A. (2005). Modelo de dispersión de contaminantes en aguas rasas. Revista de Investigación En Física, 8(1), 46–53. https://doi.org/https://doi.org/10.15381/rif.v8i01.8838

IX. APPENDIX

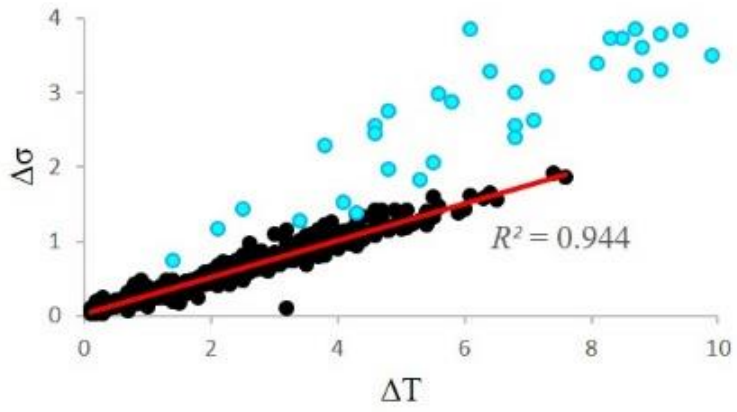

Figure A.A1. Scatter plot of the density difference between the surface and bottom waters (Δσ) in Paracas Bay versus that of temperature (ΔT), calculated from records of the IMARPE dataset in the 2010-2015 period. Cyan dots correspond to data whose salinity difference (ΔS) is greater than 0.50, representing less than 7% of the total.

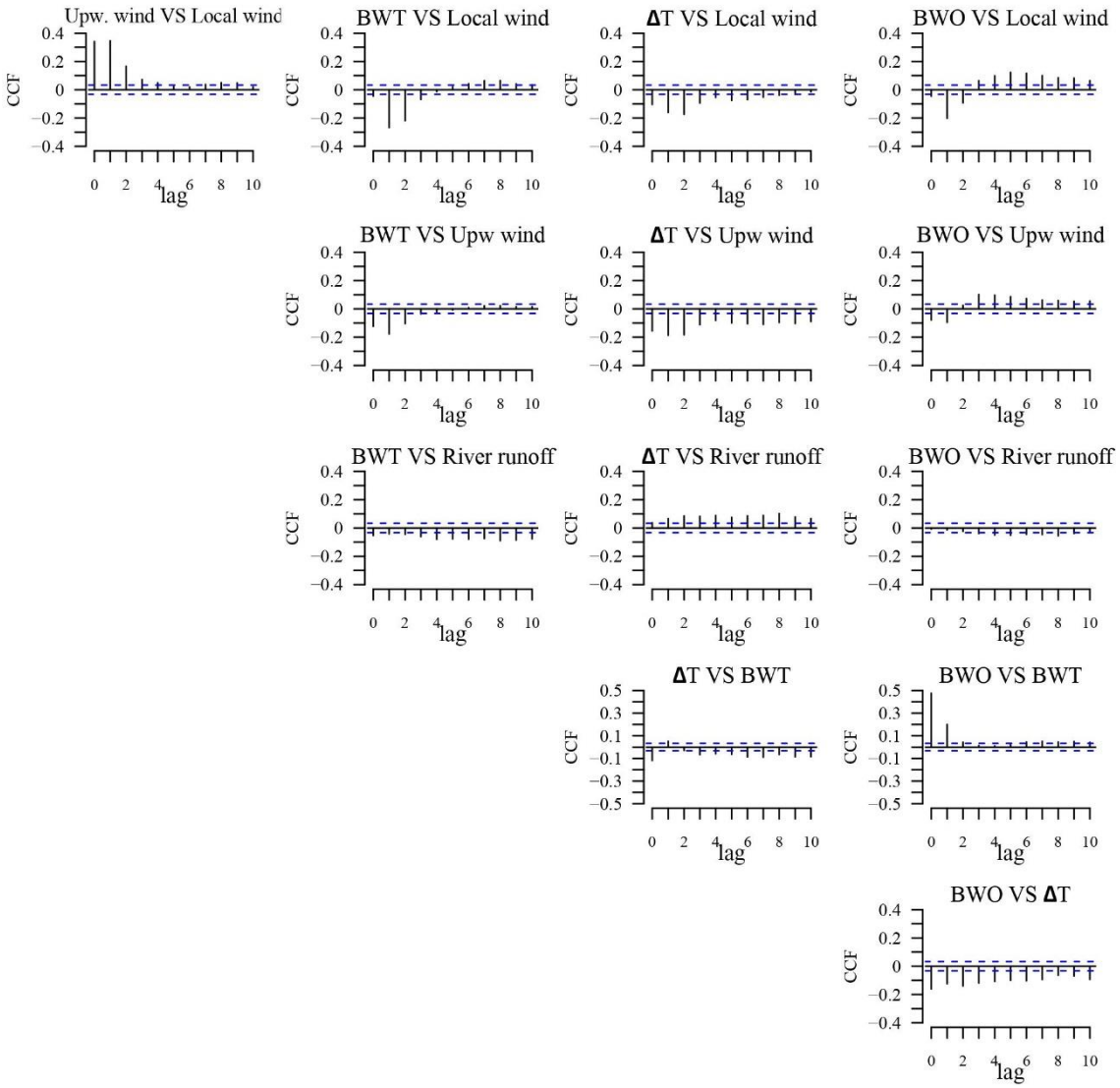

Figure A.A2. Cross-correlations between the daily anomalies of the upwelling wind, local wind, river runoff, and the ΔT, bottom temperature and BWDO of Paracas Bay, over the 2006-2015 period.

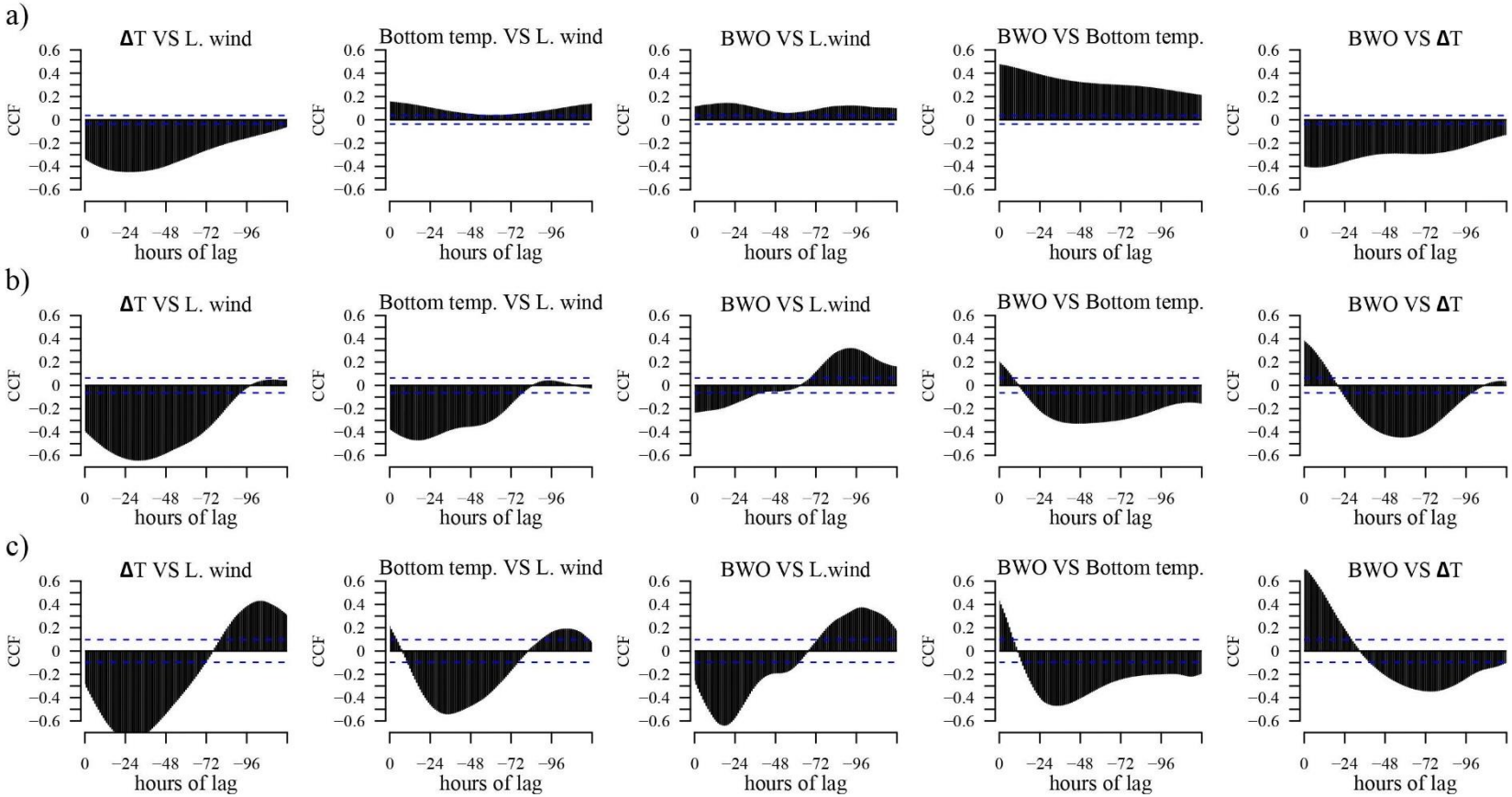

Figure A.A3. Cross-correlations between the smoothed hourly time series of meridional local wind component, ΔT, bottom temperature and BWDO, over the March 2015 – January 2016 period, for (a) the June-September season, (b) the March-April interval, and (c) the December-January interval.

Table A.B1. Two-way crossed PERMANOVA univariate of bottom water properties, based on 9999 permutations. Df = degree of freedom, SS = sum of squares, MS = mean squares.

Variable	Source	Df	SS	MS	Pseudo-F	p-value
Temperature	Time	2	18.9023	9.4512	142.098	**0.0001**
	Zone	3	2.5896	0.8632	12.978	**0.0006**
	Time x Zone	6	3.5104	0.5851	8.796	**0.0015**
	Residuals	15	0.9977	0.0665		
	Total	26	26.0000			
Salinity	Time	2	17.9746	8.9873	23.867	**0.0001**
	Zone	3	0.6955	0.2318	0.616	0.6106
	Time x Zone	6	1.6816	0.2803	0.744	0.6178
	Residuals	15	5.6483	0.3766		
	Total	26	26.0000			
Oxygen	Time	2	13.1000	6.5500	30.759	**0.0001**
	Zone	3	1.7582	0.5861	2.752	0.0855
	Time x Zone	6	7.9475	1.3246	6.220	**0.0046**
	Residuals	15	3.1942	0.2129		
	Total	26	26.0000			
pH	Time	2	11.9193	5.9597	25.329	**0.0001**
	Zone	3	1.5804	0.5268	2.239	0.1188
	Time x Zone	6	8.9708	1.4951	6.354	**0.0010**
	Residuals	15	3.5294	0.2353		
	Total	26	26.0000			
Nitrates	Time	2	15.7552	7.8776	82.830	**0.0001**
	Zone	3	3.4312	1.1437	12.026	**0.0010**
	Time x Zone	6	5.3871	0.8978	9.441	**0.0014**
	Residuals	15	1.4266	0.0951		
	Total	26	26.000			
Phosphates	Time	2	13.5357	6.7679	10.952	**0.0013**
	Zone	3	0.1205	0.0402	0.065	0.9772
	Time x Zone	6	3.0740	0.5123	0.829	0.5748
	Residuals	15	9.2697	0.6180		
	Total	26	26.0000			

Table A.B2. Two-way crossed PERMANOVA univariate of sedimentary properties, based on 9999 permutations. Df = degree of freedom, SS = sum of squares, MS = mean squares.

Variable	Source	Df	SS	MS	Pseudo-F	p-value
Sand	Time	2	0.1198	0.0599	0.050	0.9551
	Zone	3	6.3469	2.1156	1.767	0.1902
	Time	x6	1.5701	0.2617	0.219	0.9707
	Zone	15	17.9631	1.1975		
	Residuals	26	26.0000			
	Total					
Silt	Time	2	0.3638	0.1819	0.171	0.8436
	Zone	3	8.4550	2.8183	2.652	0.0915
	Time	x6	1.2375	0.2063	0.194	0.9707
	Zone	15	15.9437	1.0629		
	Residuals	26	26.0000			
	Total					
Clay	Time	2	0.6257	0.3128	0.337	0.7117
	Zone	3	9.3852	3.1284	3.365	**0.0482**
	Time	x6	2.0455	0.3409	0.367	0.8855
	Zone	15	13.9436	0.9296		
	Residuals	26	26.0000			
	Total					
LOI	Time	2	6.4604	3.2302	11.480	**0.0014**
	Zone	3	14.1099	4.7033	16.715	**0.0002**
	Time	x6	1.2089	0.2015	0.716	0.6443
	Zone	15	4.2208	0.2814		
	Residuals	26	26.000			
	Total					
CPE	Time	2	2.8726	1.4363	2.178	0.1352
	Zone	3	9.3408	3.1136	4.721	**0.0132**
	Time	x6	3.8927	0.6488	0.984	0.4589
	Zone	15	9.8939	0.6596		
	Residuals	26	26.0000			
	Total					
C:P	Time	2	1.3682	0.6841	0.857	0.4570
	Zone	3	6.8166	2.2722	2.845	0.0721
	Time	x6	5.8362	0.9727	1.218	0.3346
	Zone	15	11.9790	0.7986		
	Residuals	26	26.0000			
	Total					

Table A.B3. Two-way crossed PERMANOVA multivariate (*i.e.*, the assemblage data), and univariate (*i.e.*, assemblage structure parameters N, S, H' and D), based on 9999 permutations. Df = degree of freedom, SS = sum of squares, MS = mean squares.

Variable	Source	Df	SS	MS	Pseudo-F	p-value
Assemblage	Time	2	12.7980	6.3990	2.0451	0.0588
	Zone	3	100.0360	33.3450	10.6569	**0.0001**
	Time x Zone	6	15.8140	2.6360	0.8423	0.6581
	Residuals	15	46.9350	3.1290		
	Total	26	175.5820			
Total density (N)	Time	2	9.3916	4.6958	6.1022	**0.0118**
	Zone	3	0.8756	0.2919	0.3793	0.7639
	Time x Zone	6	4.1899	0.6983	0.9075	0.5271
	Residuals	15	11.5428	0.7695		
	Total	26	26.0000			
Species Richness (S)	Time	2	3.3665	1.6832	3.3333	0.0673
	Zone	3	13.3306	4.4435	8.7996	**0.0011**
	Time x Zone	6	1.7283	0.2881	0.5704	0.7402
	Residuals	15	7.5746	0.5050		
	Total	26	26.0000			
Shannon's diversity (H)'	Time	2	1.2454	0.6227	1.6943	0.2115
	Zone	3	16.0694	5.3565	14.5737	**0.0002**
	Time x Zone	6	3.1720	0.5287	1.4384	0.2615
	Residuals	15	5.5131	0.3675		
	Total	26	26.0000			
Simpson's Dominance (D)	Time	2	1.7269	0.8635	1.3024	0.3039
	Zone	3	9.3974	3.1325	4.7248	**0.0197**
	Time x Zone	6	4.9311	0.8219	1.2396	0.3373
	Residuals	15	9.9446	0.6630		
	Total	26	26.0000			

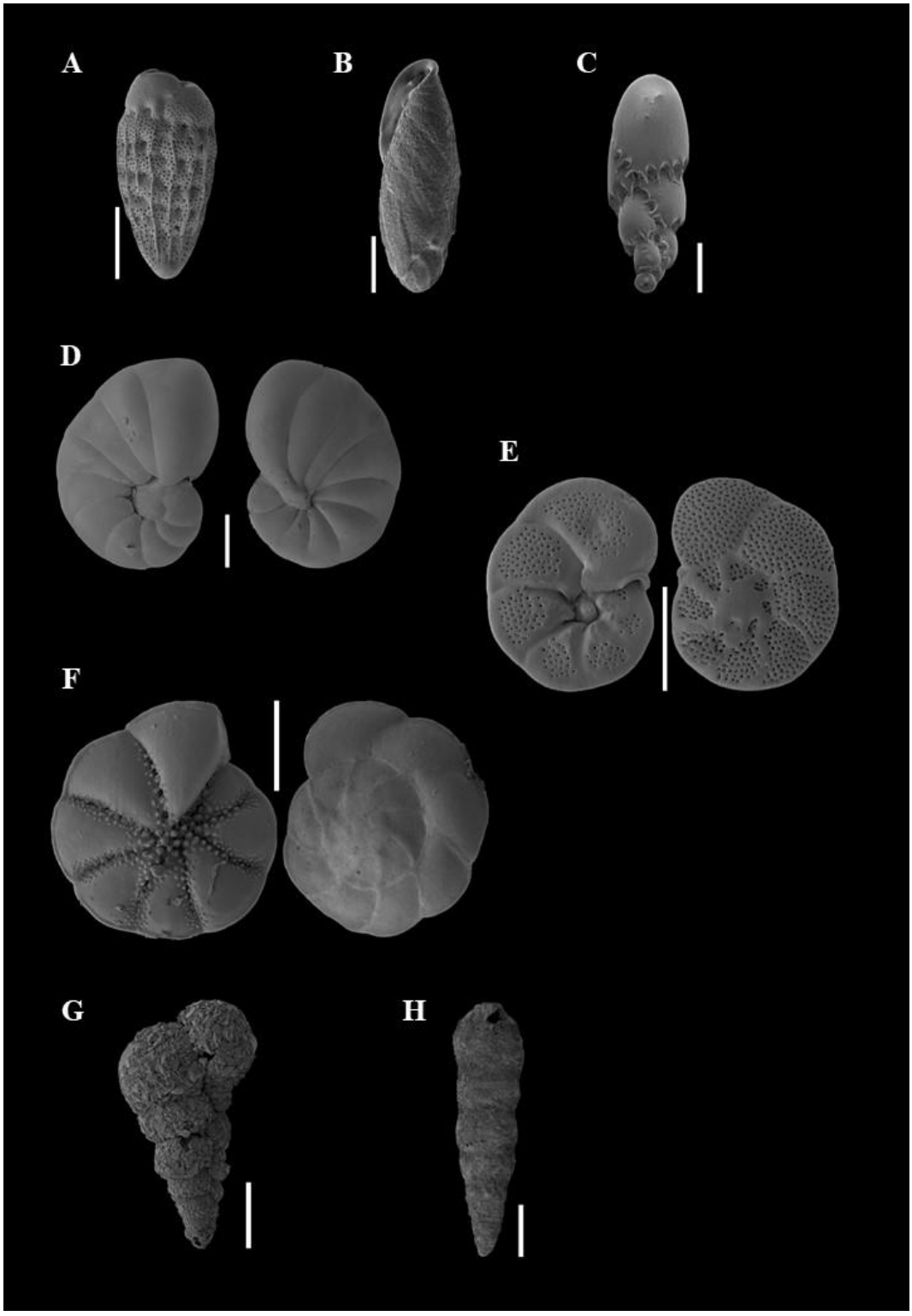

Figure A.B1. The most representative taxa of the living benthic foraminiferal assemblage of the Pisco-Paracas coastal area. A: *Bolivina costata*. B: *Buliminella elegantissima*. C: *Virgulinella fragilis*. D: *Nonionella auris*. E: *Discorbis* sp. F: *Buccella peruviana*. G: *Textularia* sp. H: *Reophax* sp. Scale bar is 100 µm.

Table A.C1. List of benthic foraminiferal species identified in the monitoring period 2019-2021. *Species found alive (Rose Bengal stained). **Species found alive only on a single occasion.

P1	P2	P3
*Bolivina costata**	*Bolivina costata**	*Bolivina costata**
*Buliminella elegantissima**	*Buliminella elegantissima**	*Buliminella elegantissima**
*Nonionella auris**	*Nonionella auris**	*Nonionella auris**
*Virgulinella fragilis**	*Virgulinella fragilis**	*Virgulinella fragilis**
*Buccella peruviana**	*Buccella peruviana**	*Discorbis* sp.
Discorbis sp.	*Discorbis* sp.*	*Bulimina* sp.
Bulimina sp.	*Bulimina* sp.*	*Bolivina* sp.
Bolivina sp.	*Bolivina* sp.	*Cibicides* sp.
Cibicides sp.**	*Cibicides* sp.	*Ammonia* sp.
Ammonia sp.	*Ammonia* sp.	*Quinqueloculina* sp.
Reophax sp.	*Quinqueloculina* sp.**	*Reophax* sp.
Textularia sp.	*Reophax* sp.	*Textularia* sp.**
Rotaliammina sp.	*Textularia* sp.	*Rotaliammina* sp.
Cribrostomoides sp.	*Rotaliammina* sp.	*Cribrostomoides* sp.
	Cribrostomoides sp.	

Table A.D1. CFCS age model results. MAR: Mass accumulation rate.

Depth (cm)	Mass depth (g cm^{-2})	CFCS Mean Age	CFCS Min. Age	CFCS Max. Age	MAR (g cm^{-2} y^{-1})
0.5	0.11	2020.34	2020.32	2020.37	0.173
1.5	0.35	2018.93	2018.85	2019.01	0.173
2.5	0.65	2017.20	2017.06	2017.34	0.173
3.5	0.94	2015.55	2015.35	2015.76	0.173
4.5	1.20	2014.03	2013.76	2014.29	0.173
5.5	1.46	2012.53	2012.21	2012.84	0.173
6.5	1.72	2011.05	2010.68	2011.43	0.173
7.5	2.00	2009.44	2009.00	2009.87	0.173
8.5	2.27	2007.85	2007.36	2008.35	0.173
9.5	2.52	2006.44	2005.89	2006.99	0.173
10.5	2.76	2005.05	2004.45	2005.65	0.173
11.5	3.02	2003.52	2002.87	2004.18	0.173
12.5	3.30	2001.91	2001.19	2002.63	0.173
13.5	3.57	2000.35	1999.57	2001.13	0.173
14.5	3.84	1998.79	1997.95	1999.63	0.173
15.5	4.12	1997.18	1996.28	1998.07	0.173
16.5	4.43	1995.42	1994.45	1996.38	0.173
17.5	4.76	1993.48	1992.45	1994.52	0.173
18.5	5.12	1991.43	1990.32	1992.55	0.173
19.5	5.46	1989.47	1988.28	1990.66	0.173
20.5	5.80	1987.48	1986.22	1988.75	0.173
21.5	6.16	1985.43	1984.09	1986.77	0.173
22.5	6.49	1983.53	1982.12	1984.94	0.173
23.5	6.84	1981.48	1979.99	1982.97	0.173
24.5	7.22	1979.29	1977.71	1980.86	0.173
25.5	7.60	1977.12	1975.47	1978.78	0.173
26.5	7.98	1974.93	1973.19	1976.67	0.173
27.5	8.38	1972.59	1970.77	1974.42	0.173
28.5	8.79	1970.23	1968.31	1972.14	0.173
29.5	9.21	1967.80	1965.80	1969.81	0.173
30.5	9.63	1965.38	1963.28	1967.48	0.173
31.5	10.07	1962.87	1960.68	1965.07	0.173
32.5	10.48	1960.51	1958.22	1962.79	0.173
33.5	10.85	1958.34	1955.98	1960.71	0.173
34.5	11.26	1956.00	1953.55	1958.46	0.173
35.5	11.66	1953.67	1951.13	1956.21	0.173
36.5	12.08	1951.27	1948.64	1953.90	0.173
37.5	12.51	1948.79	1946.07	1951.52	0.173
38.5	12.94	1946.31	1943.49	1949.13	0.173
39.5	13.34	1943.97	1941.07	1946.88	0.173
40.5	13.71	1941.84	1938.85	1944.83	0.173
41.5	14.08	1939.73	1936.66	1942.80	0.173
42.5	14.47	1937.48	1934.33	1940.63	0.173
43.5	14.86	1935.20	1931.96	1938.44	0.173
44.5	15.25	1932.95	1929.63	1936.28	0.173
45.5	15.67	1930.53	1927.11	1933.94	0.173
46.5	16.13	1927.87	1924.36	1931.39	0.173
47.5	16.60	1925.16	1921.54	1928.78	0.173
48.5	17.06	1922.51	1918.79	1926.23	0.173
49.5	17.52	1919.85	1916.03	1923.67	0.173

Table A.D2. CRS age model results. MAR: Mass accumulation rate.

Depth (cm)	Mass depth (g cm^{-2})	CRS Mean Age	CRS Min. Age	CRS Max. Age	MAR (g cm^{-2} y^{-1})
0.5	0.11	2020.38	2020.33	2020.44	0.090
1.5	0.35	2019.02	2018.87	2019.17	0.174
2.5	0.65	2017.24	2017.02	2017.46	0.169
3.5	0.94	2015.50	2015.23	2015.77	0.163
4.5	1.20	2013.83	2013.52	2014.14	0.158
5.5	1.46	2012.14	2011.79	2012.48	0.168
6.5	1.72	2010.59	2010.21	2010.96	0.184
7.5	2.00	2009.03	2008.63	2009.43	0.196
8.5	2.27	2007.59	2007.16	2008.01	0.212
9.5	2.52	2006.40	2005.96	2006.84	0.208
10.5	2.76	2005.22	2004.76	2005.68	0.183
11.5	3.02	2003.73	2003.25	2004.21	0.163
12.5	3.30	2001.96	2001.45	2002.47	0.159
13.5	3.57	2000.21	1999.67	2000.75	0.161
14.5	3.84	1998.49	1997.93	1999.06	0.178
15.5	4.12	1996.86	1996.27	1997.45	0.211
16.5	4.43	1995.38	1994.77	1996.00	0.226
17.5	4.76	1993.86	1993.22	1994.51	0.206
18.5	5.12	1992.08	1991.41	1992.75	0.168
19.5	5.46	1989.97	1989.27	1990.68	0.144
20.5	5.80	1987.48	1986.74	1988.23	0.142
21.5	6.16	1984.88	1984.09	1985.66	0.150
22.5	6.49	1982.59	1981.76	1983.42	0.178
23.5	6.84	1980.52	1979.65	1981.39	0.196
24.5	7.22	1978.52	1977.61	1979.42	0.191
25.5	7.60	1976.49	1975.55	1977.44	0.190
26.5	7.98	1974.42	1973.44	1975.41	0.175
27.5	8.38	1971.98	1970.94	1973.02	0.157
28.5	8.79	1969.25	1968.15	1970.35	0.146
29.5	9.21	1966.22	1965.05	1967.39	0.135
30.5	9.63	1962.94	1961.69	1964.18	0.137
31.5	10.07	1959.60	1958.28	1960.93	0.145
32.5	10.48	1956.63	1955.22	1958.04	0.134
33.5	10.85	1953.64	1952.14	1955.14	0.112
34.5	11.26	1949.79	1948.17	1951.42	0.101
35.5	11.66	1945.52	1943.75	1947.28	0.096
36.5	12.08	1940.86	1938.93	1942.79	0.090
37.5	12.51	1935.66	1933.53	1937.79	0.082
38.5	12.94	1929.91	1927.53	1932.29	0.085
39.5	13.34	1924.67	1922.03	1927.30	0.098
40.5	13.71	1920.62	1917.75	1923.48	0.122
41.5	14.08	1917.42	1914.36	1920.47	0.127
42.5	14.47	1914.12	1910.86	1917.39	0.101
43.5	14.86	1909.92	1906.32	1913.52	0.103
44.5	15.25	1905.81	1901.88	1909.75	0.123
45.5	15.67	1902.20	1898.03	1906.37	0.122
46.5	16.13	1898.17	1893.75	1902.58	0.107
47.5	16.60	1893.41	1888.70	1898.13	0.091
48.5	17.06	1887.88	1882.77	1893.00	0.076
49.5	17.52	1881.12	1875.45	1886.78	0.062

Table A.D3. Piecewise CRS age model results. MAR: Mass accumulation rate.

Depth (cm)	Mass depth (g cm^{-2})	CRS Age	CRS Min. Age	CRS Max. Age	MAR (g cm^{-2} y^{-1})
0.5	0.11	2020.45	2018.96	2021.95	0.102
1.5	0.35	2019.26	2016.32	2022.20	0.199
2.5	0.65	2017.71	2014.90	2020.52	0.195
3.5	0.94	2016.20	2013.52	2018.88	0.190
4.5	1.20	2014.77	2012.22	2017.32	0.185
5.5	1.46	2013.33	2010.92	2015.74	0.199
6.5	1.72	2012.02	2009.74	2014.30	0.219
7.5	2.00	2010.71	2008.57	2012.85	0.234
8.5	2.27	2009.51	2007.50	2011.52	0.256
9.5	2.52	2008.53	2006.63	2010.44	0.253
10.5	2.76	2007.56	2005.77	2009.36	0.224
11.5	3.02	2006.35	2004.70	2008.00	0.201
12.5	3.30	2004.92	2003.47	2006.38	0.198
13.5	3.57	2003.52	2002.27	2004.78	0.203
14.5	3.84	2002.17	2001.12	2003.22	0.226
15.5	4.12	2000.89	2000.04	2001.73	0.272
16.5	4.43	1999.75	1999.10	2000.40	0.294
17.5	4.76	1998.59	1998.32	1998.86	0.255
18.5	5.12	1997.12	1992.11	2002.14	0.193
19.5	5.46	1995.30	1985.37	2005.24	0.168
20.5	5.80	1993.17	1983.46	2002.89	0.167
21.5	6.16	1990.97	1981.50	2000.44	0.178
22.5	6.49	1989.06	1979.81	1998.30	0.215
23.5	6.84	1987.35	1978.32	1996.38	0.238
24.5	7.22	1985.72	1976.91	1994.52	0.235
25.5	7.60	1984.08	1975.50	1992.65	0.236
26.5	7.98	1982.43	1974.10	1990.76	0.220
27.5	8.38	1980.52	1972.49	1988.54	0.201
28.5	8.79	1978.41	1970.75	1986.07	0.191
29.5	9.21	1976.12	1968.89	1983.35	0.180
30.5	9.63	1973.70	1966.97	1980.44	0.189
31.5	10.07	1971.32	1965.11	1977.53	0.205
32.5	10.48	1969.24	1963.52	1974.96	0.195
33.5	10.85	1967.23	1962.02	1972.43	0.169
34.5	11.26	1964.72	1960.22	1969.23	0.158
35.5	11.66	1962.06	1958.38	1965.74	0.158
36.5	12.08	1959.32	1956.61	1962.03	0.157
37.5	12.51	1956.45	1955.36	1957.54	0.123
38.5	12.94	1952.45	1945.04	1959.85	0.100
39.5	13.34	1948.06	1933.68	1962.45	0.119
40.5	13.71	1944.77	1931.20	1958.34	0.153
41.5	14.08	1942.22	1929.35	1955.09	0.161
42.5	14.47	1939.66	1927.57	1951.75	0.131
43.5	14.86	1936.48	1925.43	1947.53	0.138
44.5	15.25	1933.46	1923.53	1943.40	0.171
45.5	15.67	1930.90	1922.11	1939.69	0.175
46.5	16.13	1928.15	1920.79	1935.51	0.159
47.5	16.60	1925.05	1919.54	1930.55	0.143
48.5	17.06	1921.65	1919.41	1923.89	0.077
49.5	17.52	1919.85	1919.85	1919.85	0.018

Table A.D4. Accumulation rate of benthic foraminiferal tests and relative abundances of the species preserved by average depth in the core.

Depth (cm)	Age	BFAR #tests/cm^2/y	*Bolivina costata*	*Buliminella elegantissima*	*Nonionella auris*	*Bulimina* sp.	*Ammonia* sp.	*Buccella peruviana*	*Rotaliammina* sp.	*Fursenkoina* sp	*Virgulinella fragilis*	*Discorbis* sp.	*Cibicides* sp.	*Bolivina* sp1.
0.5	2020.4	43.0	20.6	78.1	0.4	0.0	0.0	0.4	0.0	0.4	0.0	0.0	0.0	0.0
1.5	2019.2	44.0	26.8	71.7	1.5	0.0	0.0	0.0	0.0	0.0	0.0	0.0	0.0	0.0
2.5	2017.6	19.7	24.6	71.6	2.2	0.0	0.7	0.7	0.0	0.0	0.0	0.0	0.0	0.0
3.5	2016.0	19.2	40.0	55.8	3.3	0.0	0.8	0.0	0.0	0.0	0.0	0.0	0.0	0.0
4.5	2014.5	20.8	54.4	42.7	2.3	0.0	0.0	0.6	0.0	0.0	0.0	0.0	0.0	0.0
6.5	2011.6	12.4	56.6	39.8	1.2	1.2	0.0	0.0	0.0	1.2	0.0	0.0	0.0	0.0
8.5	2009.0	31.5	63.6	30.8	2.8	2.1	0.0	0.0	0.7	0.0	0.0	0.0	0.0	0.0
10.5	2006.9	37.0	67.5	30.0	2.0	0.5	0.0	0.0	0.0	0.0	0.0	0.0	0.0	0.0
12.5	2004.1	46.7	66.7	31.3	1.3	0.5	0.3	0.0	0.0	0.0	0.0	0.0	0.0	0.0
14.5	2001.2	67.1	60.1	32.4	5.9	0.0	0.6	0.0	0.2	0.2	0.2	0.2	0.2	0.0
16.5	1998.6	60.7	50.4	28.6	16.7	2.4	0.5	0.0	0.0	0.7	0.2	0.0	0.5	0.0
18.5	1995.6	43.1	48.2	26.2	21.0	3.5	0.2	0.0	0.0	0.2	0.6	0.0	0.2	0.0
19.5	1993.6	70.7	55.2	37.4	6.8	0.4	0.0	0.0	0.0	0.1	0.0	0.0	0.1	0.0
20.5	1991.3	131.8	54.2	37.0	7.8	1.0	0.0	0.0	0.0	0.1	0.0	0.1	0.0	0.0
22.5	1986.8	131.4	62.1	19.6	17.0	0.5	0.1	0.0	0.1	0.2	0.0	0.1	0.1	0.1
24.5	1983.1	114.7	26.4	9.3	62.3	1.1	0.3	0.2	0.1	0.4	0.0	0.0	0.0	0.0
26.5	1979.3	83.6	38.1	28.9	30.7	1.5	0.1	0.1	0.1	0.3	0.0	0.1	0.0	0.0
28.5	1974.7	64.1	53.4	37.5	7.0	1.9	0.1	0.0	0.0	0.2	0.0	0.0	0.0	0.0
30.5	1969.2	49.2	51.8	39.8	4.3	3.8	0.3	0.0	0.0	0.0	0.0	0.0	0.0	0.0
32.5	1963.9	110.4	60.8	33.5	4.7	0.8	0.2	0.1	0.0	0.0	0.0	0.0	0.0	0.0
34.5	1958.3	53.4	60.2	38.3	0.6	0.3	0.3	0.0	0.2	0.0	0.0	0.0	0.0	0.0
36.5	1951.3	23.6	60.6	39.0	0.2	0.0	0.2	0.0	0.0	0.0	0.0	0.0	0.0	0.0
38.5	1943.4	10.1	50.6	41.8	4.1	2.4	0.0	0.0	1.2	0.0	0.0	0.0	0.0	0.0